

https://dspace.org/

The biosorption of heavy metals by immobilised green microalgae Desmodesmus sp. biosmass

Diale, Palesa Promise

2016

http://hdl.handle.net/10539/20029

Downloaded from a DSpace repository. https://dspace.org/

THE BIOSORPTION OF HEAVY METALS BY IMMOBILIZED GREEN MICROALGAE *DESMODESMUS SP.* BIOMASS



Palesa Promise Diale

A thesis submitted to the Faculty of Engineering and the Built Environment, University of the Witwatersrand, Johannesburg, in fulfillment of the requirements for the degree of Doctor of Philosophy in Engineering.

October 2015

DECLARATION

I declare that this thesis is my own unaided work. It is being submitted for the Degree of Doctor of Philosophy in Engineering to the University of the Witwatersrand, Johannesburg. It has not been submitted before for any degree or examination to any other University.

(Signature of Candidate)

..... day of ..... year .....

ABSTRACT

Gold mining had a prominent place in the South African economy since its discovery in 1886. However, its fall in production and imminent resource exhaustion over the years has come with extensive environmental problems. This therefore calls for sustainable and cost-effective technologies that can reduce toxic levels of heavy metal concentrations in water streams to environmentally acceptable levels. A green microalgae such as *Desmodesmus sp.* has a potential to be a sustainable and cost-effective solution, due to its proficient capability of heavy metal sequestration in aqueous solutions. This study is therefore governed by two key complimentary components: (i) in-depth optimization study of Ca-alginate matrix composition for the purpose of immobilizing *Desmodesmus sp.* and (ii) the immobilized *Desmodesmus sp.* being used for biosorption of heavy metals from aqueous solutions. Following the preliminary optimization studies, bead diameter of 3 mm; calcium chloride concentration of 9 % w/v; sodium alginate concentration of 6 % w/v and biomass loading of 8 % w/v were used for subsequent biosorption experiments. High correlation coefficients was found for the Freundlich model indicating that it can be used to best describe the sorption of Fe (II) and other heavy metals on immobilized algal biomass. The correlation coefficient study showed the R^2 value of Fe (II) sorption kinetics for pseudo-second order kinetic equation was close to 1, making it a better fit to the experimental data compared to pseudo-first order where R^2 values were 0.18; 0.38; 0.76; 0.41; 0.48 and 0.76 for 5; 60; 120; 240; 480 and 1000 mg / L. The trend in binding of heavy metal ions is as follows: Ni (II) > Mn (II) >Cr (III) > Fe (II). The increase in loading capacity as a function to time when Fe (II), Ni (II), Mn (II) and Cr (III) are adsorbed by the immobilized microalgae *Desmodesms sp.* is an indication that microalgae cells are tolerant of toxic heavy metals in aqueous solutions. According to this study a flow rate of 4 mL/min with a packing height of 82 cm (C_o = 120 mg / L) seems to be the most effective combination, which has a potential to increase the

metal removal rate significantly. Further work will be required to develop models that will best describe the biosorption of heavy metals in a continuous flow system, packed bed column. From this study the immobilized green microalgae *Desmodesmus sp.* has shown to have a high loading capacity for Fe (II), it has a potential to be re-used and regenerated for multiple cycles of heavy metal uptake.

DEDICATION

In memory of my late parents

Mashabela Henry Diale

Duduzile Junias Diale

ACKNOWLEDGEMENTS

The author would like to express her deepest gratitude to Dr. Tonderayi Matambo; Prof. Diane Hildebrandt; Prof. David Glasser for their dedicated supervision of my PhD project.

I would like to thank the National Research Foundation (NRF), Canon Collins Trust and Material and Process Synthesis (MaPS) research unit for their support and excellent administration of funding y degree.

A special thank you to my mentor Dr. Josephat Zimba and my fellow colleague Velinjani Mthethwa for helping editing this thesis before submission.

I would like to thank Prof. Ewa Cukrowska, professor in Environmental Analytical Chemistry, University of Witwatersrand for allowing me to use her labs to carry out analysis needed for all experimental work in the study.

I would like to thank Dr. Lu (Alex) Xiaojun for insightful ideas and advice into this research topic.

Thank you to the administrative assistance offered by the staff in the Material and Process Synthesis (MaPS) research unit: Alicia Konzani, Genevieve Ngubeni and Lee-an Abrahams.

My mother and my sister for their encouragement and support and believing in me.

CONFERENCE PRESENTATIONS

Special Seminar talk: The Biosorption of Heavy Metals by Immobilised Green Microalgae *Desmodesmus sp.* Biomass. University of California San Diego, Scripps Institution of Oceanography (SIO), Vaughan Hall, Room 100, November 24, 2014, 12:00 Noon.

Rapid fire oral and poster presentation, in AIChE Annual Meeting 2014, *Experimental and mathematical modelling of breakthrough curves of Fe (II) on immobilized biomass in a packed column*. November 16 - 21 2014, Atlanta, Georgia, USA.

Oral presentation, in ICCT/SAIChE conference 2014: *Dynamic adsorption study of immobilized Desmodesmus sp. for heavy metal removal* and Poster presentation: *Modelling and study of sorption breakthrough behaviour of Iron (II) by Immobilized Microalgae Desmodesmus sp. in a Packed Bed Bioreactor*. 27 July to 1 August 2014, Durban, KwaZulu Natal, South Africa.

Poster presentation, in the SAIChE conference 2012: *Modelling of Iron (II) Biosorption by Immobilized Microalgae (Desmodesmus sp.) in a Packed Bed Bioreactor*. 16 -19 September 2012, Champagne Sports Resort Conferencing Venue (Drakensberg), KwaZulu Natal, South Africa.

TABLE OF CONTENTS

CHAPTER 1: INTRODUCTION AND LITERATURE SURVEY 2

1.1 Introduction 2

1.1.1 Witwatersrand Basin 2

1.1.2 Lime treatment for AMD in the Witwatersrand Basin 4

1.2 AMD treatment process as approved by government for Witwatersrand Basin clean-up 6

1.3 AMD contamination in the West Witwatersrand Basin 11

1.3.1 AMD chemistry 11

1.3.2 Other techniques for heavy metal removal from water bodies 13

1.4 Green microalgae (*Desmodesmus sp*.) 15

1.4.1 Taxonomy 15

1.4.2 Morphology 17

1.5 Growth kinetics 21

1.6 Immobilization of microalgae cells 23

1.6.1 Types of immobilization matrix and choice of usage 24

1.6.2 Natural polysaccharides as an entrapment support 26

1.7 Heavy metal biosorption by *Desmodesmus sp.* 28

1.8 HYPOTHESIS AND OBJECTIVES 30

1.8.1 Hypothesis 1 30

1.8.2 Hypothesis 2 30

1.8.3 Research key questions 30

CHAPTER 2: IMMOBILIZATION OF *DESMODESMUS SP.* USING CA-ALGINATMATRIX 32

2.1 Introduction 33

2.1.1 Immobilization 33

2.1.2 Immobilization of *Desmodesmus sp.* 33

2.1.3 Objectives 34

2.2 Experimental methods and material 35
2.2.1 Algae and growth conditions 35
2.2.2 Immobilization of microalgae preparation 36
2.2.3 Effects of curing time on bead stability 38
2.2.4 Fe (II) removal by immobilized *Desmosdesmus sp.* (IDS) and clear beads (CB) from solution 39
2.2.5 Storage test for sstability of alginate-immobilized algal cells 39
2.3 Results and Discussion 40
2.3.1 Microalgae identification and cultivation 40
2.3.2 Immobilization of microalgae preparation 44
2.3.3 Effects of curing time on bead stability 46
2.3.4 Fe (II) removal by IDS and CB from solution 48
2.3.5 Storage test on stability of alginate-immobilized microalgae cells 51
2.4 Conclusion 53
C H A P T E R 3: CHARACTERIZATION OF IMMOBILIZED MICROALGAE AND FE (II) SORPTION 55
3.1 Introduction 55
3.1.1 Immobilization of microalgae cells 55
3.1.2 Objectives 56
3.2 Experimental methods and materials 57
3.2.1 Reagents 57
3.2.2 Characterisation of immobilized *Desmodesmus sp.* (IDS) 57
3.2.3 Fe (II) removal from solution in batch conditions 61
3.3 Results and Discussion 63
3.3.1 Characterisation of immobilized *Desmodesmus sp.* (IDS) 63
3.3.2 Batch adsorption studies 71
3.4 Bead parameters for further adsorption study 79
3.5 CONCLUSION 81
C H A P T E R 4: FE (II) SORPTION MECHANISM AND KINETIC MODELLING STUDY ON IMMOBILIZED *DESMODESMUS SP.* 83

4.1 Introduction 83
4.1.1 Adsorption isotherms and kinetic models for immobilized microalgae 83
4.1.2 Objectives 83
4.2 Experimental methods and materials 84
4.2.1 Chemicals 84
4.2.2 Preparation of immobilized algae cells 84
4.2.3 Batch adsorption study 84
4.2.4 Sorption isotherm and kinetic modelling 85
4.2.5 Determination of the Effective Diffusivity 88
4.3 Results and Discussion 91
4.3.1 Metal sorption system 91
4.3.2 Metal binding mechanism 95
4.3.3 Comparative study of the removal of Cr (III), Fe (II), Ni (II) and Mn (II) by IDS 97
4.3.4 Biosorption isotherm 99
4.3.5 Adsorption kinetics modelling 102
4.4 Conclusion 108
C H A P T E R 5: EXPERIMENTAL AND MATHEMATICAL MODELING OF BREAKTHROUGH CURVES OF FE (II) SORPTION ON IMMOBILIZED BIOMASS IN A PACKED BED COLUMN 110
5.1 Introduction 110
5.1.1 Packed bed column 110
5.1.2 Objectives 110
5.2 Materials and Method 111
5.2.1 Preparation of CB and IDS beads 111
5.2.2 Preparation of heavy metal solution 111
5.2.3 Packed bed continuous system set-up 111
5.2.4 Break through curves analysis 113
5.2.5 The adsorption mechanisms of Fe (II) 114
5.3 Results and Discussion 91
5.3.1 Breakthrough curves 117
5.3.2 Modelling of breakthrough curves 126

5.4 Conclusion 133

C H A P T E R 6: GENERAL CONCLUSIONS 135

6.1 Conclusions 135

6.2. Future work 138

REFERENCES 139

APPENDICES 156

Appendix A – Beijerinck medium 157

Modified Beijerinck medium composition 157

Appendix B – Immobilization, gelling forming system design 158

LIST OF FIGURES

FIGURE 1.1: A GEOLOGICAL MAP SHOWING THE WITWATERSRAND BASIN AND KAROO SUPERGROUP, PICTURE COURTESY OF MCCARTHY (2011) 3

FIGURE 1.2: THE PROPOSED HDS PROCESS FOR THE TREATMENT OF AMD FOR THE IMMEDIATE AND SHORT TERM INTERVENTIONS. 7

FIGURE 1.3: A SIMPLIFIED ILLUSTRATION OF TAXONOMY OF ALGAE IN THE ENVIRONMENT. ILLUSTRATION ADAPTED FROM FUNDAMENTAL OF ENVIRONMENTAL MEASUREMENTS: (HTTP://WWW.FONDRIEST.COM/ENVIRONMENTAL-MEASUREMENTS/PARAMETERS/WATER-QUALITY/ALGAE-PHYTOPLANKTON-CHLOROPHYLL/)..... 15

FIGURE 1.4: TYPES OF UNICELLS AND COLONIES FORMED BY *DESMODESMUS SP.*..... 17

FIGURE 1.5: SEM OF OUTER WALL OF *DESMODESMUS* ILLUSTRATING ULTRASTRUCTURAL FEATURES SUCH AS A SHORT SPINE, LONG SPINE, WARTS, RIDGE AND OPENING (SHUBERT ET AL., 2014).. 18

FIGURE 1.6: DIAGNOSTIC PHENOTYPIC FEATURES ARE HARD TO DIFFERENTIATE FOR DESMODESMUS (D) AND SCENEDESMUS (S) GENUS AND SHOWN (A) DESMODESMUS COMMUNI (D); (B) SCENEDESMUS QUADRICAUDA (S); (C) DESMODESMUS SUBSPICATUS (D) AND (D) SCENEDESMUS RUBESCENS (S)..... 20

FIGURE 1.7: ILLUSTRATES AN IDEAL SHAPE OF THE RESPECTIVE GROWTH PHASES OF MICROALGAE IN MEDIA. 22

FIGURE 1.8: IMMOBILIZED ENZYME SYSTEMS: ENZYME COVALENTLY ATTACHED TO AN INSOLUBLE PARTICLE; ENZYME ENTRAPPED WITHIN AN INSOLUBLE PARTICLE BY A CROSS-LINKED POLYMER; ENZYME CONFINED WITHIN A SEMIPERMEABLE MEMBRANE; AND CROSS-LINKING ENZYMES (GUISÁN, 2006). 25

FIGURE 1.9: LINEAR BLOCK POLYMERS OF B-D-MANNURONATE (M) AND -L-GULURONATE (G) WITH A VARIATION IN COMPOSITION AND SEQUENTIAL ARRANGEMENTS BEING CROSS-LINKED BY CA^{2+} IONS TO FORM CALCIUM ALGINATE MATRIX. 27

FIGURE 2.1: AN ILLUSTRATION OF ALGAE GROWTH SET-UP. GREEN MICROALGA CELLS CULTURED IN A MODIFIED BEIJERINCK MEDIUM, WITH PERIODICAL CO2 BUBBLING 35

FIGURE 2.2: PREPARATION FOR IMMOBILIZED MICROALGAE BEADS FORMATION ILLUSTRATION, WHICH INVOLVES: (A) HARVESTING MICROALGAE BY CENTRIFUGATION; (B) MIXING MICROALGAE WITH NA-ALGINATE, (C) PUTTING THE MIXTURE OF MICROALGAE AND NA-ALGINATE INTO A SYRINGE, (D) DROPPING MIXTURE FROM THE SYRINGE INTO A CACL2 SOLUTION, (E) SPHERICAL BEADS FORM FROM DROPPING MIXTURE INTO CACL2 SOLUTION AND BEAD ARE CURED FOR TIME SUFFICIENT FOR MAXIMUM CROSS-LINKAGE TO OCCUR AND (F) RETRIEVAL OF FORMED BEADS FROM CACL2 SOLUTION, RINSED AND STORED FOR LABORATORY APPLICATION. (ELDRIDGE, 2008). 36
FIGURE 2.3: DR. BEN LOOS, CAF, STELLENBOSCH UNIVERSITY VIEWED THE SAMPLES USING AN INVERTED FLUORESCENCE MICROSCOPE. (A) AND (B) ARE PHOTOS SHOWING ALGAE FOUND IN THE SAMPLE FROM DONALDSON DAM AND (C) ALGAE FOUND IN THE SAMPLE FROM ZOO LAKE (DIALE ET AL., 2011). 40
FIGURE 2.4: GROWTH CURVE OF DESMODESMUS SP. MICROALGAE IN BEIJERINCK MEDIUM. 41
FIGURE 2.5: DEMONSTRATION OF MATURATION STEP IN THE BEAD FORMATION PROCESS: (A) NA-ALGINATE MIXTURE WITH MICROALGAE DROPPED INTO CACL2 SOLUTION BEADS STAYED ON TOP OF THE SOLUTION FOR ABOUT A MINUTE UNTIL, (B) THEY WERE SEEN DROPPING FURTHER AFTER 5 MINUTES, (C) SOLUTION HAS MINIMAL BEADS ON TOP OF THE SURFACE AND (D) AFTER 10 MINUTES ALL BEADS WHERE AT THE BOTTOM OF THE SOLUTION. 43
FIGURE 2.6: TGA CURVE FOR CB WITH 3 % NA-ALGINATE CONCENTRATION AFTER CURING FOR VARIOUS PERIODS..... 46
FIGURE 2.7: THE STUDY OF LOADING CAPACITY OF CB AND IDS IN THE PRESENCE OF FE (II) AT 120 MG/L AND PH 2.5. THREE MM BEAD DIAMETER OF BEADS WAS USED. 47
FIGURE 2.8: CHEMICAL REACTION THAT DESCRIBES MECHANISM OF FE (II) ADSORPTION BY IDS AND CB. 48
FIGURE 2.9: PH LEVELS IN SOLUTION DURING THE ADSORPTION OF FE (II) BY CB AND IDS. 49
FIGURE 2.10: (A) & (B) CB AND IDS STORED IN DISTILLED WATER; BEIJERINCK MEDIUM AND CACL2 SOLUTIONS. 50
FIGURE 3.1: THE FTIR SPECTRA OF (A) IDS BEFORE FE (II) ADSORPTION AND (B) AFTER FE (II) ADSORPTION. 63
FIGURE 3.2: FTIR SPECTRA OF CB (A) BEFORE FE (II) ADSORPTION AND (B) AFTER FE (II) ADSORPTION 64
FIGURE 3.3: SURFACE TOPOGRAPHY BY ESEM OF CB BEFORE ADSORPTION OF FE (II): (A) MAG =100 X, WD = 7.4 MM, 500 μM; (B) MAG = 200 X, WD = 6.5 MM, 400 μM; (C) MAG = 500 X, WD = 7.4 MM, 100 μM AND (D) MAG = 1000 X, 7.6 MM, 100 μM..... 66

FIGURE 3.4: SURFACE TOPOGRAPHY BY ESEM OF IDS BEFORE ADSORPTION OF FE (II): (A) MAG =100 X, WD = 6.8 MM, 500 μM ;(B) MAG = 500 X, WD = 6.8 MM, 100 μM; (C) MAG = 1000 X, WD = 6.8 MM, 100 μM AND (D) MAG = 2000 X, 6.8 MM, 50 μM. 67
FIGURE 3.5: SHOWS TGA CURVES OF CB WHEN VARIOUS CONCENTRATIONS OF NA-ALGINATE WERE USED. 68
FIGURE 3.6: THE POINT OF ZERO CHARGE (PHPZC) FOR BIOSORBENTS IDS AT PH 8.8 AND CB OBTAINED AT PH 9.3. 71
FIGURE 3.7 THE FE (II) ION UPTAKE AT DIFFERENT SURFACE PH OF CB. 72
FIGURE 3.8: REMOVAL FE (II) ION CONCENTRATION WITH TIME WHEN 1; 2; 3 AND 4 MM CB ARE USED. 73
FIGURE 3.9: REMOVAL OF FE (II) ION CONCENTRATION WITH TIME WHEN 1; 2; 3 AND 4 MM IDS ARE USED. 74
FIGURE 3.10: REMOVAL OF FE (II) ION CONCENTRATION IN THE PRESENCE OF BEADS WITH VARIOUS BIOMASS CONCENTRATIONS. 75
FIGURE 3.11: REMOVAL OF FE (II) ION CONCENTRATION IN THE PRESENCE OF BEADS WITH VARIOUS NA-ALGINATE CONCENTRATIONS. 77
FIGURE 3.12: THE REMOVAL OF FE (II) ION CONCENTRATION IN THE PRESENCE OF BEADS WITH VARIOUS CACL2 CONCENTRATIONS. 78
FIGURE 3.13: REMOVAL OF FE (II) ION CONCENTRATION IN THE PRESENCE OF CB AND IDS USING PARAMETERS OBSERVED TO BE BEST FOR METAL FE (II) ADSORPTION AND COMPARED TO THE DS PERFORMANCE. 80
FIGURE 4.1: SCHEMATIC REPRESENTATION OF SHRINKING CORE MODEL OF A SPHERICAL PARTICLE (NAIYA ET AL., 2009). 89
FIGURE 4.2: FE (II) ION CONCENTRATION IN SOLUTION WAS INCREASED FROM 5 – 1000 MG/L, THESE PLOTS SHOW THE LOADING CAPACITY OF IDS AT VARIOUS CONCENTRATIONS USED. 91
FIGURE 4.3: MAXIMUM AMOUNT OF FE (II) ADSORBED PER UNIT AMOUNT OF ABSORBENT AT VARIOUS INITIAL CONCENTRATIONS 92
FIGURE 4.4: EVOLUTION OF METAL ADSORPTION AT VARIOUS INITIAL CONCENTRATIONS. C0 = C∞ AND C~ = ... 94
FIGURE 4.5: SCHEME OF OCTAHEDRAL COORDINATION FORMED BY FE (II) ADSORPTION ON THE FUNCTION GROUPS FOUND IN IDS (ARYAL & LIAKOPOULOU-KRYRIAKIDES, 2013) 97
FIGURE 4.6: EVOLUTION OF METAL ADSORPTION AT VARIOUS INITIAL CONCENTRATIONS 98
FIGURE 4.7: SEPARATION FACTOR OF FE (II) IONS ADSORBED ON DIFFERENT BIOMASS 102

FIGURE 4.8: ADSORPTION OF FE (II) BY IMMOBILIZED ALGAL BEADS ON PSEUDO-FIRST-ORDER KINETIC MODEL 103
FIGURE 4.9: SORPTION OF FE (II) BY IMMOBILIZED ALGAL BEADS ON PSEUDO-SECOND-ORDER KINETIC MODEL 104
FIGURE 4.10: SCM PLOTS: (A) CB & (B) IDS WHEN USING FILM DIFFUSION CONTROL EQUATION. (C) CB & (D) IDS PARTICLE DIFFUSION CONTROL EQUATION. 106
FIGURE 5.1: SCHEMATIC DIAGRAM OF THE EXPERIMENTAL COLUMN, (1). FEED STORAGE (2); PERISTALTIC PUMP (3); ADSORPTION COLUMN AND ADSORPTION BED; (4). OUTLET LIQUID; (5) SAMPLE COLLECTION 113
FIGURE 5.2: A TYPICAL S-SHAPED BREAKTHROUGH CURVE 114
FIGURE 5.3: BREAKTHROUGH CURVES FOR FE (II) ADSORPTION BY CB BIOMASS AT, Z = 16 CM; CO = 120 MG/L AND Q = 22 ML/MIN. 118
FIGURE 5.4: BREAKTHROUGH CURVES FOR FE (II) ADSORPTION BY CB BIOMASS AT, Z = 29 CM; CO = 120 MG/L AND Q = 22 ML/MIN. 119
FIGURE 5.5: BREAKTHROUGH CURVES FOR FE (II) ADSORPTION BY CB BIOMASS AT, Z = 29 CM; CO = 120 MG/L AND Q = 4 ML/MIN. 121
FIGURE 5.6: BREAKTHROUGH CURVES FOR FE (II) ADSORPTION BY IDS BIOMASS AT, Z = 29 CM; CO = 120 MG/L AND Q = 4 ML/MIN. 122
FIGURE 5.7: BREAKTHROUGH CURVES FOR FE (II) ADSORPTION BY IDS BIOMASS AT, L = 82 CM; CO = 120 MG/L AND QO = 4 ML/MIN. 123
FIGURE 5.8: LINEAR PLOT OF THOMAS MODEL WITH EXPERIMENTAL DATA AT DIFFERENT BED HEIGHTS OF CB. Z = 16 AND 29 CM; CO = 120 MG/L AND Q = 22 ML/MIN. 127
FIGURE 5.9: LINEAR PLOT OF THOMAS MODEL WITH EXPERIMENTAL DATA AT FLOW RATES OF CB. Z = 29 CM; CO = 120 MG/L AND Q = 4 AND 22 ML/MIN. 128
FIGURE 5.10: LINEAR PLOT OF THOMAS MODEL WITH EXPERIMENTAL DATA AT DIFFERENT HEIGHTS OF IDS. Z = 29 CM AND 82 CM; CO = 120 MG/L AND Q = 4 ML/MIN. 129
FIGURE 5.11: LINEAR PLOT OF ADAM-BOHART MODEL WITH EXPERIMENTAL DATA AT DIFFERENT HEIGHTS OF CB. Z = 16 AND 29 CM; CO = 120 MG/L AND Q = 22 ML/MIN. 131
FIGURE 5.12: LINEAR PLOT OF ADAM-BOHART MODEL WITH EXPERIMENTAL DATA AT DIFFERENT FLOW RATES OF CB. Z = 29 CM; CO = 120 MG/L AND Q = 4 AND 22 ML/MIN. 131
FIGURE 5.13: LINEAR PLOT OF ADAM-BOHART MODEL WITH EXPERIMENTAL DATA AT DIFFERENT HEIGHTS OF IDS. Z = 29 AND 82 CM; CO = 120 MG/L AND Q = 4 ML/MIN. 132

LIST OF TABLES

TABLE 1.1: HEAVY METALS CONTAMINATING THE WEST (WB) AS FOUND BY DIALE ET. AL, (2011) .. 12

TABLE 1.2: THE CLASSIFICATION OF THE DESMODESMUS GENUS. 16

TABLE 2.1: PRIMER SEQUENCES USED FOR ALGAL IDENTIFICATION (DIALE ET AL., 2011). 42

TABLE 4.1: THE FTIR SPECTRAL CHARACTERISTICS OF IMMOBILIZED ALGAL BEADS BEFORE AND AFTER ADSORPTION OF FE (II) IONS 95

TABLE 4.2: LANGMUIR ISOTHERM AND FREUNDLICH ISOTHERM PARAMETERS 100

TABLE 4.3: THE PSEUDO-SECOND ORDER KINETIC CONSTANTS FOR BIOSORPTION OF FE (II) ON IMMOBILIZED ALGAL BEADS 105

TABLE 5.1: SUMMARY OF DIFFERENT PROCESS PARAMETERS OBTAINED FROM PACKED BED ADSORPTION FE (II). * T_E BREAKTHROUGH TIME WAS NOT OBTAINED. 123

TABLE 5.2: SUMMARY OF DIFFERENT PROCESS PARAMETERS OBTAINED FROM A PACKED BED COLUMN ADSORPTION OF FE (II) 125

TABLE 5.3: THOMAS MODEL PARAMETERS FOR THE ADSORPTION OF FE (II) ONTO CB AND IDS AT DIFFERENT CONDITIONS USING LINEAR REGRESSION ANALYSIS 129

TABLE 5.4: ADAM-BOHART PARAMETERS FOR THE ADSORPTION OF FE (II) ONTO CB AND IDS AT DIFFERENT CONDITIONS USING LINEAR REGRESSION ANALYSIS 131

CHAPTER 1

INTRODUCTION AND LITERATURE SURVEY

1.1 Introduction

1.1.1 Witwatersrand Basin

The Witwatersrand basin (WB) (mesoarchaean), is an underground geological formation found in an ancient crustal block called Kaapvaal Craton, in an arc of about 400 km across the Free State; North West and Gauteng provinces (Figure 1.1) (Riemer & Durrheim, 2011). It holds the world's largest known gold reserves and has produced over 1.5 billion ounces (over 40,000 metric tons) of gold, which represents about 50 % of all the gold ever mined on earth. Gold (Au) in this basin occurs as metamorphic terrains such as granite complexes (i.e. greenstone belts) and placers. Placers are deposits that have accumulated through weathering and mechanical concentration. When gold was discovered in 1886, its mining involved extracting gold-bearing and coarse-grained conglomerates from an approximately 7000 m thick sequence of sedimentary rocks of the Witwatersrand Supergroup (McCarthy, 2011). Au is found in association with uranium (U), quarts and pyrite in the basin. Since conglomerates are not uniformly gold-bearing and gold is present in only certain localized areas, a lot of the conglomerates are left unmined and stored as waste. The conglomerates in slimes or tailings dumps typically contain a high amount of pyrite. Their reaction with dissolved oxygen from rainwater forms sulphuric acid which further dissolves other heavy metals, a phenomenon called acid mine drainage (AMD). The dissolved heavy metals in water draining from the tailings dumps seep into nearby water streams. This is one form water bodies (e.g rivers, streams, lakes and ponds) around the mines get contaminated. Another form of water contamination caused by the WB mining occurs when mine operations ceases.

Typically when a mine is operational water is continuously pumped out of the cavities in the underground mining work to prevent flooding.

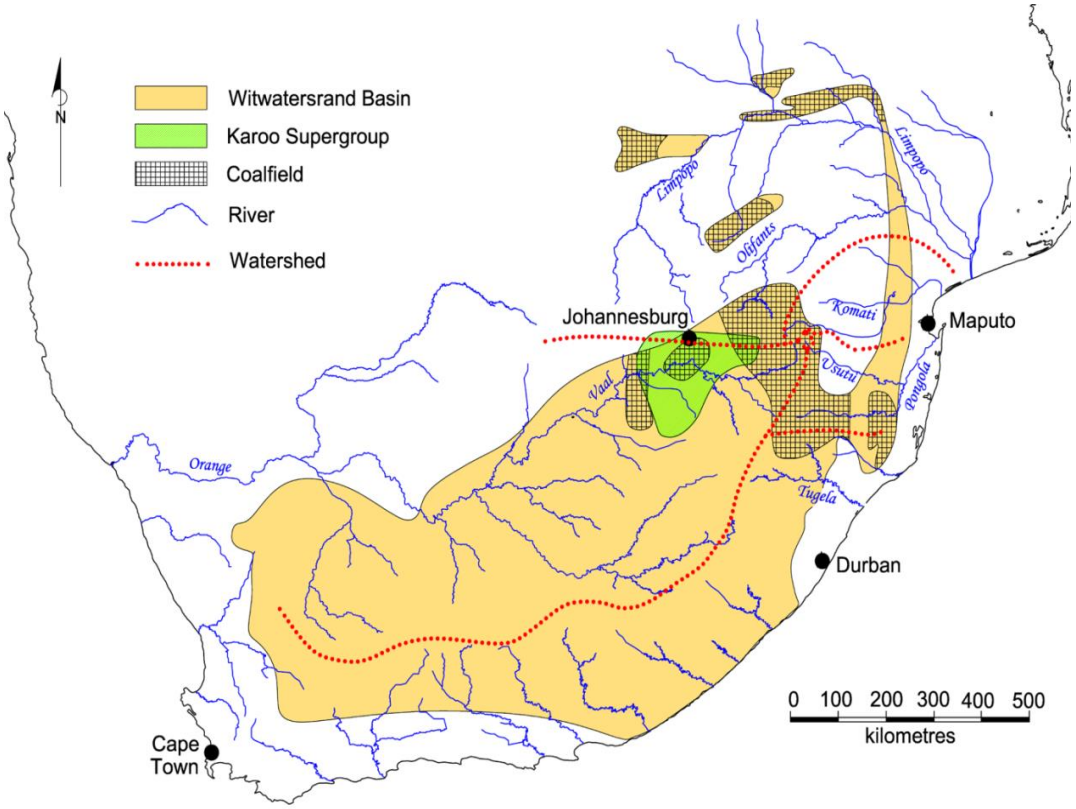


Figure 1.1: A geological map showing the Witwatersrand Basin and Karoo Supergroup, picture courtesy of McCarthy (2011)

However, when mine operations stop, so does the pumping of water, this causes mine voids to fill completely. Consequently, decants occur where water with toxic heavy metals and very low pH from underground reach the surface and contaminate surface water. The Western basin in Krugersdorp is currently decanting (started 2012) from an old shaft and partially treated and untreated AMD contaminated water is being released into a river called Tweelopiesspruit (Horak, 2012). The Central and Eastern Basins were forecasted to start decanting in 2013 and 2015, respectively. One method

to prevent or deal with decants is to keep underground water levels below an Environmental Critical Level (ECL). These levels were determined to be and measured by meter above mean sea level (m amsl). Western Basin: 1,550 m amsl; Central Basin 1,467 m amsl; and Eastern Basin: 1,280 m amsl (Horak, 2012). Remediation plans have been proposed in a form of immediate and short term interventions to treat mine water to a level that it can be discharged to the environment. Chemical treatment method in a form of lime neutralization has been chosen as the treatment method to be used for AMD water remediation in the Witwatersrand west basin, as briefly discussed below.

1.1.2 Lime treatment for AMD in the Witwatersrand Basin

Lime neutralization is one of the most widespread methods used to mitigate acidic effluents in AMD contaminated water bodies (Johnson & Hallberg, 2005). In South Africa, research on AMD treatment using limestone neutralization was been done by (Maree et al., 2013). Maree et al., 2013, found that limestone can be used for complete removal of iron (II) in an SBR system within 90 min reaction time with the estimated capital cost for the SBR process amounts to R3.5 m. per Mℓ/d. There are other remediation methods that can be used for treating AMD contaminated water and this is outlined in the sections to follow. They all, like lime neutralization fall short of not being cost effective. The principle of lime neutralisation lies in the insolubility of heavy metals in alkaline conditions (Aubé, 2006). Metals such as iron (Fe), zinc (Zn) and copper (Cu) are normally precipitated out at pH 9.5 and a higher pH is used (10.5 – 11) for metals such as nickel (Ni) and cadmium (Cd) (Aubé, 2006). Lime dissolution is the first step of the neutralisation process. Hydrated lime is used in large scale treatments to further increase pH in the system. Ferrous hydroxides are not as stable as ferric hydroxides when the sludge is exposed to acidic waters or natural

precipitation. For this reason, aeration is often applied to oxidise the iron to its more stable form, as per the following (reaction 1.1) (Aubé, 2006):

$$Fe(OH)_2 + \tfrac{1}{2} H_2O + \tfrac{1}{4} O_2 \Rightarrow Fe(OH)_3 \quad (1.1)$$

A common by-product of lime neutralisation is gypsum. Gypsum precipitation occurs as the AMD is often rich in sulphate and the calcium added from lime will bring the solubility product well above saturation. This reaction is often responsible for scaling in treatment processes, reaction (1.2) (Aubé, 2006).

$$Ca(OH)_2 + H_2SO_4 \Rightarrow CaSO_4 . 2H_2O \quad (1.2)$$

Another common by-product of lime neutralisation is calcium carbonate. The inorganic carbon for this reaction can either come from the AMD water or be a result of carbon dioxide from air, which is dissolved during aeration. The carbon dioxide converts to bicarbonate and then partially to carbonate. The carbonate fraction will precipitate with the high calcium content of the slurry to form calcite (calcium carbonate). This calcite can play an important role in the stability of the final sludge product as it provides neutralising potential to the sludge as it is stored. It is also an indicator of the process lime efficiency: more efficient neutralising processes will produce less calcite (reaction 1.3) (Aubé, 2006).

$$Ca(OH)_2 + CO_2 \Rightarrow CaCO_3 + H_2O \quad (1.3)$$

The overall aim of the immediate and short term interventions is to treat the mine water to a level that it can be discharged to the environment, with tolerable impacts on downstream water users. A combination of treatment technology and chemical reagent was recommended as a potential intervention for the treatment of the WB AMD, in the form of: (i) oxidation by aeration; (ii) pre-neutralisation with limestone and (iii) gypsum crystallization to remove excess sulphate from solution.

1.2 AMD treatment process as approved by government for Witwatersrand Basin clean-up

There are two main components to the proposed project. Firstly, an immediate intervention to neutralise acid water already decanting from the Western Basin at the current Rand Uranium treatment plant, and secondly, a short term intervention. Short term intervention will entail pumping water from the Western, Central and Eastern Basins to reduce and prevent surface decant so as to neutralise the water. A High Density Sludge (HDS) treatment plants (Figure 1.2) will be used to treat AMD contaminated water, before it is released into the environment.

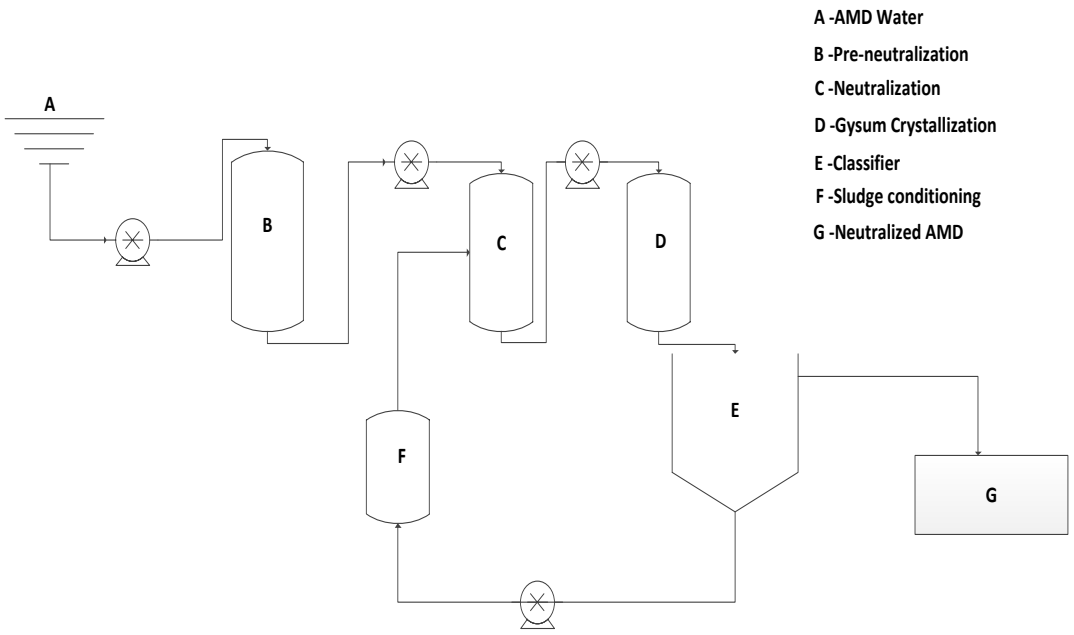


Figure 1.2: The proposed HDS process for the treatment of AMD for the immediate and short term interventions.

The HDS process is currently recognized as the method to be used for treating mine water containing high metal concentrations in the WB. A case study on active and passive treatment of mine water at the Wheal Jane Tin Mine in Cornwall, UK, uses the HDS treatment system as the preferred method for AMD water treatment (Coulton et al., 2003). HDS allows for the neutralisation of acidic waters, the removal of metals and a large proportion of the dissolved salts. A number of other processes are available, but the HDS process offers the ability of producing a relatively dense sludge. This enables the reduction of sludge volumes and assisting with the management and disposal of this sludge. The HDS process generally involves the following (Kostenbader & Haines, 1970):

i. Addition of an alkali, typically lime in the slaked lime or un-slaked lime form;
ii. Aeration to oxidise the iron and manganese;
iii. Neutralisation of the free and metal-related acidity;
iv. Precipitation of the metals in the hydroxide or carbonate form;
v. Solids separation and production of clear neutralised water; and
vi. Handling and disposal of waste sludge, which mainly contains metal hydroxides and gypsum.

The process shown in Figure 1.2, requires the oxidation of dissolved ferrous iron, Fe (II), and manganese in the AMD through aeration (Bosman, 1974). The oxygen is introduced by mechanical aeration equipment. If this stage does not occur the Fe (II) will not be oxidised prior to the introduction of an alkali (Bosman, 1974) (Murdoch et al., 1995). The next stage of the process is pre-neutralisation with limestone ($CaCO_3$) to increase the pH before the neutralisation stage. During neutralisation, lime produced by the slacking of quicklime will be used (TCTA, 2012). Unslaked quicklime has to be slaked (Ca $(OH)_2$) or hydrated prior to application. Through the neutralisation of the AMD, the pH is adjusted to a level which facilitates the formation of metal precipitates. By elevating the pH, the process facilitates the precipitation of sulphate as gypsum ($CaSO_4$) (TCTA, 2012). The precipitated gypsum sludge is recycled to seed and enhance the further precipitation of gypsum on sludge seed particles and, thus increasing the removal efficiency. After neutralisation the water will flow into a clarifier where sufficient reaction time will be allowed to provide the slow growing metal hydroxide and gypsum crystals time to form and grow. This creates a dense sludge (TCTA, 2012). The treated and neutralised water resulting from the process is then discharged into the streams. Although the proposed project will treat the AMD water to a level where it will no longer be acidic and where most of the dissolved salts

and the heavy metals have been removed, it will still not be suitable for human consumption. The discharge of the water into public streams will affect water quality downstream.

The cost of using HDS has previously been found to preclude their use on a large scale for this type of application (TCTA, 2012). The major short-comings of the proposed method of remediating AMD water in the WB is that:

i. It is expensive and the construction takes time and something needed to be done as a matter of urgency.
ii. Sludge produced by HDS process is toxic and hazardous, means of handling and disposal will need to be special and will be costly.

The proposed method for treating AMD water in the WB can remediate water to a level where it will no longer be acidic and where some of the dissolved salts and heavy metals are removed. The method will however not be able to treat water to a level suitable for human consumption and irrigation (TCTA, 2012). Consequently, the discharge of this low quality water into public water streams pose a significantly risk of heavy metal accumulation downstream. There is a possibility of treating water further from the HDS process before it is discharged in public water streams. The use of HDS must be viewed as the first step of a long term treatment solution to the AMD problem in the WB (TCTA, 2012). Long term solutions need to be sort and incorporated to the proposed short term intervention plan. While conventional AMD treatment processes such as HDS prove to be necessary, they are however expensive and not efficient. There is an over-arching need therefore for auxiliary process methods to improve efficiency in heavy metal removal. The use of techniques such

as algal based heavy metal removal process can be beneficial in enhancing the efficiency of the proposed HDS method for AMD water treatment in the WB.

During the last three decades, treatment of AMD using technologies such as algal based process have been developed as an alternative to conventional method of remediating AMD water (Das et al., 2008). Biosorption could be an alternative method for treating AMD water to conventional method such as HDS, which uses chemical precipitation as the mode of heavy metal removal. The specific interest on algal-based bioremediation processes is based on their proven prominent sorption capacity for heavy metals in liquid effluents (Ahemad & Kibret, 2013). The present study will investigate the use of green microalgae called *Desmodesmus sp.* as an adsorbent of heavy metal constituents from AMD water, with a specific focus on Fe (II) removal. Immobilization of the green microalgae will be the core of the research. Immobilization is thought to enhance the adsorption capabilities of the green microalgae. Packed bed adsorption units are the most favourable as a practical wastewater treatment process when algae are used (Das et al., 2008). Immobilized green microalgae cells will be produced and studied for heavy metal removal efficacy both in batch and continuous flow systems. Remediation efforts are most effective when the source or cause of contamination is well understood and the following section will describe process of AMD formation.

1.3 AMD contamination in the West Witwatersrand Basin

1.3.1 AMD chemistry

FeS_2 (pyrite) is responsible for acid mine drainage formation. When pyrite is exposed to oxygen and water it oxidizes resulting in hydrogen ion release, acidity, sulfate ions and soluble metal cations (reaction (1.1 – 1.4)) (Johnson & Hallberg, 2003). Mining increases the exposed surface area of sulfur-bearing rocks allowing for excess acid generation beyond the water's natural buffering capabilities.

$$FeS_2 + 3\ O_2 + 2\ H_2O \rightarrow FeSO_4 + H_2SO_4 \quad (1.1)$$

$$4\ Fe^{2+} + O_2 + 4\ H+ \rightarrow 4\ Fe^{3+} + 2\ H_2O \quad (1.2)$$

$$4\ Fe^{3+} + 12\ H_2O \rightarrow 4\ Fe(OH)_3\ (s) + 12\ H^+ \quad (1.3)$$

$$FeS_2\ (s) + 14\ Fe^{3+} + 8\ H_2O \rightarrow 15\ Fe^{2+} + 2\ SO_4^{2-} + 16\ H^+ \quad (1.4)$$

Further oxidation of Fe^{2+} (ferrous iron) to Fe^{3+} (ferric iron) occurs when sufficient oxygen is dissolved in the water or when the water is exposed to sufficient atmospheric oxygen (Costello, 2003). Ferric iron can either precipitate as ochre ($Fe(OH)_3$ the red-orange precipitate seen in waters affected by acid mine drainage or it can react directly with pyrite to produce more ferrous iron and acidity (Costello, 2003).

When the water bodies are sufficiently acidic, acidophilic bacteria - bacteria that thrive in low pH - are able to establish themselves. Microorganisms can play a significant role in accelerating the chemical reactions taking place in mine drainage situations (Kuhn, 2005). *Thiobacillus Ferroxidans*, a bacteria, is commonly found in AMD contaminated water bodies (Prescott et al., 1999) (Costello et. al, 2003).

These bacteria catalyze the oxidation of ferrous iron, further perpetuating AMD formation.

AMD contamination in the west (WB) has been documented by Diale et. al, (2011c) where certain water bodies were sampled and analyzed (Table 1.1).

Table 1.1: Heavy metals contaminating the west (WB) as found by Diale et. al, (2011c)

Sampled sites	pH	Fe (mg/L)	Mn (mg/L)	Co (mg/L)	Ni (mg/L)	U (mg/L)
Hippo Dam	3.98	28.79	68.27	0.58	1.83	> 0.001
Aviary Dam	3.1	4.57	48.59	0.4589	1.02	0.001
Robinsons Lake	2.4	115	121.14	8.78	26.50	2.02
Donaldons Dam	6.84	0.02	0.50	0.015	0.06	0.02
Tarlton River	2.8	77.96	58.35	0.44	1.04	0.014

Major contamination was observed in Robinsons Lake and Tarlton River. Robinsons Lake had Fe exceeding SANS 241:2006 standards by about 576 times. Other heavy metals such as Mn, Co and Ni exceeded the regulated limits by 1211, 18 and 177 times, respectively. The levels of pH were extremely low in these water bodies, 2.4 and 2.8 for Robinsons Lake and Tarlton River, respectively. Chromium was also found in the water samples; however it was within regulated limits. The site sampling data / results gave a context on which heavy metals, metal concentrations and pH levels should be focused on when studying possible remediating methods.

1.3.2 Other techniques for heavy metal removal from water bodies

Different methods can be used to treat water bodies contaminated by AMD. The most common techniques are: addition of chemicals, reverse osmosis, electro dialysis, oxidation-reduction, activated carbon adsorption and solvent extraction. The use of these methods for heavy metal removal is often expensive and tend to generate toxic chemical sludge. There is a need therefore to develop not only cost-effective, but sustainable remediation processes.

(a) Reverse osmosis

Filtration techniques used for AMD treatment can be classified into four groups: reverse osmosis (RO); nanofiltration; ultrafiltration and microfiltration (Amjad, 1998). When using RO, a solution is normally pressured through a semi-permeable membrane. The semi-permeable membrane allows pure solvents to pass through the membrane, leaving the solute in the entering site. The membrane separation occurs due to the presence of a dense barrier layer in the polymer matrix. The major drawback of RO is the high power consumption due to the pumping pressures, and the restoration of the membranes (Fu & Wang, 2011).

(b) Electro dialysis

The electro dialysis (ED) process uses electrical potential to influence the transportation of the ions of a solution through a semi-permeable membrane (Applegate, 1984) (Schoeman, 1985) (Valero et al., 2010). The membrane can be, anion- or cation-selective which means that only positive or negative ions can pass through. The idea of the cation-selective membrane is that it only allows positively charged ions to flow through and the negatively charged ones are rejected. This can happen because the membrane is built up of negatively charged matter,

polyelectrolytes responsible for the rejection (Applegate, 1984). Several membranes can be placed in a row to allow negative or positive ions to pass through thus enabling comparatively easy separation of ions from wastewater. If a particle has no charge, it will also pass through the membrane. The constructing material of anion-selective membranes is polystyrene with quaternary Ammonium and for cation-selective membranes consist of sulphonated polystyrene (Applegate, 1984). If a solution has large particles, it can plug the pores of the membrane. This technique is also rather cost intensive, like the RO described previously.

(c) Oxidation-reduction

The oxidation-reduction is partially catalytic and an electrochemical mechanism. This technology is widely used for the removal of cadmium, arsenic, lead, nickel, copper, mercury, chromium, antimony and cobalt ions from water bodies (Réka, 2014). This process is limited therefore for removing Fe. The efficiency rate of this method can be as high as 98%, however it is cost intensive.

(d) Activated carbon adsorption

Active carbon is used as a solid to remove soluble substances from a solution during activated carbon adsorption process. Active carbon does have a big internal surface of 500-1500 m^2/g necessary to achieve adsorption (Pohan, 2010) (Henning & Kienle, 2012). During the activated carbon adsorption process the water is pumped though a column containing active carbon and leaves the column across the draining system (AD Guide, 2001). The nature of the substances in the water and the temperature are factors affecting the activity of the active carbon column. While the water runs through the column, the substances can accumulate in the filter. This used filter can be regenerated and in case of granular carbon, the

organic matter can be oxidized. Synthetic adsorbents such as these are costly to prepare and subsequently their use.

1.4 Green microalgae (*Desmodesmus sp*.)

1.4.1 Taxonomy

'Algae' is a name given to an organisms of diverse groups of oxygenic, phototrophic and eukaryotic microorganisms (Graham & Wilcox, 2000). Algae are differentiated from bacteria and photosynthetic cynobacteria by having a nucleus and they are referred to as eukaryotic. Features such as cell structure, biochemistry, molecular (amino acid and nucleic acid) sequences and molecular architectural data can be used to identify and differentiate algae species (Graham & Wilcox, 2000). Algae are widely present in freshwater environments, such as lakes and rivers, where they are typically present as microorganisms and visible only with the aid of a light microscope. Figure 1.3 shows a simplified taxonomy of algae.

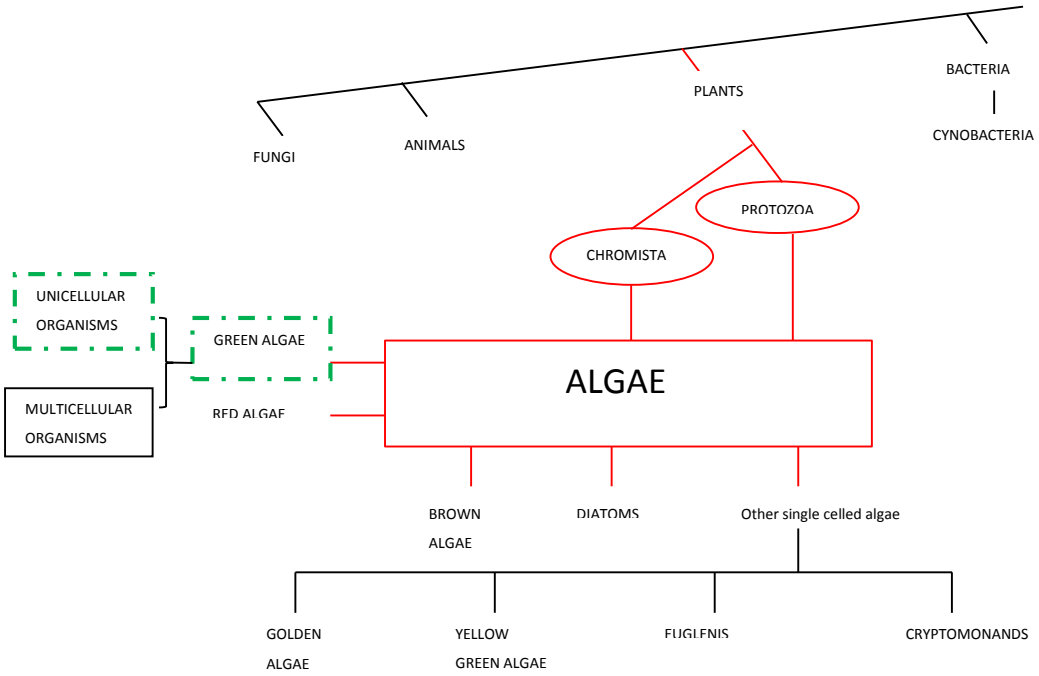


Figure 1.3: A simplified illustration of taxonomy of algae in the environment. Illustration adapted from Fundamental of environmental measurements: (http://www.fondriest.com/environmental-measurements/parameters/water-quality/algae-phytoplankton-chlorophyll/)

Although relatively inconspicuous, they have a major importance in the freshwater environment, both in terms of fundamental ecology and in relation to human use of natural resources (Bellinger & Sigee, 2010). Green microalgae are classified as charophyta. *Charophyta* also written as *Charaphyceae* and *Characeae* are ancient monophyletic group with conserved features (Caisová & Gąbka, 2009). Green microalgae found in freshwater form part of the base of aquatic food chain. Green microalgae contribute to major roles such as: (i) climate control, (ii) oxygen supply and (iii) food production. In addition to oceanic and freshwater environments, some algae have adapted to extreme habitats such as hot springs, brine lakes, acidic lakes and AMD contaminated water. It is this factor that has made green microalgae to be earmarked as a possible mode of water quality control in AMD contaminated water. *Desmodesmus* is classified in Table 1.2. *Desmodesmus* has been found in freshwater contaminated by AMD (Diale et al., 2011b). This therefore, proves this strain of algae can adapt to change in aquatic environment, especially when water has a low pH and is contaminated by toxic heavy metals. It is based on this fact that this particular species of algae will be used in this study. The aim is to study the efficacy of *Desmodesmus sp.* heavy metal removal process for remediating water stream contaminated by WB AMD.

Table 1.2: The classification of the Desmodesmus genus.

Scientific classification	
Domain	Eukaryota
Kingdom	Viridiplantae
Phylum	Chlorophyta
Class	Chloropyceace
Order	Sphaeropleales

1.4.2 Morphology

Desmodesmus sp. (DS) are green photosynthetic unicellular organisms. Their green pigment is due to the presence of chlorophyll, which is found in the chloroplasts of green plants. Porphyrin rings that are co-ordinated to the central atom form the main structure of the chlorophyll molecule (May, 2008). The *Scenedesmaceae* family has two subegnii: (i) *Scenedesmus* and (ii) *Desmodesmus* (Réka, 2014). These colonies are generally 2-, 4-, or 8-celled but rarely 16-, 32-celled ones also can occur and the cells are often lying parallel to each other and joined laterally Figure 1.4.

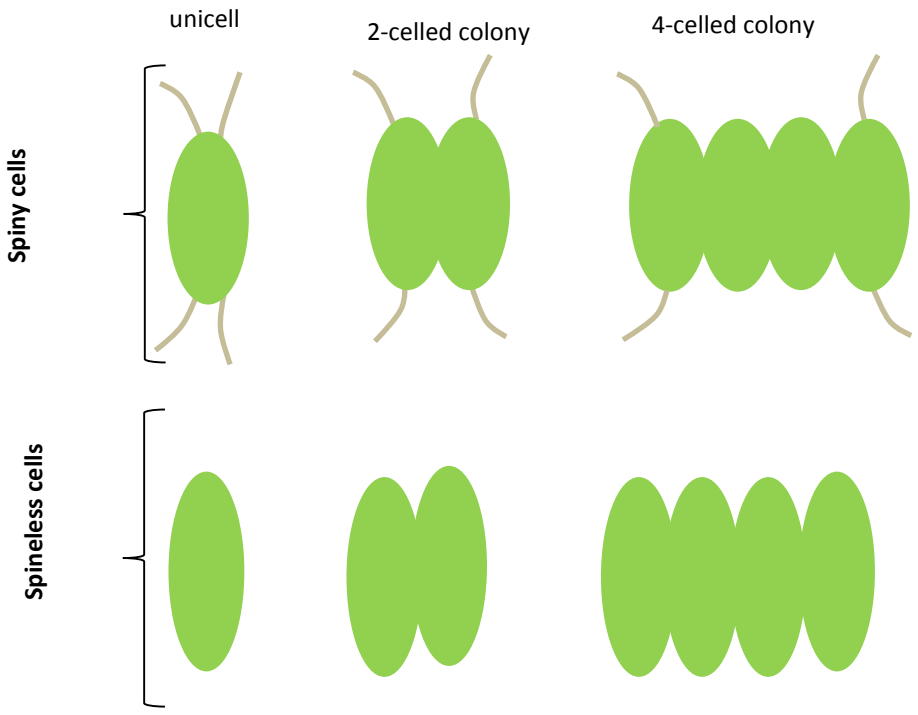


Figure 1.4: Types of unicells and colonies formed by *Desmodesmus sp.*

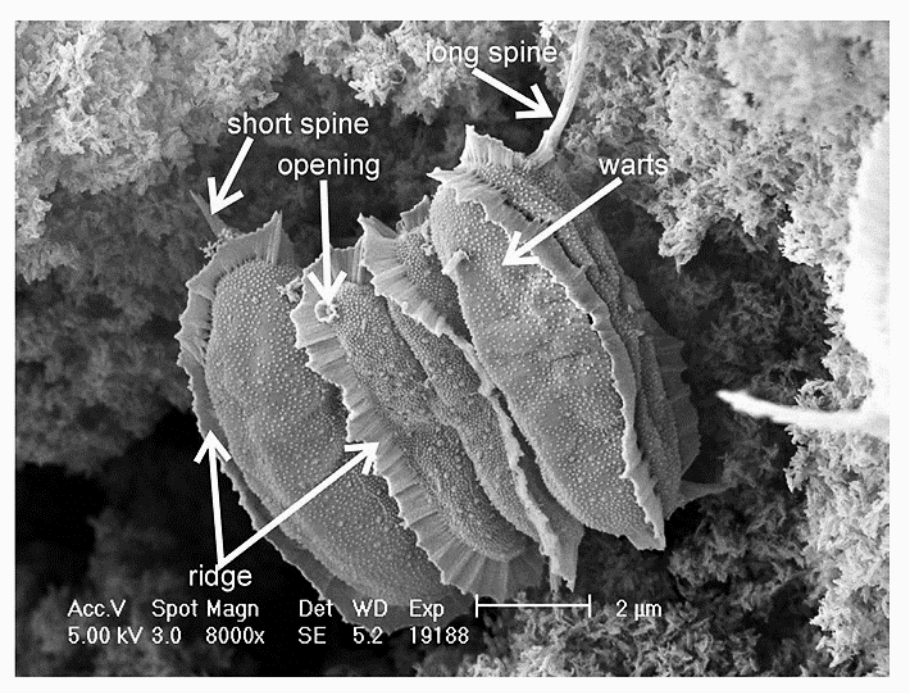


Figure 1.5: SEM of outer wall of *Desmodesmus* illustrating ultrastructural features such as a short spine, long spine, warts, ridge and opening (Shubert et al., 2014).

The cell wall of DS is toothed or spiny, granular and there are ribs and / or wart-like projections (Figure 1.5). The chloroplast of DS is parietal with a single pyrenoid. Shubert et al. (2014) reported that during the reproduction of DS auto spores are released by the fracture of the lateral cell wall as an asexual mechanism. DS has the ability to change its form as a response to the changing environmental conditions, thus exhibiting phenotypic plasticity. Depending on the changing environmental conditions the DS can have different morphs, as shown in Figure 1.4. The most resistant form of DS is the colonies but the single cells (unicells) are also common. The unicell can occur also spineless. By increasing the phosphorus or nitrogen concentration, the morphological variation can be triggered (Shubert et al., 2014). When the DS is isolated and grown in culture media free of other organisms with enough nutrients, clonal culture is formed by the unicells (Shubert et al., 2014).

In algal systematics, the taxonomy of *Scenedesmus* and *Desmodesmus* genera has been the centre of debate as there are hardly clear diagnostic phenotypic features that differentiate between them (Wozniak et al. (2008). The *Scenedesmus* genus was originally described as freshwater, non-motile green-alga by (Meyen, 1829). This description outlined the colony-forming habit of that genus and indicated the possibility of presence of spiny and non-spiny morphological forms. For a long period, this was largely accepted until Trainor et al. (1976) proposed that spiny and non-spiny forms were in fact two distinct genera according to their different phenotypic and physiological characters. Additionally, An et al. (1999) used ITS-2 region as a molecular marker that supported the separation of *Desmodesmus* genus, as a spiny taxon. Most of the DS were found to have one or several spines on the cells (Hegewald & Hanagata, 2000) (Johnson et al., 2007) whereas those of *Scenedesmus* genus were regarded as non-spiny. Another characteristic feature of *Desmodesmus* genus is the presence of cell wall layers with ornamentations formed by the outermost layer often visible under the light microscope as granulations (Hegewald & Deason, 1989) (An et al., 1999). Based on those characteristic features as well as phylogenetics based on 18S and ITS-2 rDNA, *Desmodesmus* genus was given the taxonomic rank of a genus (Kessler et al., 1997) (An et al., 1999) (Van Hannen et al., 2002). A morphological overlap between *Desmodesmus* and *Scenedesmus* gena can cause a lot of identification problems. Recently, Wozniak et al. (2008) suggested that several methodologies should be combined to provide a holistic understanding of *Desmodesmus* and *Scenedesmus* taxa. Figure 1.6 shows morphological similarities of *Desmodesmus* and *Scenedesmus* species. Identification based solely on morphology can lead to mischaracterization of microalgae taxa that share common morphological features and the extreme plasticity of morphological characters can certainly lead to erroneous interpretations (Trainor et al., 1990) (Kessler et al., 1997) (Trainor, 1998).

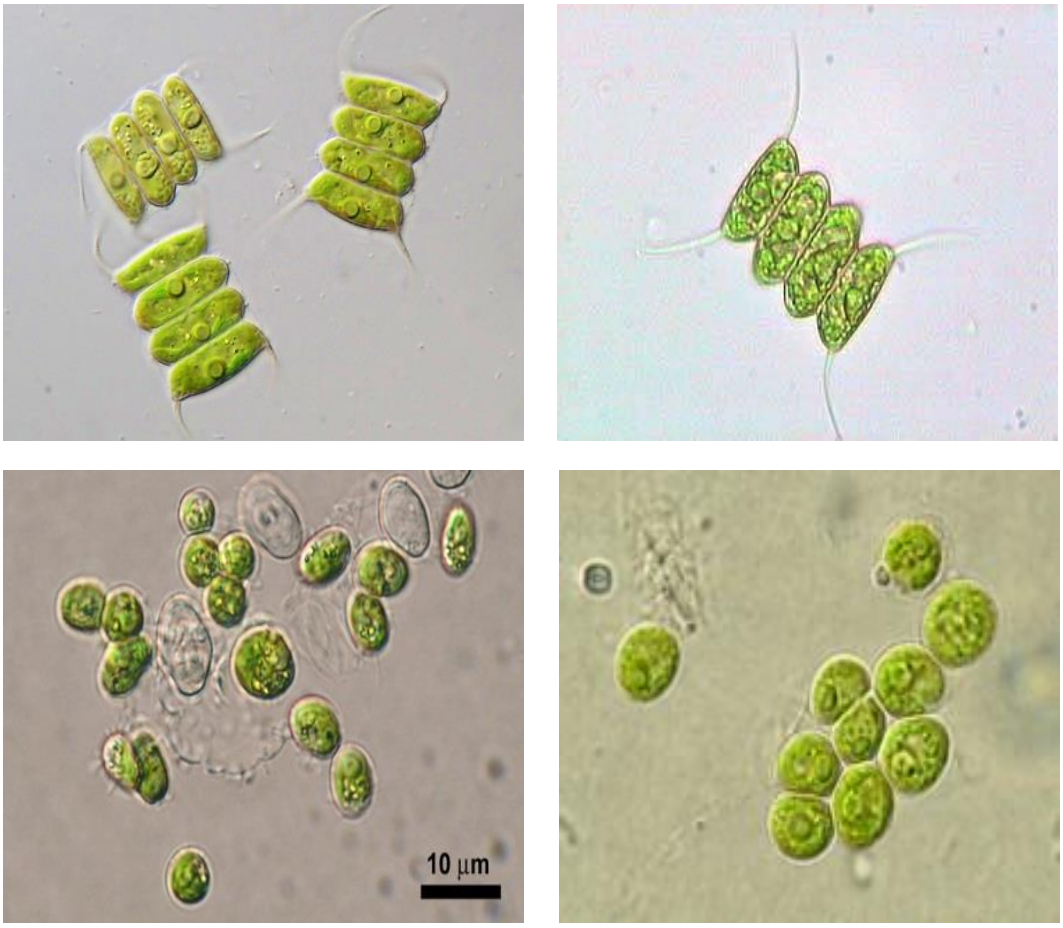


Figure 1.6: Diagnostic phenotypic features are hard to differentiate for Desmodesmus (D) and Scenedesmus (S) genus and shown (a) Desmodesmus communi (D); (b) Scenedesmus quadricauda (S); (c) Desmodesmus subspicatus (D) and (d) Scenedesmus rubescens (S).

Despite the ubiquity of these gena worldwide and its biotechnological potentials in heavy metal biosorption (Monterio et al., 2010), literature lacks a thorough record of its use for AMD water treatment.

1.5 Growth kinetics

Microalgae cells division's rate of proliferation largely depends on the availability of nutrients, light and carbon dioxide (Kativu et al., 2011). Alberts et al. (2002) defined factors that promote organism growth into three major classes:

i. Mitogens: which stimulate cell division, primarily by relieving intracellular negative controls that otherwise block progress through the cell cycle.

ii. Growth factors: which stimulate cell growth (an increase in cell mass) by promoting the synthesis of proteins and other macromolecules and by inhibiting their degradation.

iii. Survival factors: which promote cell survival by suppressing apoptosis.

Populations of organisms is said to be growing when there is an increase in a number of organisms by replication; synthesis and a new organized structure is produced (Becker, 1994). The growth of microorganisms such as DS can be measured by cell concentration or cell mass / density. Cell concentration refers to the number of individual cells per unit volume and cell mass / density refers to weight of cells or biomass per unit volume (Becker, 1994). Growth is measured as cell density versus the incubation time. Rate of growth is characterized by several different phases as illustrated in Figure 1.7.

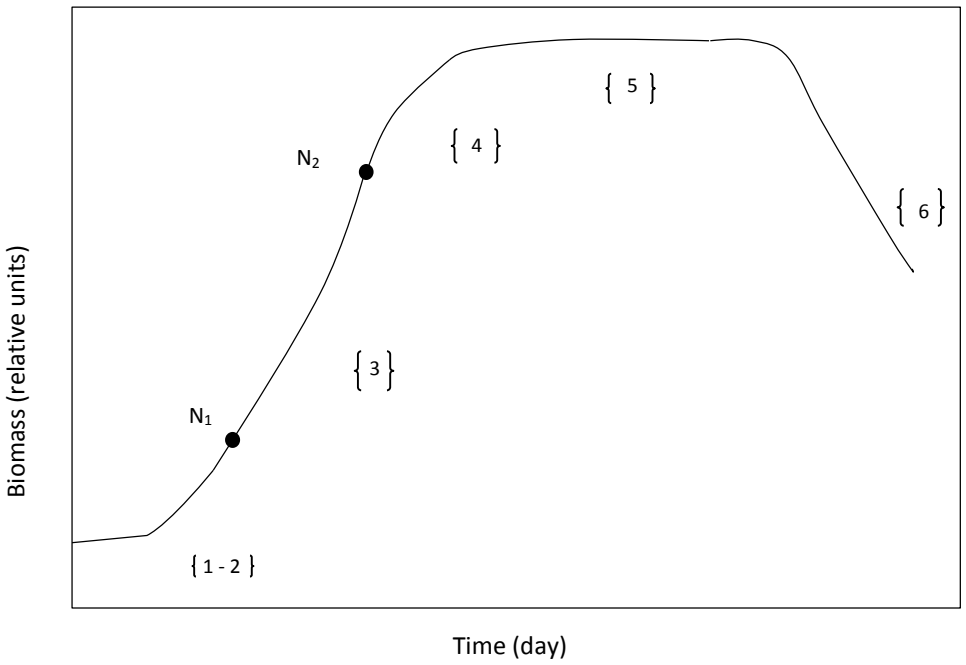


Figure 1.7: Illustrates an ideal shape of the respective growth phases of microalgae in media.

The individual phases are not always clearly pronounced and the growth curve can be different depending on the conditions of the culture (Becker, 1994). The phases that describe reaction of microalgae population in the homogenous batch culture are:

1 – 2: Represent the lag phase and accelerating growth phase.

3: Exponential growth (log).

4: Decreasing log growth (linear growth).

5: Stationary phase.

6: Accelerated death (log death).

Once the growth phase has been plotted, careful determination of the exponential phase of growth is needed. Two points, N_1 and N_2, at the extremes of this linear

phase are taken and substituted into the equation 1.4 to determine the alga specific growth rate.

Growth rate → $K' = Ln (N_2 / N_1) / (t_2 - t_1)$ (1.4)

Where Ln = natural logarithm, N_1 and N_2 = biomass at time1 (t_1) and time2 (t_2) respectively; Levasseur et al. (1993). Divisions per day and the generation or doubling time can also be calculated once the specific growth rate is known using equations 1.5 and 1.6, respectively.

Divisions per day → $Div.day^{-1} = K' / Ln^2$ (1.5)

Generation time → $Gen't = 1 / Div.day^{-1}$ (1.6)

1.6 Immobilization of microalgae cells

Brena et al., (2013) described the term immobilized enzymes and cells as physical confinement or localization in a certain defined region of space with retention of their catalytic activities, and which can be used repeatedly and continuously. Besides the industrial process applications, the immobilization techniques are the basis for making a number of biotechnological products with applications in diagnostics, bio-affinity chromatography and biosensors (Guisán, 2006). The major components of an immobilized cell system are: i) the cell; ii) the matrix and iii) the mode of attachment (Zacheus et al., 2000). The cells can be attached to the support by interactions ranging from reversible physical adsorption and ionic

linkages to stable covalent bonds. The covalent reactions commonly employed give rise to binding through amide, ether, thio-ether, or carbonate bonds (Guisán, 2006). As a consequence of cell immobilization, some properties such as catalytic activity or thermal stability become altered. These effects have been demonstrated and exploited. The concept of stabilization has been an important driving force for immobilizing cells. Stabilization at the molecular level has been widely demonstrated, an example is proteins immobilized through multipoint covalent binding.

1.6.1 Types of immobilization matrix and choice of usage

There are four principal methods available for immobilising enzyme adsorption: (i) covalent binding; (ii) entrapment; (iii) microencapsulation and (iv) cross linking (Guisán, 2006) (Figure 1.8).

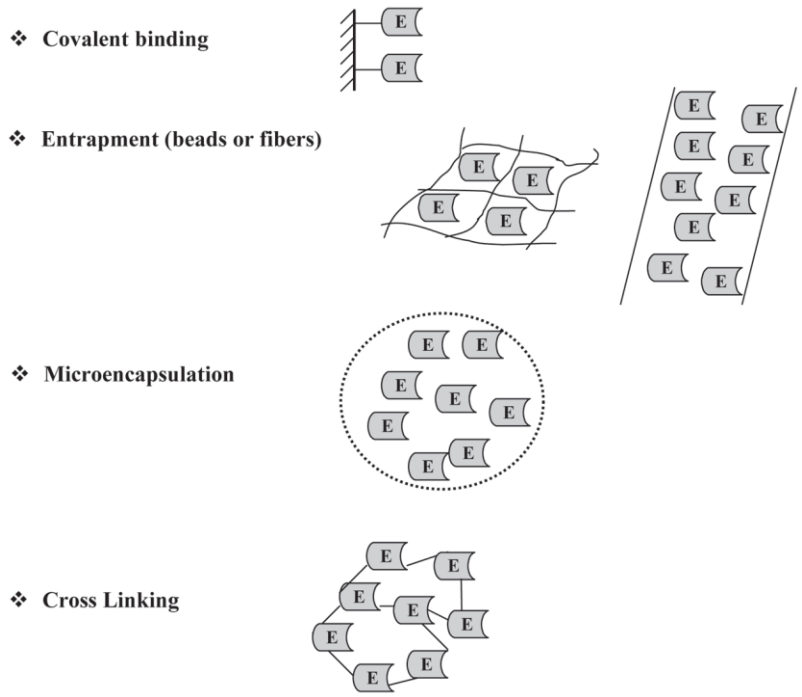


Figure 1.8: Immobilization systems: covalent attachment to an insoluble particle; entrapment within an insoluble particle by a cross-linked polymer; confinement within a semipermeable membrane; and cross-linkage (Guisán, 2006).

Carrier matrices immobilization selection is one of the crucial decisions to be made in the course of preparing for immobilization process (Zacheus et al., 2000). Some of the important aspects to be considered are: relevance to their use in industrial processes; cost effectiveness in relation to the overall process costs; and ideally they should be cheap enough to discard. An ideal support is cheap, inert, physically strong and stable (Guisán, 2006). A substantial saving in costs occurs where the carrier may be regenerated after the useful lifetime of the immobilized cells. The form, shape, density, porosity, pore size distribution, operational stability and particle size distribution of the supporting matrix will influence the reactor configuration in which the immobilized cells may be used (Guisán, 2006).

The particular choice of adsorbent depends principally upon minimizing leakage of the cells during use. Although the physical links between the cells and the support are often very strong, they may be reduced by many factors including the introduction of the substrate. Care must be taken that the binding forces are not

weakened during use by inappropriate changes in pH or ionic strength (Chaplin & Burke, 1990). Ion-exchange matrices, although more expensive than these other supports, may be used economically due to the ease with which they may be regenerated when their bound cells has come to the end of its active life (Guisán, 2006).

1.6.2 Natural polysaccharides as an entrapment support

Gel entrapment in natural polysaccharide matrixes is the most widely used immobilization technique for microorganisms (and microalgae in particular). Among them, carrageenan, agar and alginate are the most employed. Carrageenan is a collective term for polysaccharides prepared by water alkaline extraction from some Rhodophyceae (red algae), overall from the families of Gigartinacieae and Solieriaceae. Carrageenan consists of alternating 3-linked-β-D-galactopyranose and 4-linked-α-D-galactopiranose units. It precipitates as a gel in the presence of cationic compounds: metal ions, amines, amino acid derivates and water-miscible organic solvents (Tosa et al., 1979). Different isomeric forms of carrageenan can be found, in function of the algal specific origin. For instance, i, j and k-carrageenan are primarily produced by *Aghardhiella subulata* and the gametophyte and tetrasporophyte of *Chondrus crispus*, respectively (Burdin & Bird, 1994). Hardening processes in order to increase the mechanical stability of carrageenan-based matrixes have a major advantage of alginate gel entrapment in that immobilized cells do not suffer extreme physical–chemical condition changes during the immobilization process. Alginates are used in industry as viscosifiers, stabilizers and gel-formers, film-formers or water-binding agents (Ertesva˚g & Valla, 1998). The polymer is soluble in cold water and forms thermostable gels. Gelation of monovalent salts of this polysaccharide (i.e. Na-alginate) dissolved in water occurs when droplets of a mixture of cells (or enzymes) and alginate monovalent salts are mixed with a solution containing

gel-forming ions. Gel formation is a very quick process and the most common cation used to form alginate gels is Ca^{2+}. Figure 1.9, illustrates gel formation using Na-alginate and Ca^{2+} solution.

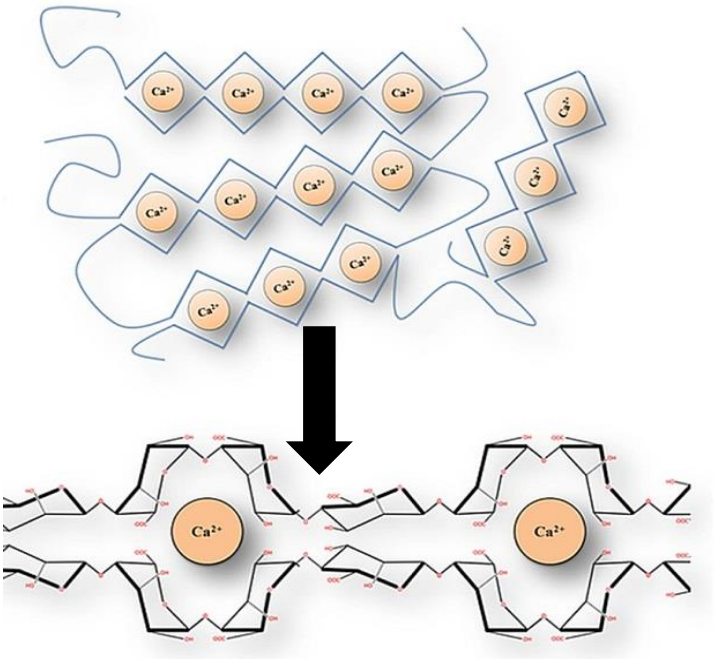


Figure 1.9: Linear block polymers of β-d-mannuronate (M) and -l-guluronate (G) with a variation in composition and sequential arrangements being cross-linked by Ca^{2+} ions to form calcium alginate matrix.

Calcium cations responsible for cross-linking Na-alginate polymers can be sequestered by soluble anions or can be substituted in the matrix by monovalent and can destabilize the structure. When the immobilization techniques is applied, immobilized microalgae cells show, as minimum, a longer lag period when these are compared with free cells (Vı´lchez et al., 1997) (Mallick, 2002). Some authors consider this similar to that occurring in free cultures (Lukavsky et al., 1986). After this period the specific growth rate (k) can be very similar in free and immobilized cells (Lau et al., 1998) (Mallick, 2002) although some reports confirmed that it is lower than in the latter case: Pane et al. (1998) reported a lag-phase of 5 – 6 days for immobilized *T. suecica* in Ca-alginate beads. It is common to find higher

chlorophyll production in immobilized cells (Lau et al., 1998) (Pane et al., 1998) (Robinson et al., 1986). This is a phenomenon that should be taken into account when estimations of biomass by chlorophyll are intended to be done. Hertzberg and Jensen (1989) demonstrated that the maximum amount of cells in culture could be higher for immobilized algae (*P. tricornutum*, in this case) than for free cells. The type of alginate and, overall, the initial cellular concentration seems to be very important in maximum cellular density that can be reached in immobilized cultures: the higher initial cellular density, the higher final cellular density to be reached in cultures. The latter phenomenon can be explained because growing cells inside the immobilizing matrix tend to form colonies. Maximum number of cells per colony must be limited by some factors as nutrient diffusion or light (colonies are smaller in the inner part of the beads than in the surface). Thus, the higher number of colonies, the higher number of cells in the culture. The most widely used method for microalgae immobilization using Ca-alginate matrix is the dripping method. This method entails making individual droplets using a nozzle. The size of the droplets is determined by its weight and surface tension, as well as the nozzle perimeter.

1.7 Heavy metal biosorption by *Desmodesmus sp.*

Biomass (Spinti et al., 1995) and especially macro- (Valdman et al., 2001) (Al-Rub et al., 2004) and microalgae are known to accumulate high amounts of metal from their environment (Stark & Rayson, 2000) (Travieso et al., 2002). This capacity has been exploited for different purposes (Greene & Bedell, 1990) (Burdin & Bird, 1994) (Aksu & Ac¸ikel, 1999) (Hashim et al., 2000). Silica immobilized-algal biomass (*Pilayella littoralis*) has been proposed to be used as a biosorbent for metal pre-concentration before measuring in analytical devices (inductively coupled plasma optical emission spectrometry) (Carrilho et al., 2003). The main purpose of the use of immobilizing algae binding metals has been detoxification and metal

recovery (Greene & Bedell, 1990). The latter is possible because a great part of the metal bound to cellular surfaces and immobilizing systems is able to be desorbed via acid treatment. Other resins, such as Amberlite, have been used in order to immobilize microorganisms set aside for metal removal (Baytak & Tu¨rker, 2005). Sorption of metals on microalgae seems to be not only a simple adsorption process, but also an exchange of ions, where Ca^{2+} is often replaced (Crist et al., 1994).

Binding of metals to algal surface occurs in living and non-living algae (Greene & Bedell, 1990), cell surface area being a major parameter in the binding of metals by microalgae (Khoshmanesh et al., 1997). Dead cells can be very efficient in accumulating metals (Do¨nmez et al., 1999). Blanco et al. (1999) used biomass of the cyanobacterium *P. laminosum* immobilized in polysulphone and epoxy resin beads for Cu (II), Fe (II), Ni (II) and Zn (II) sequestering. They found that the amount of biosorbed metal increased with biomass and the amount of metal available. Biosorption–desorption (acid-mediated) cycles with this immobilized system maintain the efficiency after at least 10 cycles. Copper is selectively adsorbed by alginates (Jang et al., 1995a) (Jang et al., 1995 b, c) (Nestle & Kimmich, 1996) (Alhakawati & Banks, 2004).

Microalgae such as DS have been found to be efficient is adsorbing toxic heavy metals at low concentrations (Réka, 2014) (Chekroun & Baghour, 2013). No sufficient evidence exist however that its performance can be proficient when adsorbing heavy metals at high concentration levels. DS is non-acidophilic and its ability to thrive in harsh environments such as pH < 2 and concentration above 100 mg / L will give it a competitive edge as one of the adsorbents to be considered for AMD treatment processes. The phenotypic plasticity of DS will be put under immense stress in the presence of high heavy metal concentrations like not studied before. This study will consists of two key complimentary components: (i)

in-depth optimization study of Ca-alginate matrix composition for the purpose of immobilizing *Desmodesmus sp.* and (ii) the immobilized *Desmodesmus sp.* being used for biosorption of Fe (II) from aqueous solutions.

1.8 Hypothesis and objectives

1.8.1 Hypothesis 1

The fresh water green microalgae *Desmodesmus sp.* found in Zoo Lake will exhibit phenotypic plasticity properties when exposed to high heavy metal concentrations and low pH to facilitate sequestration of toxic heavy metals from aqueous solutions.

1.8.2 Hypothesis 2

The immobilization of *Desmodesmus sp.* using a natural polysaccharide matrix Calcium-alginate will afford easy separation, protecting microalgae cells from the toxic AMD environment from inhibiting its metabolic activity and immobilized microalgae cells will be reused and regenerated for multiple cycles of heavy metal treatment

1.8.3 Research key questions

- What effect does immobilizing parameters have on the biosorption efficiency of heavy metals by *Desmodesmus sp.*?

- What is the maximum sorption capacity of immobilized *Desmodesmus sp.* biosorbent?

- What are the biosorption kinetics of the immobilized *Desmodesmus sp.* in batch conditions?

- Do the kinetics and equilibrium conditions of the immobilized microalgae in a continuous process compare to its batch conditions?

- What effect does bed height and flow rate have on the biosorption efficiency of heavy metals by immobilized *Desmodesmus sp.*

CHAPTER 2

IMMOBILIZATION OF *Desmodesmus sp.* USING Ca-ALGINATE MATRIX

2.1 Introduction

2.1.1 Immobilization

Entrapment media such as Ca-alginate, gelatin and polyacrylamide have similar gel formation procedures and all can be used for microalgae cell entrapment. They are all widely used for this purpose. However, Ca-alginate matrix is more conducive for microalgae cell immobilization, because bead formation occurs under extremely mild conditions compared to other media. Ca-alginate matrix is easy to prepare, nontoxic to humans, nontoxic to the entrapped microalgae cells and inexpensive (Martins et al., 2013). The most significant property of Ca-alginate matrix is that the immobilization technique does not cause cells to undergo extreme changes in physiochemical conditions (Bashan & Bashan, 2010).

2.1.2 Immobilization of *Desmodesmus sp.*

Desmodesmus sp. (DS) is a green freshwater microalgae, that plays an important role in freshwater ecosystems and it is also frequently found in polluted environments (Monteiro et al., 2009). It has also been applied in bioremediation studies in which heavy metals such as Arsenic (As); Lead (Pb; Cadmium (Cd) were studied (Willey, 2007). However, the performance of DS entrapped in Ca-alginate matrix is not well documented as an adsorbent for metal iron (Fe (II)). Fe (II) removal is a major constituent in AMD contaminated aqueous solution.

2.1.3 Objectives

The broad objective of this study is to investigate the formation of beads by entrapping DS into Ca-alginate matrix for Fe (II) uptake from aqueous solutions. In the attempt to determine the efficacy of the immobilized microalgae cells in adsorbing Fe (II), the research will focus on determining:

- The effect of bead-curing time on the bead stability
- The loading capacity of the immobilized microalgae
- The effects of storing beads in various media

2.2 Experimental methods and material

2.2.1 Algae and growth conditions

The chlorophyta microalgae was isolated from fresh water at Zoo Lake, Parkview, Johannesburg, South Africa, located 26°09'29.33" S, 28°01'42.45" E (Google earth, 2014). Sampling was also done at Donaldson Dam, Westonaria, South Africa, located 26°16'47.55" S, 27°41'07.02" E (Google earth, 2009). A Polymerase chain reaction (PCR) and DNA sequencing was used to determine the genus of the microalgae sampled (Diale et al., 2011b). Samples were observed by Dr. Ben Loos, CAF, of Stellenbosch University on an Olympus Cell^{R} system attached to an IX-81 inverted fluorescence microscope equipped with an F-view-II cooled CCD camera (Soft Imaging Systems). A Xenon-Arc burner (Olympus Biosystems GMBH) was used as a light source, where images were excited with a 472 nm excitation filter. Emission was collected using a UBG triple- bandpass emission filter cube (Chroma). Image acquisition was performed with an Olympus UPlan Sapo N 60x/1.4. Images were processed and background-subtracted using the Cell^R software.

All vessels used for culturing were autoclaved using a HA-300 MD, HICLAVE (Japan) autoclave at 0.1MPa and 190 °C, to inactivate any microbial activity. The microalgae cells were cultured using a modified Beijerinck medium (Kativu et al., 2011). An illustration of algae growth set-up is presented in Figure 2.1. Beijerinck medium was prepared from premixed stock solutions in a 1L Erlenmeyer flask (see Appendix A). CO_2 was bubbled at 50 ml/min into the culturing medium for an hour daily. Continuous bubbling has a dynamic way of affecting microalgae growth (Kativu et al., 2011). Bubbling CO_2 is necessary for photosynthesis occurrence and it also ensures that the CO_2: HCO^{-3} is balanced, which is essential for microalgae growth. Sylvania, Gro-lux (F35W/GRO-T8) lights were used as photosynthetic light source during the culturing process. Mixing was achieved by the use of a magnetic stirrer plate, Boeco, MS 300 (Germany) magnetic stirring plate. Mixing is

necessary to prevent sedimentation of the microalgae and to ensure all microalgae cells are equally exposed to the light and nutrients, so as to avoid thermal stratification.

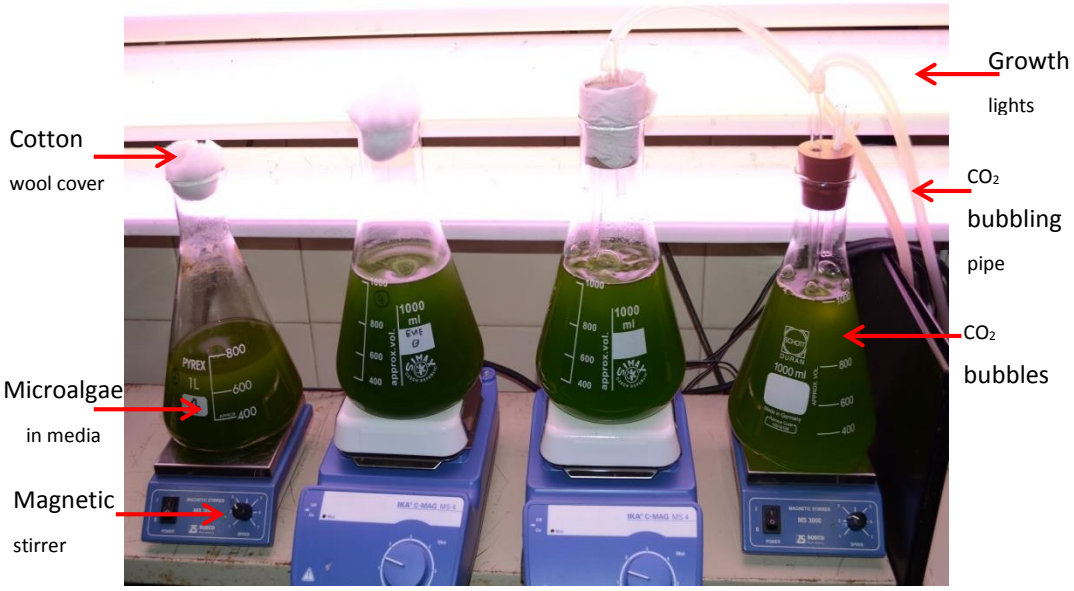


Figure 2.1: An illustration of algae growth set-up. Green microalga cells cultured in a modified Beijerinck medium, with periodical CO_2 bubbling

The successive growth of the microalgae cells population under batch condition was monitored using a 4802 UV / VIS Double beam spectrophotometer at a wavelength of 680 nm. Harvesting was done by centrifuging 50 mL of microalgae biomass at 4 000 x g for 30 minutes. The medium was then decanted and the algal biomass was filtered to remove excess water.

2.2.2 Immobilization of microalgae preparation

Na-alginate solution was reacted with $CaCl_2$ solution using the drop-technique, to immobilize microalgae cells into calcium alginate (Ca-alginate) beads, according to the process used by (Figure 2.2) (Eldridge, 2008). Both Na-alginate and $CaCl_2$ were

obtained from Sigma-Aldrich, South Africa. Prior to that, Na-alginate was dissolved proficiently in water for immobilization preparation. Na-alginate is hygroscopic and tends to clump to the surface of the liquid (Fraser & Bickerstaff, 1997). Na-alginate powder therefore, was slowly added to well-stirred distilled water to assist with the dissolution process. Stirring was allowed to continue for at least an hour after addition of Na-alginate powder.

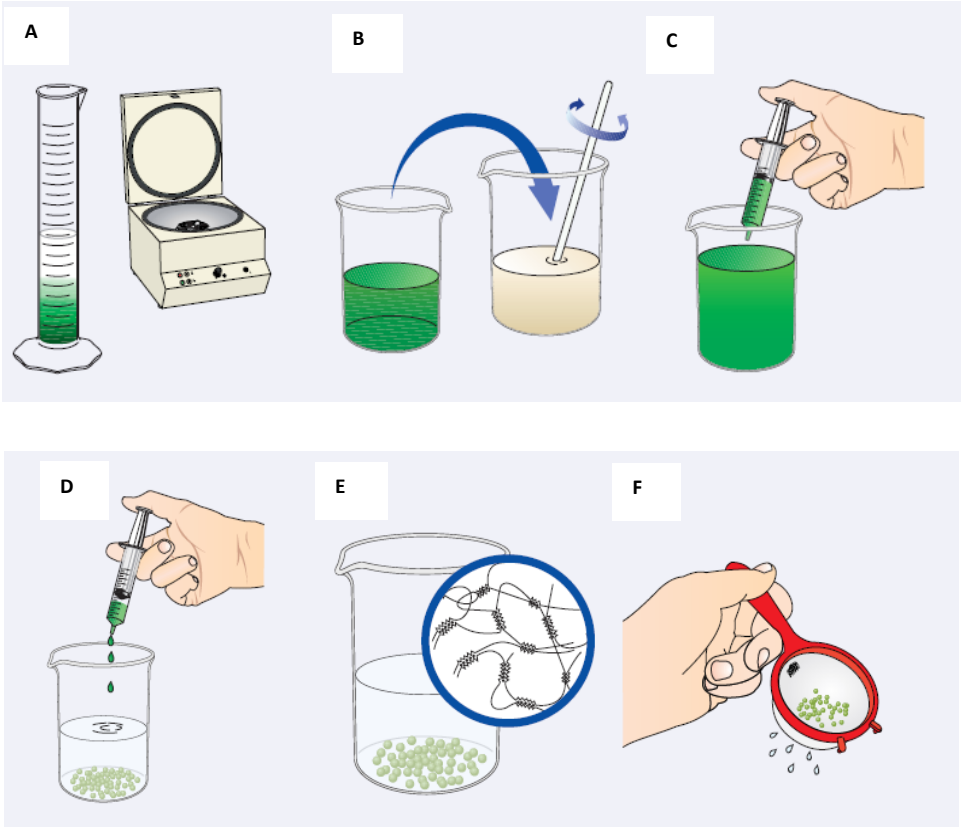


Figure 2.2 : Preparation for immobilized microalgae beads formation illustration, which involves: (a) harvesting microalgae by centrifugation; (b) mixing microalgae with Na-alginate, (c) putting the mixture of microalgae and Na-alginate into a syringe, (d) dropping mixture from the syringe into a $CaCl_2$ solution, (e) spherical beads form from dropping mixture into $CaCl_2$ solution and bead are cured for time sufficient for maximum cross-linkage to occur and (f) retrieval of formed beads from $CaCl_2$ solution, rinsed and stored for laboratory application. (Eldridge, 2008).

The solution was allowed to stand at room temperature for at least an hour with occasional manual stirring to expel excess air bubbles. Microalgae biomass of 1.5 g was mixed with 50 mL of 3 % wt Na-alginate solution. Beads of 3 % w/v were

formed by dropping the polymer solution from a height of approximately 20 cm into 500 mL of stirred 0.2 M $CaCl_2$ solution with a syringe and a needle. Figure 2.2 (a – f) shows a step-by-step immobilization process for live microalgae cells.

The chemical reaction characterizing the Na-alginate and $CaCl_2$ interaction in forming Ca-alginate gel / beads is presented in reaction 2.1.

$$2\ Alg - COONa + CaCl_2 \rightarrow (Alg - COO)_2\ Ca + 2\ NaCl \qquad (2.1)$$

Ca-alginate beads formed consist of β – D – mannuronic and α – L – guluronic units that are linked to form 1, 4 – glycosidic bonds when contacted with $CaCl_2$ solution, as illustrate in section 1.3.2. The 'egg-box' model (Grant et al., 1973) is generally invoked to explain how the divalent metal ions, bounded in the inter-chain cavities, essentially polyguluronate sequences, give rise to a rod-like cross-link complex (Velings & Mestdagh, 1995).

2.2.3 Effects of curing time on bead stability

Experiments were conducted to study the effect of curing time on bead stability. Na-alginate solution was dropped into Ca^{2+} solution and curing time intervals varied from 0.5; 1; 3 and 24 hours. The prepared gel beads were examined on a Thermogravimetric Analysis unit, Perkin Elmer Pyris 1 TGA Thermogavimetric Analyser (Massachusetts, USA) using nitrogen as the purge gas, at a flow rate of 20 mL min^{-1} and a heating rate of 5 ^oC per minute from 0 – 1000 ^oC. Mass change in the material was measured as a function of temperature whilst the substance was subjected to a controlled temperature programme. The steps of weight-loss assisted in describing the effect curing time has on the stability of the beads.

2.2.4 Fe (II) removal by immobilized *Desmosdesmus sp.* (IDS) and clear beads (CB) from solution

The biopolymeric beads IDS and CB (1 g) were added to a 100 mL known solution of Fe (II) with a concentration of 120 mg/L at constant pH 2.5. All experiments were conducted at room temperature. The suspension was shaken on an orbital shaker for 120 minutes at 180 rpm. This was found to be sufficient time to attain equilibrium adsorption. Time intervals used for sample collection were 5; 10; 15; 30; 60 and 120 minutes. After shaking, the suspension was filtered and the amount of Fe (II) present in the solution obtained after contacting the metal with biomass was determined using Atomic Absorption Spectrometry (AAS) (equation (2.1)). AAS measurements were made on a PG-990 AAS model (Leicestershire, UK).

$$Fe(II)removal(\%) = \left(\frac{C_1 - C_0}{C_1} \right) \times 100 \qquad (2.1)$$

Where, C_0 = initial concentration of metal ions in aqueous solution (mg/L); C_1 = final concentration of metal in aqueous solution (mg/L)

2.2.5 Storage test for sstability of alginate-immobilized algal cells

Ca-alginate has high sensitivity towards precipitating compounds such as: phosphate; citrate and lactase (Thu et al., 1996). The beads need to be kept in media that do not interfere with their chemical and physical properties. The stability of the Ca-alginate matrix used for alga cells immobilization in this work was determined by storing IDS and CB in various media. IDS and CB were stored in petridishes consisting of 20 ml of i) Distilled water; ii) Beijerinck medium; and iii) $CaCl_2$ solution. Petridishes were observed for a period of 30 days.

2.3 Results and Discussion

2.3.1 Microalgae identification and cultivation

Figure 2.3 (a – c), show microscopic results obtained from Zoo lake and Donaldson dam sampled algae. Figure 2.3 (a) shows slightly curved, 2-celled, and spineless flat colonies joined laterally and lying parallel to each other resembling *Scenedesmus obliquus* (Shubert et al., 2014). This species of microalgae has been studied for its potential source for biodiesel production by (Mandal & Mallick, 2009). Figures 2.3 (b) and (c) show ellipsoid spineless cells that resembles *Desmodesmus subspicatus* and *Scenedesmus rubescens*, as shown in section 1.2.1. Sequences for both samples were run through NCBI and the internal transcriber spacer 2 database (Schultz et al., 2006). The genuses of the unknown algal Zoo Lake and Donaldson dam samples was found to be *Desmodesmus.* This genus is ubiquitous in freshwater habitats as single to 32-celled coenobia and is phenotypically plastic (Johnson et al., 2007). The best hit for an alga was found to be *Desmodesmus sp.* for Zoo lake algae and *Desmodesmus sp*. for Donaldson dam algae samples. Tables 2.1 represent the primer sequences used for algal identification from Donaldson dam sample, as reported previously by Diale et al. (2011b).

DS is an autotrophic microalgae requiring light, carbon dioxide (CO_2), and trace nutrients for its growth. It can change its form in response to changing environmental conditions, exhibiting a phenomenon called phenotypic plasticity. Phenotypic plasticity is viewed as a mode in which organisms cope with environmental changes and these changes can be: morphological, physiological, behavioural and phonological. This study has found *Desmodesmus sp.* microalgae have demonstrated a morphological type phenotypic plasticity. This is the case due to the microalga found in two fresh water sources contaminated differently and exhibited different morphs as shown in Figure 2.3.

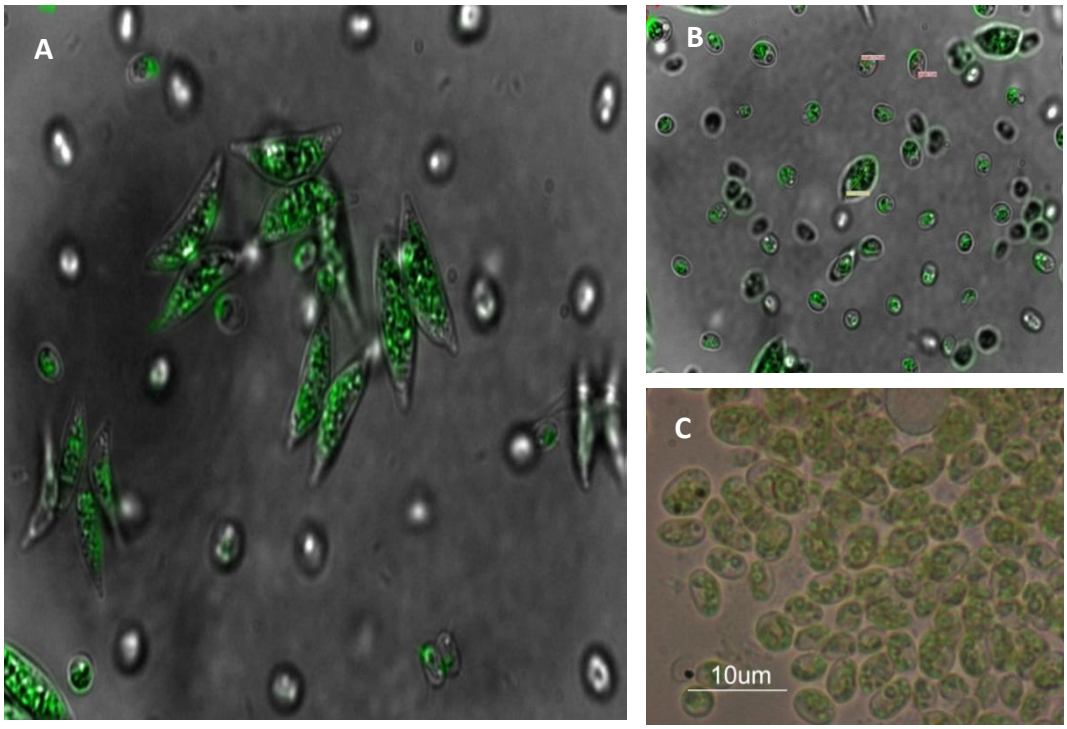


Figure 2.3: Dr. Ben Loos, CAF, Stellenbosch University viewed the samples using an inverted fluorescence microscope. (A) and (B) are photos showing algae found in the sample from Donaldson Dam and (C) algae found in the sample from Zoo Lake (Diale et al., 2011b).

Zoo lake's main pollutants are silt and sewage, whereas Donaldson's dam is AMD seeping from surrounding mine dumps and spent mines. The ability of these microalgae to thrive in harsh conditions makes it highly favoured for use in rehabilitating AMD contaminated water in the Witwatersrand basin. Immobilization of the microalgae will improve its chance of commercialization as a method for AMD water treatment solution.

Table 2.1: Primer sequences used for algal identification (Diale et al., 2011b).

Primer Name	Region	Primer Sequence	Reference
Gaz F1	COI	TCAACAAATCATAAAGATATTGG	Robba et al., 2006
Gaz R1		ACTTCTGGATGTCCAAAAAAYCA	
ITS 03F-800	ITS	CGATGAAGAACGYAGCGA	Hoef-Emden, 2007
ITS 05R-700		TACTTGTTCGCTATCGGTCTCT	

Figure 2.4 shows the growth curve of DS obtained using the conditions described in section 2.3.1. The lag and acceleration growth phases of the growth curve were observed between day 1 and day 10. The exponential (log) phase proceeded from day 10 to day 20. The diminishing growth (linear growth) phase was observed after 23 days.

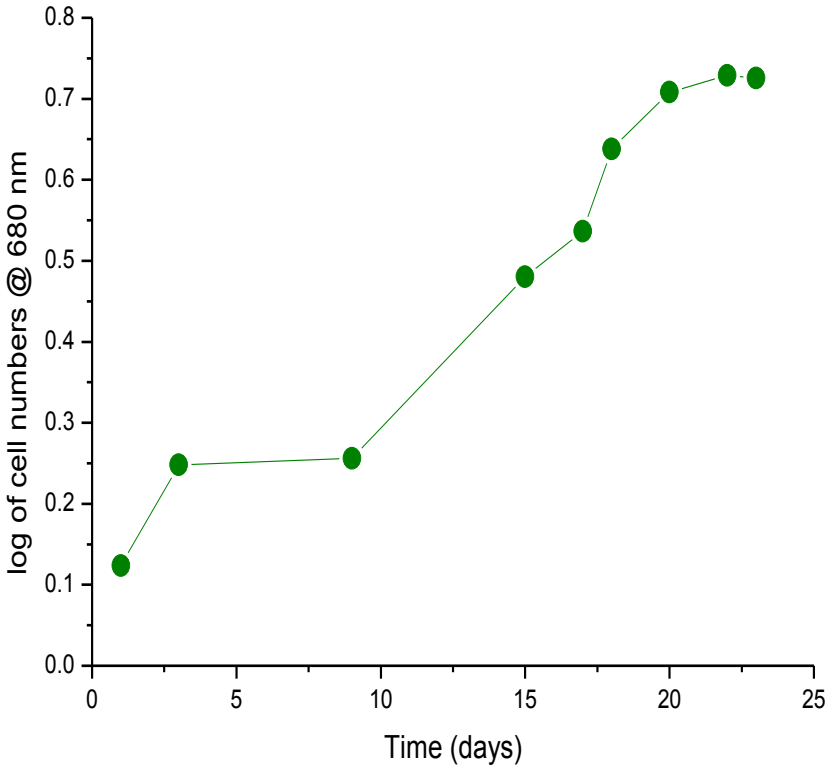


Figure 2.4: Growth curve of *Desmodesmus sp.* microalgae in Beijerinck medium.

The specific growth rate (SGR) of the cultured microalgae was calculated using equation 2.3 (Clesceri et al., 1989):

$$\mu = \frac{\ln X_2 - \ln X_1}{t_2 - t_1} \qquad (2.2)$$

Where;

X_1 = Biomass concentration at the end of selected time interval

X_2 = Biomass concentration at the beginning of selected time interval

$t_2 - t_1$ = Elapsed time between selected time in the day

The calculated SGR for DS in the Beijerinck medium was 0.11 day $^{-1}$. Similarly (Kativu, 2011) obtained a SGR of 0.10 day^{-1} when culturing DS. The SGR obtained for the microalgae in this study is low compared to *Scenedesmus sp.* which produced a maximum SGR of 0.76 day^{-1} when cultured at 25 ^{o}C (Xin et al., 2011). Habib (1998) found SGR of *Chlorella vulgaris* ranging from 0.33 to 0.45 day^{-1} when cultured in Nitrogen, Phosphorous and Potassium (NPK) and different concentrations of standard Malaysian rubber effluent (SMRE) media (Toyub et al., 2008). Growth conditions for DS could have been optimized to improve its SGR; however this is outside the scope of current research work.

2.3.2 Immobilization of microalgae preparation

DS was immobilized into Ca-alginate matrix and spherical beads were formed. When drops of a Na-alginate solution get into a Ca^{2+} solution, beads are immediately formed. During the first few minutes, the beads stay on the top of the solution. After a while (depending on the cation concentration and the type of cation) they sink due to an increase of the density. This period is known as the *maturation step* (Velings & Mestdagh, 1995). The maturation step during bead formation was observed when immobilizing DS (Figure 2.6 (a – d)). It was observed that when a mixture of Na-alginate and microalgae cells interacted with $CaCl_2$ solution the beads that form retain their shape and remained at the top of the solution (Figure 2.5 (a)). After 5 minutes the beads slowly started dropping to the bottom of the solution (Figure 2.5 (b) & (c)) until all were completely settled at the bottom, Figure 2.5 (d), within 10 minutes. This observation confirms the bead maturation step. The rate of maturation step in bead formation process depends on a number of factors and the concentration of Ca^{2+} is one of them. The implication therefore is that the more Ca^{2+} ions available for cross-linking the Na-alginate polymer, the faster the rate of maturation step.

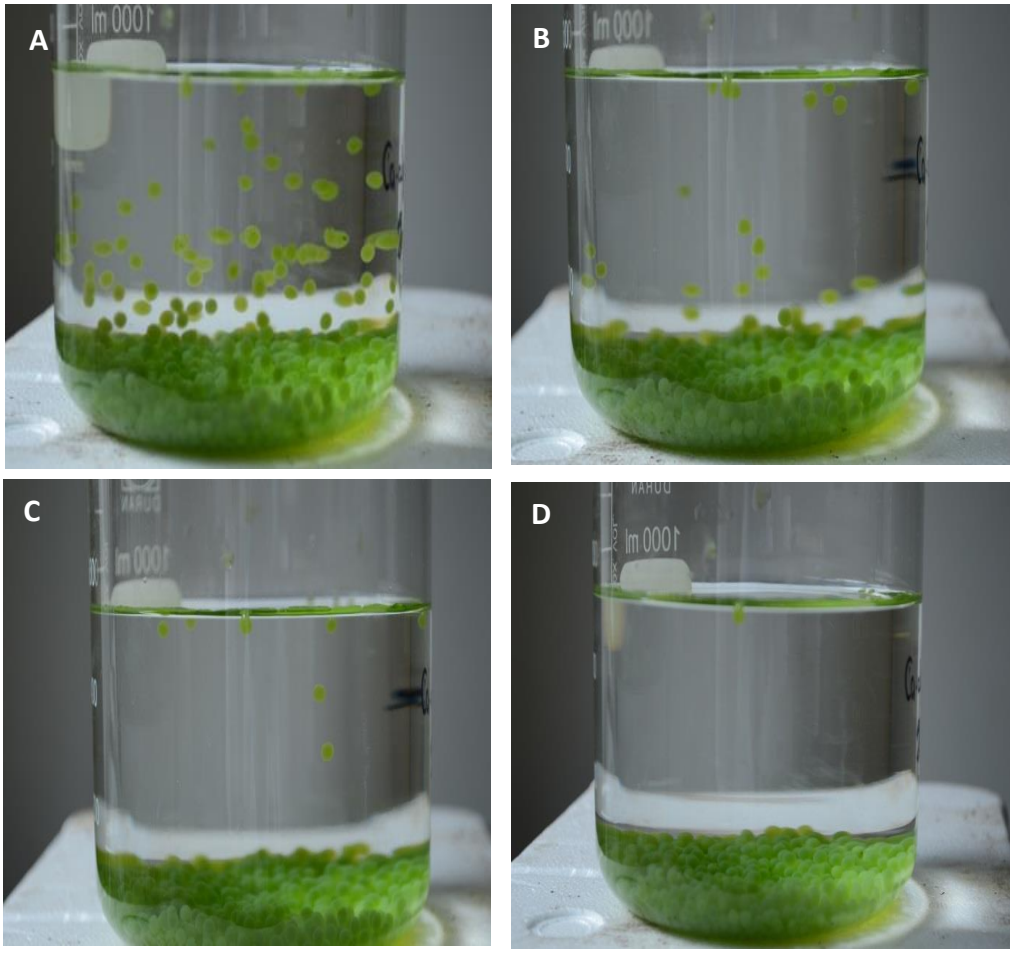


Figure 2.5: Demonstration of maturation step in the bead formation process: (a) Na-alginate mixture with microalgae dropped into $CaCl_2$ solution beads stayed on top of the solution for about a minute until, (b) they were seen dropping further after 5 minutes, (c) solution has minimal beads on top of the surface and (d) after 10 minutes all beads where at the bottom of the solution.

When Na-alginate solution is dropped into the $CaCl_2$ solution, initially the center is unreacted, then over time the Ca^{2+} ions will diffuse into the center and form a complete Ca-alginate structure (Kim, 1990). During the maturation step the boundary of Ca-alginate gel will move toward the center from the surface while Ca^{2+} ions penetrate the Na-alginate layer. Kim, 1990 conducted an in-depth study on the kinetics of Ca-alginate bead formation. The study proposed a kinetic equation based on shrinking-core model with assumptions dominant pore-diffusion kinetics and pseudo-steady-state approximation. By taking into account the transfer rate of Ca^{2+} ions; rate of consumption of Na-alginate and

concentration distribution of Ca^{2+}, the proposed kinetic equation could be represented in equation 2.4 (Kim, 1990):

$$\frac{2C_o D_e}{pqR_o^2} t = 1 - \gamma^2 - \frac{1-\phi^2}{1-\varepsilon} \equiv \varphi \qquad (2.3)$$

Where,

Co = concentration Ca^{2+} ion in the gelled layer (mol/L)

De = diffusion coefficient of Ca^{2+} ion in the micropores (cm^2 / min)

p = composition of Na-alginate in the solution (g/cm^3)

q = moles of Ca^{2+} required for gelation based on the weight of Na-alginate (mol/g)

Ro = initial radius of a spherical bead (cm)

t = gelling time (min)

γ = dimensionless core radius

ε = dimensionless gelled layer shrinkage

ϕ = dimensionless bead radius

ψ = dimensionless variable

A reasonable agreement was obtained between the gelling processes of Ca-alginate beads and proposed kinetic equation describing bead formation.

2.3.3 Effects of curing time on bead stability

The stability of beads was studied by soaking beads in a $CaCl_2$ solution over various periods of time then removed for analysis. The beads were then analysed in a TGA. Figure 2.6, represents TGA curves of CB being cured for 0.5; 1; 3 and 24 hours. The initial weight loss in the TGA curve corresponds to water evaporation, from both free water and bound water (Sartori, 1997). CB experienced a rapid

weight loss between 30 °C and 100 °C, suggesting that moisture and water of crystallization evaporated in this period. A sharp weight loss step was experienced by this sample at 200 °C. The sample was completely decomposed beyond 200 °C. The complete decomposition of the sample at this temperature and beyond corresponds to its boiling point (Widmann, 2001).

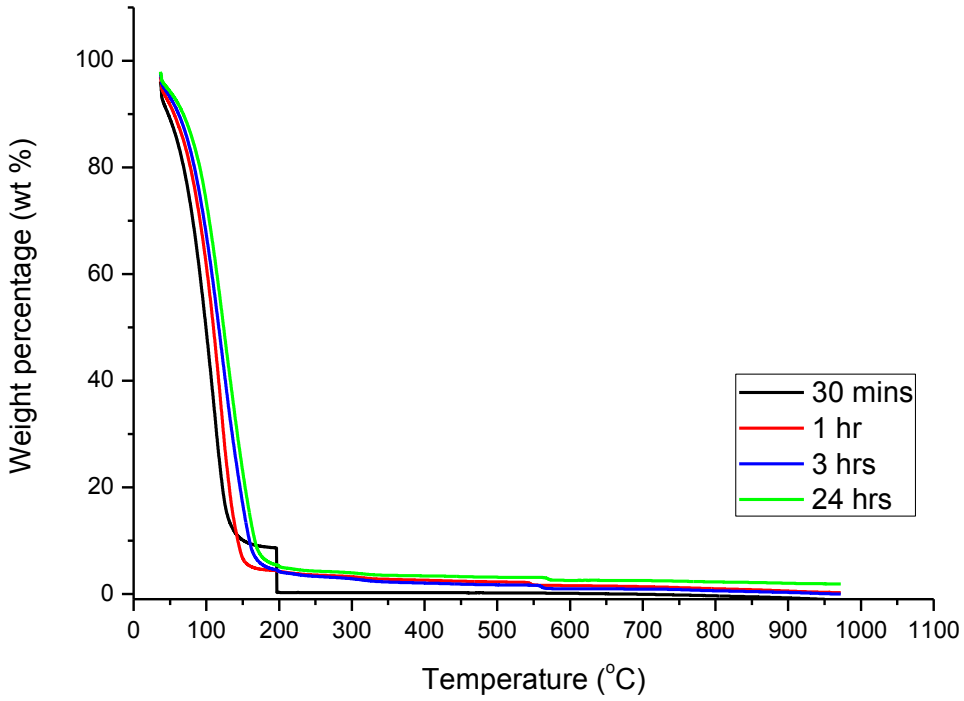


Figure 2.6: TGA curve for CB with 3 % Na-alginate concentration after curing for various periods.

The evaporation of free water and bound water was slightly delayed or occurred at higher temperatures with an increase in curing time. Weight loss step occurred at temperatures 150; 170 and 180 °C for beads cured for 1, 3 and 24 hours, respectively. It was observed that no significant weight loss was seen for samples cured for 3 and 24 hours. This therefore suggests 3 hours is sufficient for

Ca-alginate curing for gelling, but 24 hours can be used for maximum gelling of the matrix. The TGA curve shapes obtained for CB cured for 1; 3 and 24 hours, indicate that thermal decomposition with the formation of gaseous reaction products could be the chemical reaction that describes weight loss that occurred (Widmann, 2001). These results therefore demonstrate that bead-curing period has a direct effect on the stability of beads formed from Na-alginate and $CaCl_2$ interaction. Curing beads for 24 hours suggests maximum gelling; this study therefore will adopt this curing period to ensure stable beads are formed for further experimental work.

2.3.4 Fe (II) removal by IDS and CB from solution

The Fe (II) removal percent of IDS and CB biomass was studied and the outcome is shown in Figure 2.7.

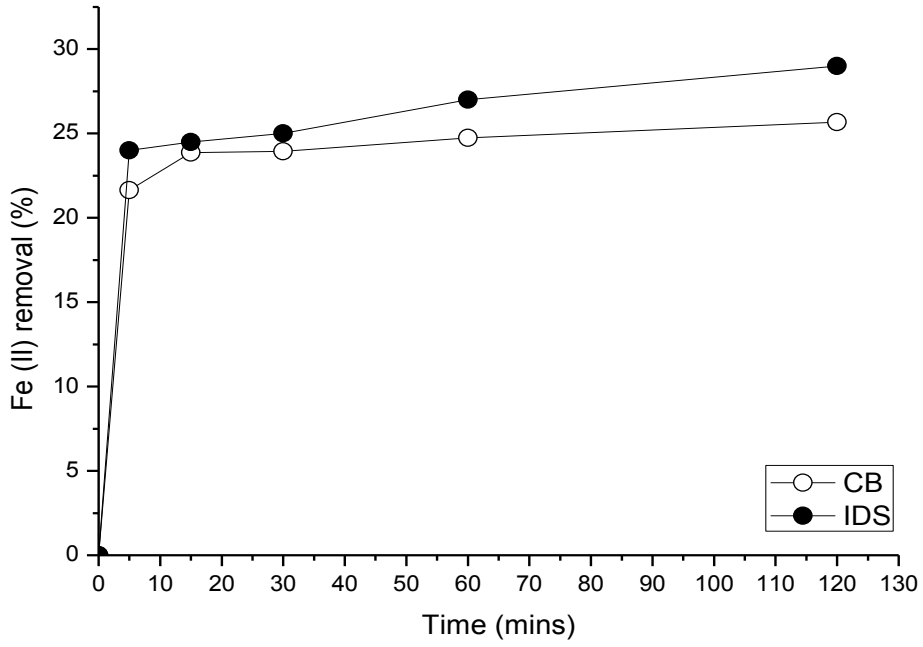


Figure 2.7: The study of loading capacity of CB and IDS in the presence of Fe (II) at 120 mg/L and pH 2.5. Three mm bead diameter of beads was used.

It was observed that Fe (II) ions were rapidly removed within 5 minutes, by IDS and CB. The Fe (II) removal rate reached 23.9 % after 15 minutes. No significant Fe (II) removal was experienced after 120 minutes. The maximum or approximated 25 % Fe (II) removal, suggested that all available binding sites of the CB biomass were saturated. The removal rate exhibited a steady increase from 15 minutes to 120 minutes when IDS biomass was used for Fe (II) ions adsorption. Equilibrium was not reached for this particular biomass. This may imply that an extension of contact time will be necessary to establish an equilibrium rate of removal of IDS. These results show a significant difference the presence of microalga in Ca-alginate has in enhancing the Fe (II) ion removal of the Ca-alginate matrix. The availability of binding sites on CB biomass can be attributed to Na-alginate being an extract from cell walls of brown seaweed (i.e. brown algae). Brown seaweed is known to have metal adsorbing functional groups and carboxylic groups are the most abundant acidic functional groups (Davis et al., 2003). Sequestration of heavy metal by brown algae has been documented by Fourest & Volesky (1996) and Schiewer & Volesky, (2000). The blend of Ca-alginate and microalgae cells, gave a higher Fe (II) removal percent after 120 minutes (29 %) as compared to CB at 25 %. The carboxylic ionic compound reacts with metal oxides or metal hydroxides to form metal carboxylates. A mechanism that might be responsible for the reaction of Fe (II) with carboxyl acid groups in IDS and CB is illustrated in Figure 2.8.

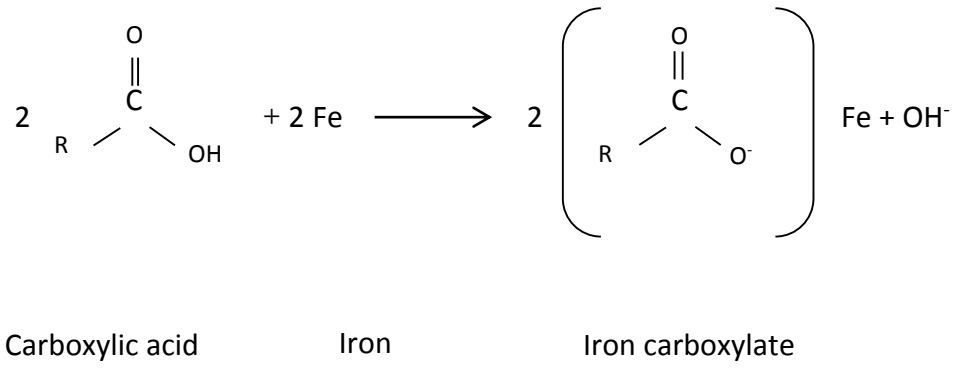


Figure 2.8: Chemical reaction that describes mechanism of Fe (II) adsorption by IDS and CB.

Biochemical reaction of microalgae and heavy metals are known to be complex. Metal complexation and its by-products tend to have an impact on the pH of the solution. This trend was observed when pH levels were monitored when IDS and CB beads were reacted with Fe (II) in solution (Figure 2.9). The pH of living cells is generally between 7 and 8.5, referred to as physiological pH (McDowell et al., 1977). At physiological pH, a functional group such as carboxyl- is an ionized deprotonated acid. Deprotonation of the algae species at low pH levels plays a role in the sorption mechanism of Fe (II) from aqueous solution. The functional group generates a negatively charged surface at acidic pH and electrostatic interaction between cationic species and the cell surface is responsible for metal adsorption (Monteiro et al., 2009). As the pH increases, the functional sites become deprotonated, so their negative charges increase and permit binding to metal cations to higher extents.

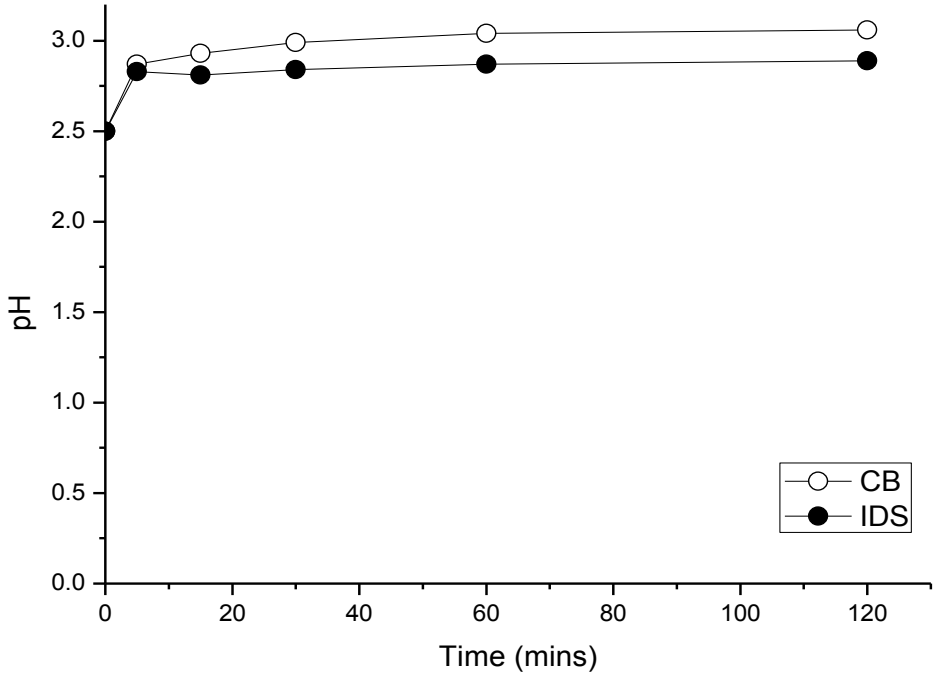


Figure 2.9: pH levels in solution during the adsorption of Fe (II) by CB and IDS.

2.3.5 Storage test on stability of alginate-immobilized microalgae cells

Experiments were conducted to study the stability of IDS and CB biomass when stored in distilled water; Beijerinck medium and $CaCl_2$ at room temperature for 30 days. Figure 2.10 (a) shows CB stored in distilled water; Beijerinck medium and $CaCl_2$ solution

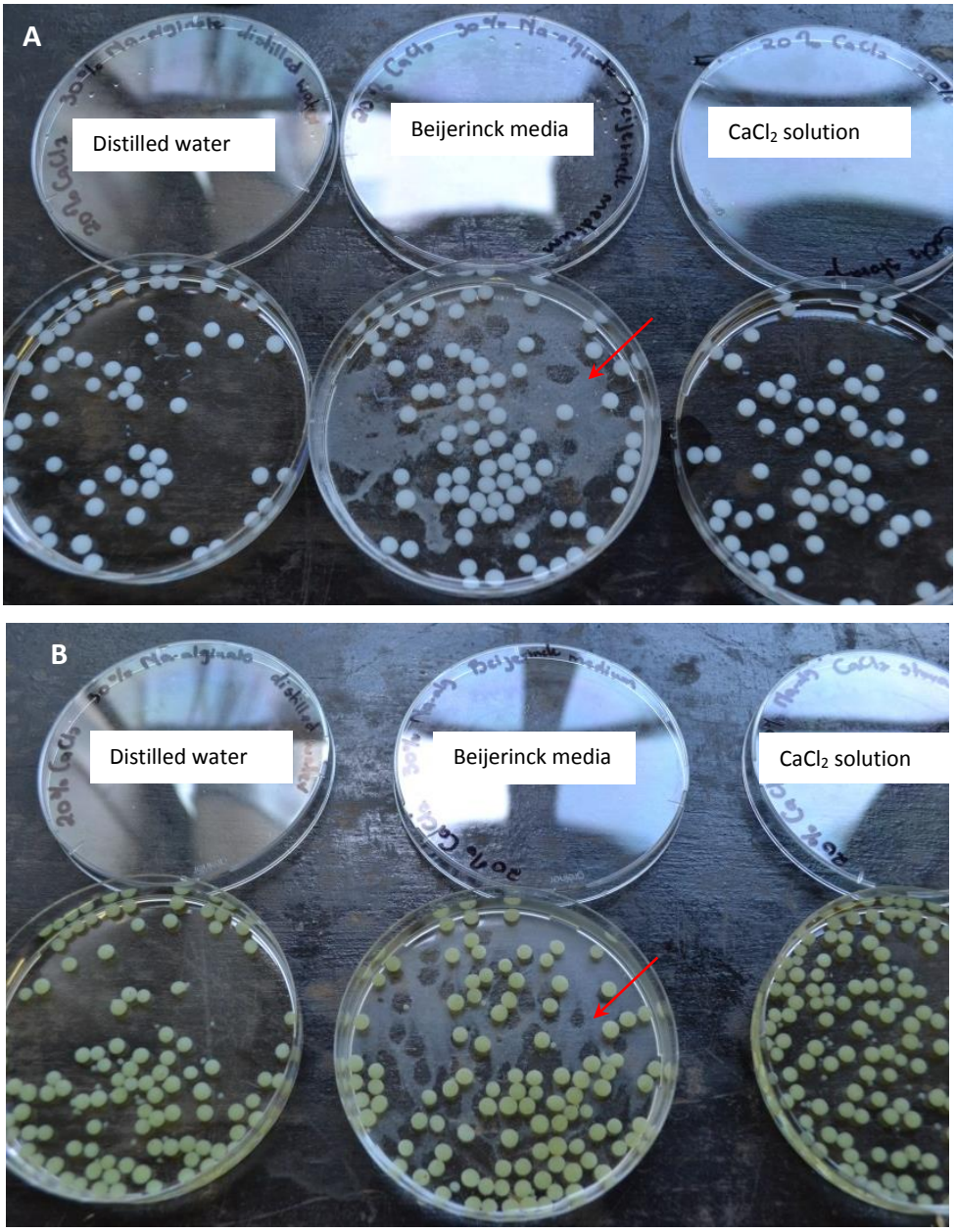


Figure 2.10: (A) & (B) CB and IDS stored in distilled water; Beijerinck medium and $CaCl_2$ solutions.

It was observed that CB biomass experienced some swelling when stored in all three solutions. Precipitation was found at the bottom of a petridish, where CB was stored in Beijerinck medium. Similarly, IDS stored in Beijerinck medium (Figure 2.10 (b)) also contained precipitates at the bottom of the petridish. Furthermore, the petridish had some traces of microalgae cells, indicating that some microalgae cells might have leaked out of the matrix. The swelling of the Ca-alginate matrix found in this study is a well-known phenomenon. Swelling of polymer gels such as Ca-alginate matrix is considered a major limitation for its use in industrial applications. This can however be avoided. Kinetics of swelling are characterised by mass transport and mechanical deformation, which depend on the interaction between the polymer network and the solvent. Bouklas & Huang (2012) presented an in depth study on linear and nonlinear theories that can be used to describe or predict the swelling kinetics of polymer gels under various conditions. Ca-alginate beads contain a polysaccharide anion, which can form insoluble compounds when interacted with chelating agents. Beijerinck medium consists of EDTA, phosphates, sodium and magnesium ions which are all components that can interact with polysaccharide anion to form precipitate. This study has shown that Beijerinck medium not only precipitates the Ca-alginate matrix, but also allows for continued cell growth in the matrix. When the microalgae cells continue to grow they eventually break out of the matrix entrapment and leak out of the beads. Beijerinck medium is therefore not a suitable medium for bead storage, because the medium deforms the alginate matrix compromising its stability.

Distilled water and $CaCl_2$ solution also proved not to be suitable storage medium, because they induced swelling on the beads. Further studies were conducted where IDS and CB were stored in a humidified environment. Schott duran glass bottles (250 ml) were used to store beads and wetted cotton wool was mounted inside the bottle's lid. The beads were tightly sealed into the bottles, where the

presence of wetted cotton created a humidified environment. After 30 days of storage, the beads still retained their original shape with no swelling or dissociation. IDS and CB showed to be stable in humid storage environment. This method was therefore adopted for storing all beads created for further experimental work.

2.4 Conclusion

This study showed that curing period in creating Ca-alginate matrix directly affects the stability of the beads or gels formed. Three hours proved to be sufficient for gelling, however maximum gelling can be obtained after 24 hours.

Immobilization of *Desmodesmus sp.* and its use for Fe (II) ions uptake in aqueous solution gave a better Fe (II) removal compared to clear beads.

This study has shown that IDS and CB are not inert, because they were seen to interact with the media in which they were stored in. The media provoked a transformation that can lead to total dissociation and possible collapse of the network. The controls of physic-chemical characteristics of the media in which the beads are put are important, because they play an important role in the behaviour and stability of the Ca-alginate beads. Storing beads in a humidified environment proved to not interfere with the bead structures of IDS and CB, this method was adopted for storage in this study.

CHAPTER 3

CHARACTERIZATION OF IMMOBILIZED MICROALGAE AND Fe (II) SORPTION

3.1 Introduction

3.1.1 Immobilization of microalgae cells

In the present work, Ca-alginate matrix was used for immobilizing *Desmodesmus sp.* (DS) by the entrapment technique. Immobilized microalgae cells have received increasing interest in the field of waste water treatment (Winnicki et al., 1982) (Westmeier & Rehm, 1987) (Hallas et al., 1992) (Cohen, 2001) (Ahmad et al., 2012). Extensive reviews on its methods, application and properties have been reported by (Bickerstaff, 1997). Industrial applications of immobilized microalgae expand over toxicity measurement; metal removal; organic pollutant removal to energy generation (electricity or hydrogen) (Moreno-Garrido, 2008).

Despite the suitability of Ca-alginate as the immobilising matrix material of microalgae cells, the technique has limitations. The low stability quotient of Ca-alginate matrix limits its use in certain environments. Substances such a phosphate or citrate have a high affinity for Ca^{2+} ions. These substances can sequester cross-linking Ca ions and consequently destabilize the gel (SmidsrØd & Skjåk-Bræk, 1990). Ca-alginate matrixes cannot be used in sea, estuarine and brackish waters. The dissolved monovalent cations (mainly sodium) in the media can substitute divalent cations and results in the loss of structure of matrixes. High porosity of the Ca-alginate matrix allows for high diffusion rates of substrate through the matrix; however it can also lead to leakage. However, the effective use of Ca-alginate matrix for immobilization relies largely on optimizing the gel formation process. An ideal Ca-alginate matrix should have: (i) high chemical and mechanical stability; (ii) controllable swelling properties, (iii) defined pore size and (iv) a narrow pore-size distribution. Creating a Ca-alginate matrix that meets these

requirements, an optimized gel formation process is required looking at the choice of immobilizing matrix, the concentration of Na-alginate and $CaCl_2$ and other factors.

3.1.2 Objectives

This chapter will discuss how the gel formation process was optimized to create a Ca-alginate matrix suitable for immobilizing DS for the purpose of heavy metal removal in aqueous solutions. Techniques employed for characterising Ca-alginate beads will be discussed. Physical characterisation of IDS and DS was performed using Nitrogen Sorption Porosimetry, Environmental Scanning Electron Microscopy and Fourier Transform Infra-Red Spectroscopy. Chemical characterisation methods employed were point of zero charge.

3.2 Experimental methods and materials

3.2.1 Reagents

Microalgae biomass collected from Zoo Lake ponds in Johannesburg, South Africa, was immobilized as mentioned in section 2.3.2. All chemicals were of analytical grade. Sodium alginate (Na-alginate) and calcium chloride ($CaCl_2$) were procured from Sigma Aldrich (South Africa). Iron (II) sulphate heptahydrate ($FeSO_4.7H_2O$) was supplied by Merck (South Africa).

3.2.2 Characterisation of immobilized *Desmodesmus sp.* (IDS)

(a) Fourier Transform Infrared (FTIR) Spectroscopy analysis of Ca-alginate beads

The FTIR spectrum was used as a fingerprint for identification, by comparing the spectrum of an 'unknown' material with previously recorded reference spectra (Coates, 2006). The spectra of Ca-alginate beads were recorded using a Bruker FTIR spectrometer, Model Tensor 27 (Ettlingen, Germany). Fourier-transform infrared spectra were recorded in the frequency range of 4500 to 1000 cm^{-1} in the transmission mode and 4 cm^{-1} resolution over 50 scans.

(b) Environmental Scanning Microscopy (ESEM)

An ESEM was used as opposed to the conventional SEM, because of its ability to make nonconductive samples conductive without desiccating and then coating samples with gold-palladium or carbon. This helps preserve the sample's original characteristics and it is essential when analysing biological / polymer material like IDS. Samples were prepared and viewed at the Council for Scientific and Industrial Research (CSIR) in Port Elizabeth, South Africa. The surface morphology of the

beads was determined using the conditions: HV = 25 kV; Mode = SE and Vac Mode = ESEM.

(c) Thermogravimetric analysis (TGA)

In order to determine the chemical stability of the Ca-alginate beads TGA was used. Perkin Elmer Pyris 1 TGA Thermogavimetric Analyser (Massachusetts, USA) using nitrogen as the purge gas, at a flow rate of 20 mL min^{-1} and a heating rate of 5^{o}C per minute from 0 – 1000 ^{o}C. Mass change in the material was measured as a function of temperature whilst the substance was subjected to a controlled temperature programme. In this study TGA was used to determine whether weight losses is caused by: (i) chemical reactions (i.e. decomposition; loss of water of crystallization; combustion; reduction of metal oxides) or; (ii) physical transitions (i.e. vaporization; evaporation; sublimation; desorption and drying).

(d) Determination of point of zero charge (pH_{pzc}) of beads

The point of zero charge (pH_{pzc}) is the pH point at which a surface charge is equal to zero. Based on this, pH would either be increased or decreased so as to make the surface more negative or positive. In this study, pH_{pzc} was determined by adding 50 mL of 0.01 M of $NaCl_2$ solution into six closed Erlenmeyer flasks. The solutions were adjusted to initial pHs of: 2, 4, 6, 8, 10, 12; using 0.1 M HCL or NaOH solutions. Immobilized alginate beads of 0.15 g were added to each solution and incubated at 25 ^{o}C, with shaking at 100 rpm for 48 hours. After which each solution was filtered and the final pH values of the supernatant liquid were recorded. The pH_{pzc} is determined by plotting a curve of pH_{final} versus $pH_{initial}$. A straight line from the origin was plotted and the point at which the line crosses $pH_{initial}$ = pH_{final} is taken as the pH_{pzc} of the beads. Experiments were repeated twice.

(e) Surface characterisation of the biosorbent

The N_2 adsorption-desorption isotherms were measured at 77.35 K on a TriStar 3000 V6.05A (Micromeritics, USA). BET specific surfaces (S_{BET}), porous volume (V_p), and average pore size (D_p) were calculated using the Brunauer-Emmett-Teller (BET) method (Brunauer et al., 1938) under a relative pressure ranging from P/P_0 = 0.051 to 0.999. The determination of specific surface by means of the BET theory is based upon the phenomenon of physical adsorption of gases on the external and internal surfaces of a porous material and BET equation is used (equation 3.1) (Lowell et al., 2004).

$$\frac{1}{W[(P_0/P)-1]} = \frac{1}{W_m C} + \frac{C-1}{W_m C}\left(\frac{P}{P_0}\right) \qquad (3.1)$$

Where,

W = weight of gas adsorbed

P/P_0= relative pressure

W_m= weight of adsorbate as monolayer

C = BET constant

The S_{BET} is determined by total surface area (S_t) by sample weight (equation 3.2), where total surface is represented by equation 3.3 (Lowell et al., 2004).

$$S_t = \frac{W_m N A_{cs}}{m} \qquad (3.2)$$

Where,

N = Avogadro's number (6.023 x 1023)

m = Molecular weight of Adsorbate

Acs = Adsorbate cross sectional area (16.2Å2 for Nitrogen)

$$S_{BET} = \frac{S_t}{w} \qquad (3.3)$$

Total pore volume is derived from the amount of vapour adsorbed at a relative temperature close to unity (assuming pores are filled with liquid adsorbate) (equation 3.4) (Lowell et al., 2004).

$$V_{liq} = \frac{PaV_{ads}V_m}{RT} \qquad (3.4)$$

Where,

V_{ads} = volume of gas adsorbed

V_{liq} = volume of liquid N_2 in pores

V_m = molar vol. of liquid adsorbate (N_2 = 34.7cm^3/mol)

Pa = ambient pressure (Pa)

T = ambient temperature (˚C)

R = gas constant

A material which is surrounded by a certain gas which has a certain temperature, T, and relative vapour pressure, P/Po, adsorbs physically a certain amount of gas. The amount of adsorbed gas is dependent on its relative vapour pressure and is proportional to the total external and internal surface of the material. The connection between relative vapour pressure and amount of adsorbed gas at a constant temperature is called an adsorption isotherm (Fagerlund, 1973).

3.2.3 Fe (II) removal from solution in batch conditions

(a) Effect of pH on Fe (II) removal from solution

Several studies have shown that pH plays an important role in metal adsorption by biological material (Monteiro et al., 2012). A study was conducted to determine the effects of pH on metal adsorption. Fe (II) (120 ppm, 50 mL solution) was added into seven closed flasks. Alginate beads of 5 g, previously prepared at pHs: 2; 6; 7; 8; 9; 10; 12, were added to the flasks and stirred at 180 rpm for 120 minutes. The solution was filtered and a final pH was recorded and analysed on an Atomic Adsorption Spectroscopy (AAS) for metal concentration. AAS measurements were made on a PG-990 AAS model (Leicestershire, UK)

(b) Effects of bead size diameter on Fe (II) removal from solution

Four hypodermic needles of different diameters were used to prepare beads of diameters 1-4 mm. The immobilized microalgae were allowed to react with 50 mL of 120 ppm Fe (II) ion solution, at pH 2.5 with shaking at 180 rpm. This was done to study the effect of bead size on metal uptake. Reaction time intervals used were: 5; 10; 15; 30; 60 and 120 minutes. Metal uptake from solution was measured using an AAS.

(c) Effect of microalgae biomass concentration on Fe (II) removal from solution

The effect of microalgae biomass concentration on metal removal in solution was studied by immobilized microalgae beads of concentrations: 3% v/w; 5 %w/v and 8 % w/v. Fe (II) (50 mL of 120 ppm) solution was added into six closed flasks with reaction times of 5; 10; 15; 30; 60 and 120 minutes. Alginate beads of 5 g were added to six Fe (II) ion solutions and allowed to mix at 180 rpm for 120 minutes.

The solution was filtered and the supernatant was analysed on an AAS for metal concentration.

(d) Effect on Na-alginate concentration on Fe (II) removal from solution

Na-alginate concentration on metal uptake was investigated by preparing different concentrations of 3; 6; 9 and 12 % wt in a 50 mL Erlenmeyer flask. The Na-alginate solutions were dropped into 2 % $CaCl_2$ solution using the drop-technique. Spherical beads were formed and cured for 24 hours at room temperature. Alginate beads (5 g), of varying Na-alginate concentration, were added to the flasks and stirred at 180 rpm for 120 minutes. The solution was filtered and the supernatant liquid was analysed on an AAS for metal concentration.

(e) Effect on $CaCl_2$ concentration on Fe (II) removal from solution

The effect of $CaCl_2$ on metal uptake was investigated by preparing concentrations: 3 %; 6 %; 9 % and 12 % in 50 mL. Na-alginate concentration was kept at 3 % wt and using the drop-technique, spherical beads were formed and cured for 24 hours at room temperature. A batch equilibrium study was undertaken to determine the effect of the $CaCl_2$ concentration on metal removal.

3.3 Results and Discussion

3.3.1 Characterisation of immobilized *Desmodesmus sp.* (IDS)

(a) FTIR spectra of IDS

For the purpose of this study clear beads will be referred to as (CB) and immobilized *Desmodesmus sp.* has already been referred to as (IDS) in chapter 2. The FTIR spectrum of IDS before and after Fe (II) biosorption is shown in Figure 3.1. The arrow shows the peak that appeared after biomass was in contact with Fe (II) in solution. The IDS biomass, exhibited stretching vibrations of O – H bonds in the range of 3000 – 3600 cm^{-1}. The most important functional group for heavy metal adsorption was observed in 1604 cm^{-1}, being attributed to the asymmetric and symmetric stretching vibrations of carboxyl ions (Daemi & Barikani, 2012). Other bands were observed at wavenumbers: 2133.2 cm^{-1},1421 cm^{-1} and 1033.8 cm^{-1}, which correspond to functional groups: alkynes, alkanes and alcohol respectively.

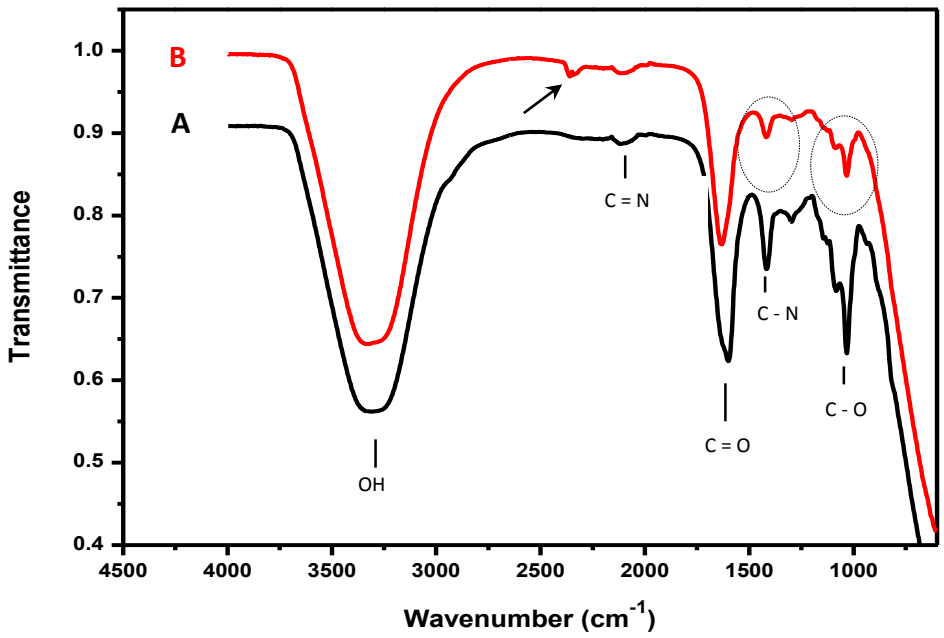


Figure 3.1: The FTIR spectra of (A) IDS before Fe (II) adsorption and (B) after Fe (II) adsorption.

Figure 3.2, represents FTIR spectrum of CB before and after Fe (II) biosorption. Functional groups; hydroxyl, alkynes, carboxylic acids, alkanes and alcohol were also observed. Davis et al., (2003) reported that these functional groups represented classes of organic compounds (carbohydrates, fatty acids, proteins, carbohydrates, nucleic acid, amino acid, cysteine, ATP, lipids and polysaccharides) found in biomass.

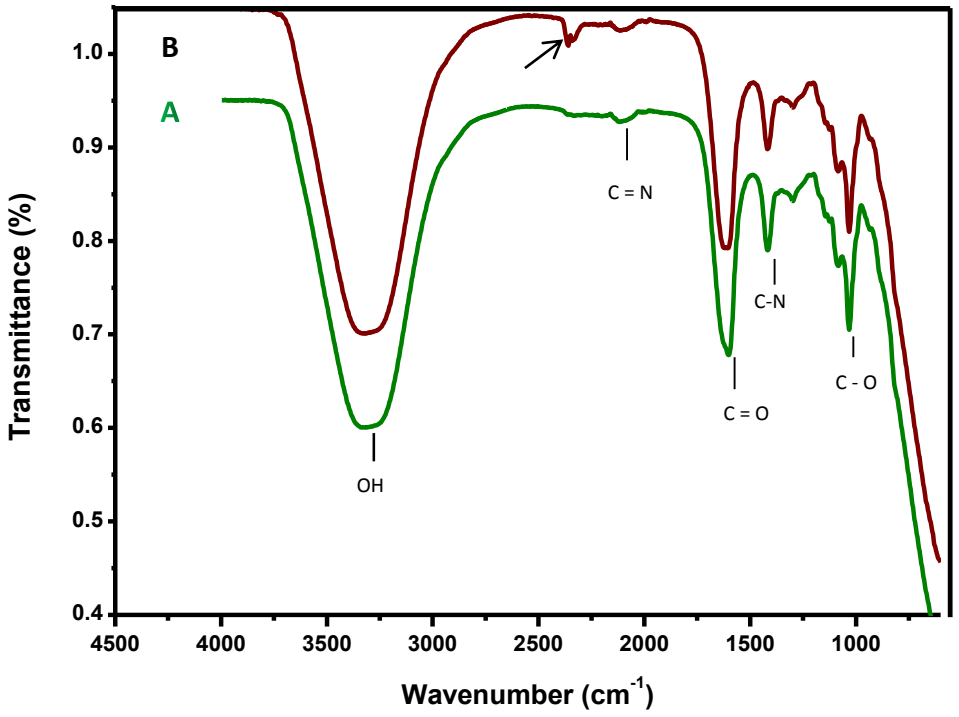


Figure 3.2: FTIR spectra of CB (A) before Fe (II) adsorption and (B) after Fe (II) adsorption

The peak density at 1604 cm^{-1} for carboxylic acidic of IDS experienced a lateral shift to 1637 cm^{-1}. The shift could be attributed to the displacement of proton by the divalent Fe (II) ion, following partial or complete esterification of the carboxylic sites (Pathak, 2015) (Smith, 2013). The same trend was observed for CB. FTIR shows that Fe (II) biosorption by IDS might have arose from bridging or bidentate complex formation with the carboxylate groups of the alginate consistent with the "egg-box" model (Davis et al., 2003). The second most abundant functional

group in IDS was the hydroxyl groups. Hydroxyl groups only become negatively charged at pH > 10, therefore, playing a secondary role in metal binding at low pH (Davis et al., 2003). A peak at 2363 cm^{-1} appeared on both IDS and CB after Fe (II) biosorption (Figure 3.1 and 3.2). The appearance of the band at 2363 cm^{-1}, can be attributed to the formation of Fe (II) chelation complexes on the microalgae membrane. Microalgae have the capacity to bind or chelate Fe in solution, due to a molecule called siderophore (Neilands, 1981). Siderophores have a high affinity for Fe. These molecules help harvest Fe, where Fe is used to build enzymes that catalyse biochemical reactions at key points in the nitrogen and carbon cycles.

(b) Environmental Scanning Microscopy (ESEM)

The surface structures of the IDS and CB were viewed under vacuum mode at various magnifications on an ESEM. The surface of the beads without microalgae showed no pores (Figure 3.3), while beads encapsulated with microalgae, IDS, showed numerous pores on the surface (Figure 3.4). The arrows aimed to clearly point out the pores found on the surface. The pores on the surface of the inoculated beads can be attributed to the gel surface cracking open due to the growth of the underlying colonies. The opening of the surface lead to the release of the colonies and Bailliez et al. (1985) reported an approximately 4 % of the microalgae biomass release in this process. The growth of the microalgae in the beads subsequently makes the beads more bulky and this might lead to a high metal uptake.

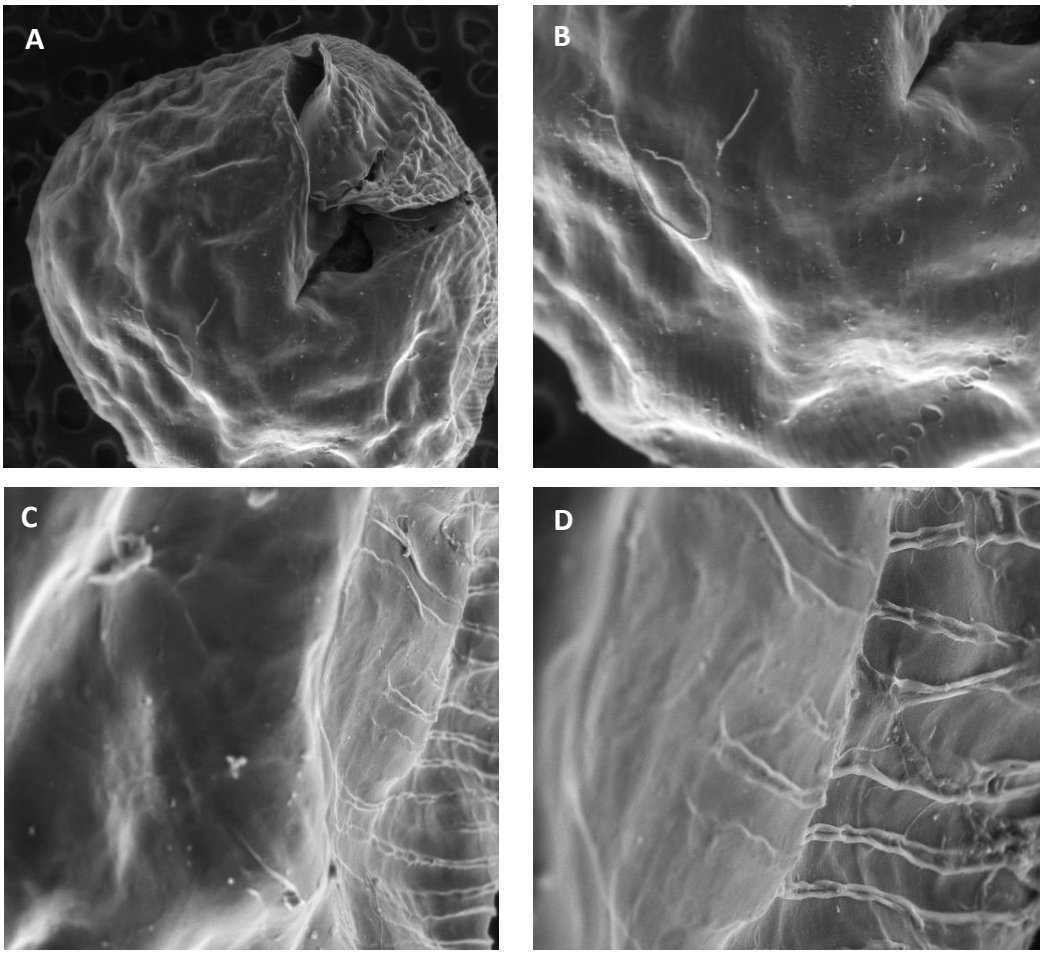


Figure 3.3: Surface topography by ESEM of CB before adsorption of Fe (II): (A) Mag =100 x, WD = 7.4 mm, 500 µm; (B) Mag = 200 x, WD = 6.5 mm, 400 µm; (C) Mag = 500 x, WD = 7.4 mm, 100 µm and (D) Mag = 1000 x, 7.6 mm, 100 µm.

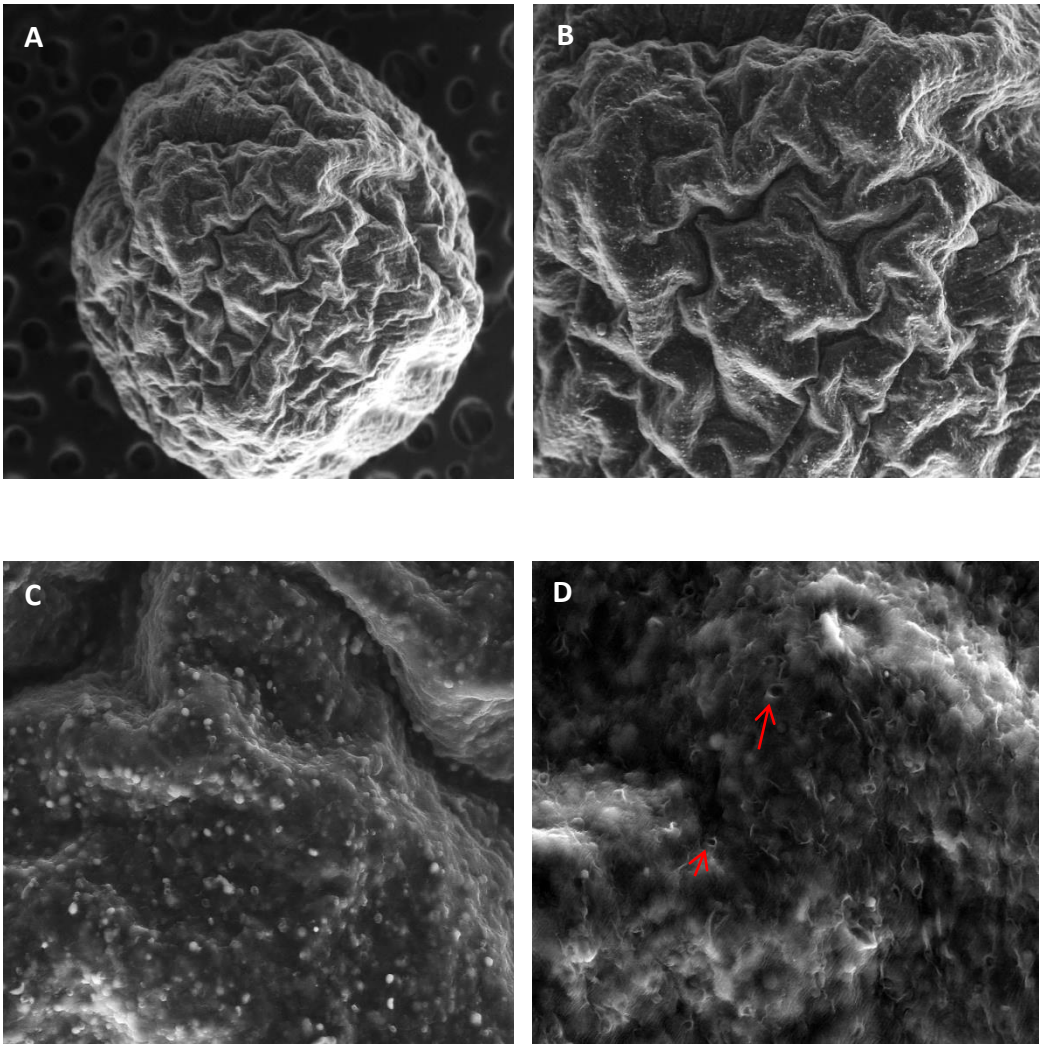


Figure 3.4: Surface topography by ESEM of IDS before adsorption of Fe (II): (A) Mag =100 x, WD = 6.8 mm, 500 µm ;(B) Mag = 500 x, WD = 6.8 mm, 100 µm; (C) Mag = 1000 x, WD = 6.8 mm, 100 µm and (D) Mag = 2000 x, 6.8 mm, 50 µm.

(c) Thermogravimetric analysis (TGA)

The evaluation of CB biomass degradation as a function of temperature was studied by using TGA on CB of various Na-alginate concentrations (3; 6; 9 and 12 % wt). Figure 3.5, shows TGA curves of CB. A rapid stepwise weight

loss was experienced between 30 °C – 200 °C for CB of 3 % wt Na-alginate, indicating a decomposition reaction during degradation. Similar results were observed and explained in depth in section 2.3.3, referring to Figure 2.6. CB of 6 %; 9 % and 12 % Na-alginate concentrations showed different types of decomposition reactions to CB at 3 %, during thermal sweeps. The major difference was that CB (3% wt Na) had two weight loss steps in the thermal degradation curve, whilst CB (6; 9 and 12 % Na) had four.

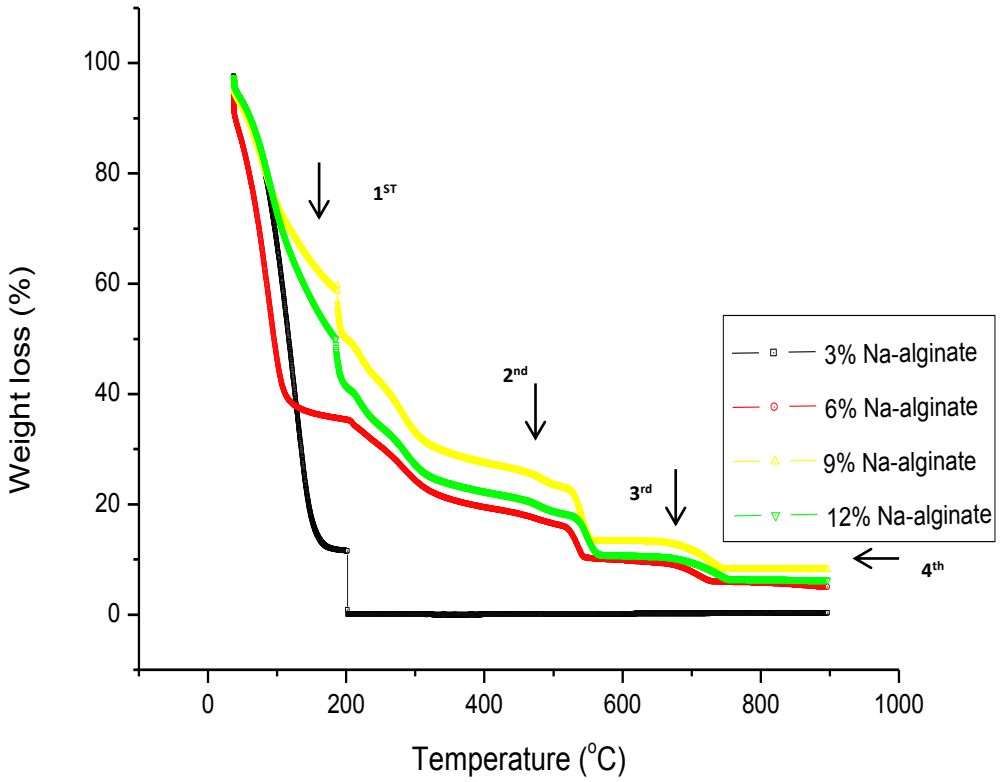


Figure 3.5: Shows TGA curves of CB when various concentrations of Na-alginate were used.

The first thermal sweep (30 °C – 200 °C) experienced by all the samples can be attributed to the presence of non-freezing water on the Ca-alginate beads (Widmann, 2001). This water reacts with polymeric chains as they form and subsequently form hydrogen bonds. During the thermal sweep, these water molecules are the first to leave the alginate samples. The second thermal sweep

(200 ^{o}C – 580 ^{o}C) reveals the decomposition of $CaC_2O_4.H_2O$ that might have formed CaC_2O_4, a stable calcium oxalate (Robinson, 1970). Further heating produced the third thermal sweep (580 ^{o}C – 760 ^{o}C). The third sweep forms $CaCO_3$, as obtained from reaction 3.1:

$$Ca(OO)_2 \underrightarrow{\Delta} CaCO_3 + CO \uparrow \qquad (3.1)$$

Since the subsequent degradation of the material is attributed to polymer matrix decomposition and reduction of metal oxides (Widmann, 2001), this therefore demonstrates that weight loss from the thermogram (Figure 3.5) is due to chemical reactions not physical transitions. It was observed that the increase in Na-alginate concentration shortened the thermal sweep extent. This can be attributed to the syneresis phenomenon (Veling & Mestdagh, 1995). This is a thermally activated reaction that leads to the shrinkage of the gel while liquid within the pores is expelled (Veling & Mestdagh, 1995). It is evident therefore, that an increase in Na-alginate concentration has an effect on the solid network texture of Ca-alginate matrix.

(d) Surface characterisation of the biosorbent

The BET, N_2-sorption surface and porosity measurements of CB (3 % wt Na) yielded 0.0504 m^2 / g; 0.0040 cm^3 / g and 314.9843 nm (SBET), (Vp), and (Dp), respectively. A single gram of the commercialized adsorbent, activated carbon, can have a surface area in the range of 500 – 2000 m^2 / g. Polymeric adsorbents have surface are in the range of 150 – 1000 m^2 / g. Diale et al. (2011a) found natural adsorbent, zeolite – clinoptilolite to have a SBET of 65 m^2 / g. The Na-alginate matrix surface area of 0.05 m^2 /g found in this study does not make the matrix suitable for effective heavy metal ion adsorption. However, with matrix

modification the material's properties could be enhanced and made suitable for effective heavy metal adsorption. The surface area of CB (6, 9 and 12 % wt) could not be calculated from the BET model, because the samples collapsed when nitrogen sorption was undertaken. To circumvent this, a mathematical model could be derived to calculate SBET from the pore volume of material.

Surface area is an important property for an adsorbent which is made for the purpose of adsorption. It is related to features such as pore volume and pore size, which are essential for accessibility of active sites and molecular transport. In this study, pore volumes for CB of 3; 6; 9 and 12 % wt was found to be 4; 2.9; 2.6 and 2.5 x 10^{-3} cm^3 / g, respectively. Pore volume drastically decreased from 4 x 10^{-3} to 2.9 x 10^{-3} cm^3 / g when Na-alginate concentration was increased from 3 to 6 % wt. A slight decrease of pore volume was observed from 6 to 9 % wt Na-alginate and no significant change occurred for 12 % wt Na-alginate when compared to 9 % wt. The decrease in pore volume experienced with an increase of Na-alginate concentration might have adverse impact on the surface chemistry of the adsorbent. The decrease of pore volume when Na-alginate concentration is increased can be attributed to the density cross-linking of the matrix being enhanced by the increase of Na-alginate concentration. A relatively solid cross-linked matrix is significant for lowering chances of enzyme leakage; however the matrix structure should still be porous enough to allow for effective diffusion through it. IUPAC classifies pores in nanometers (nm) as Trunschke (2013):

Macroporous	> 50 nm
Mesoporous	> 2 – 50 nm
Microporours	< 2 nm

The average pore diameter for CB (3 % wt Na-alginate) was found to be 314.98 nm, making the adsorbent macroporous in nature.

3.3.2 Batch adsorption studies

(a) Determination of the effect of pH on Fe (II) removal from solution

The effect of pH on adsorption capacity was studied for IDS and CB. The point of zero charge (pH_{pzc}) for biosorbents IDS and CB was obtained at pH values of 8.8 and 9.2, respectively (Figure 3.6).

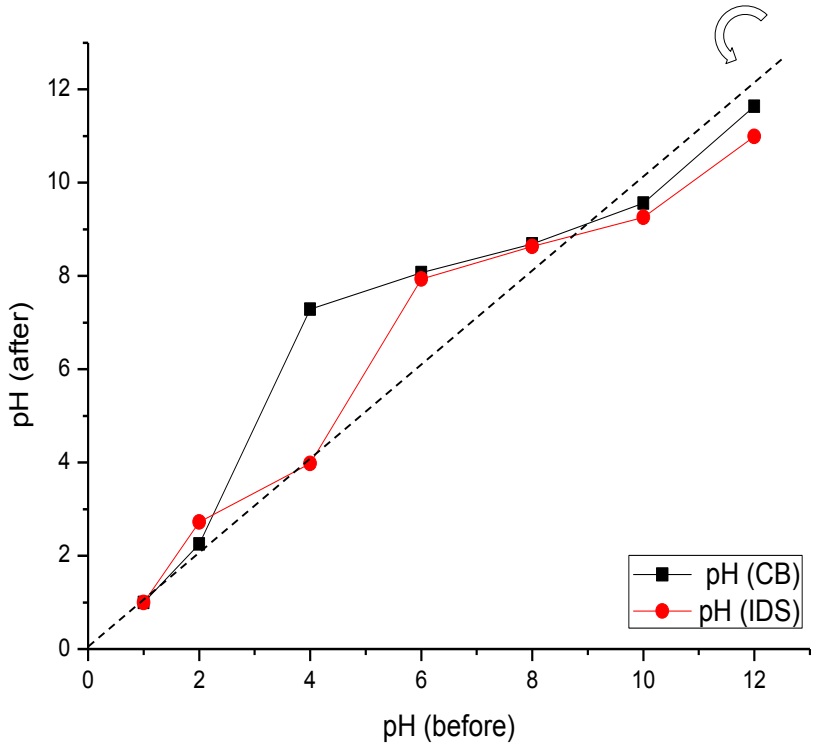


Figure 3.6: The point of zero charge (pH_{pzc}) for biosorbents IDS at pH 8.8 and CB obtained at pH 9.3.

At low pH values ($pH < pH_{pzc}$), the overall surface charge on the beads becomes positive. This has a potential to hinder biosorption of metal cations. At $pH > pH_{pzc}$, the adsorbent becomes negatively charged with a high metal uptake anticipated. When CB's surface was adjusted to pH 2, it was noted that 43 % of Fe (II) was

removed from solution (Figure 3.7). A steady increase of about 46 % was experienced at pH 6, before it plummeted at pH 7 to 38 %.

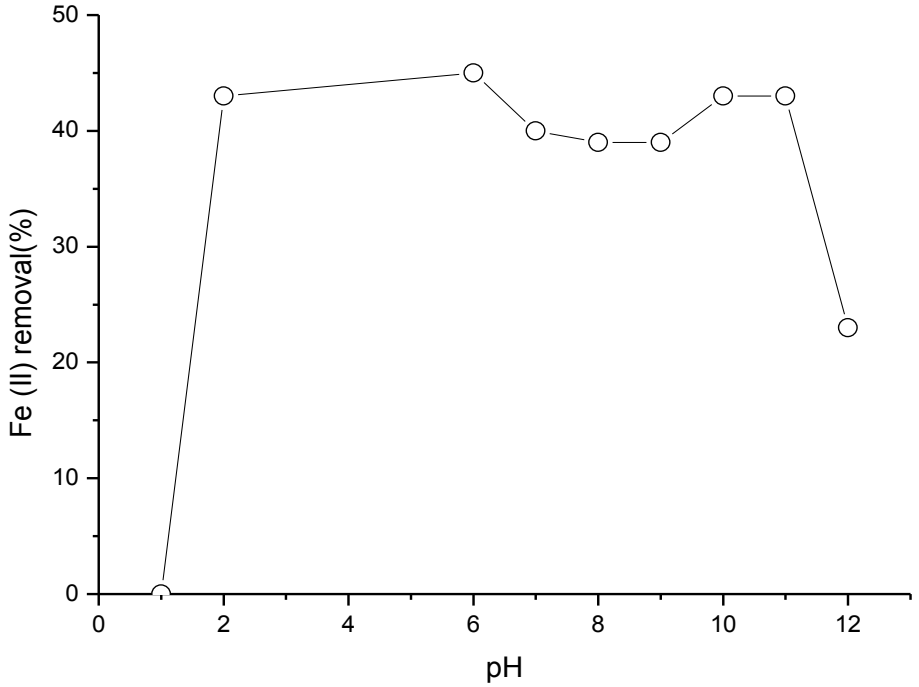


Figure 3.7: The Fe (II) ion uptake at different surface pH of CB.

Between pH 7 and 11 the metal uptake fluctuated until a dramatic dropped to 29 % at pH 12. The pH_{pzc} was experimentally determined to be pH 8.8 for CB, meaning the surface of the beads will have a positive charge at solution pH values less 8.8. This means anions may be adsorbed proficiently at this level. Conversely, the surface will have a negative charge at solution pH values greater than 8.8 and thus, the surface may adsorb cations proficiently. The surface's positivity did not inhibit the binding of positively charged Fe (II) ions between pH 1 and 6. This can be attributed to the acidic functional group (as explained in section 2.3.4) generating a negatively charged surface at acidic pH and electrostatic interaction between cationic species and surface. When pH increases, the functional sites become deprotonated, so their negative charges increase and permit binding to

metal cations to higher extents. At high pH it is expected that Fe (II) to precipitate leading to high sorption rates. This however did not happen from pH 7 – 9, as metal removal from solution decreased. A slight increase in metal removal was experienced from pH 10 to 11. Monteiro et al., (2009) reported an increase in metal sorption with increasing pH in removing Cd (II) and Zn (II) with *Desmodesmus pleiomorphus*. At higher pH levels, precipitation of Fe (II) occurs, thus explaining the decrease in extent of metal removal at pH 11.

(b) Determination of the effect of bead diameter on Fe (II) removal from solution

The effect of bead size was studied CB and IDS, Figure 3.8 and 3.9, respectively. A decrease in the immobilized biomass bead size led to an increase in metal uptake and increase in adsorption of Fe (II) ions.

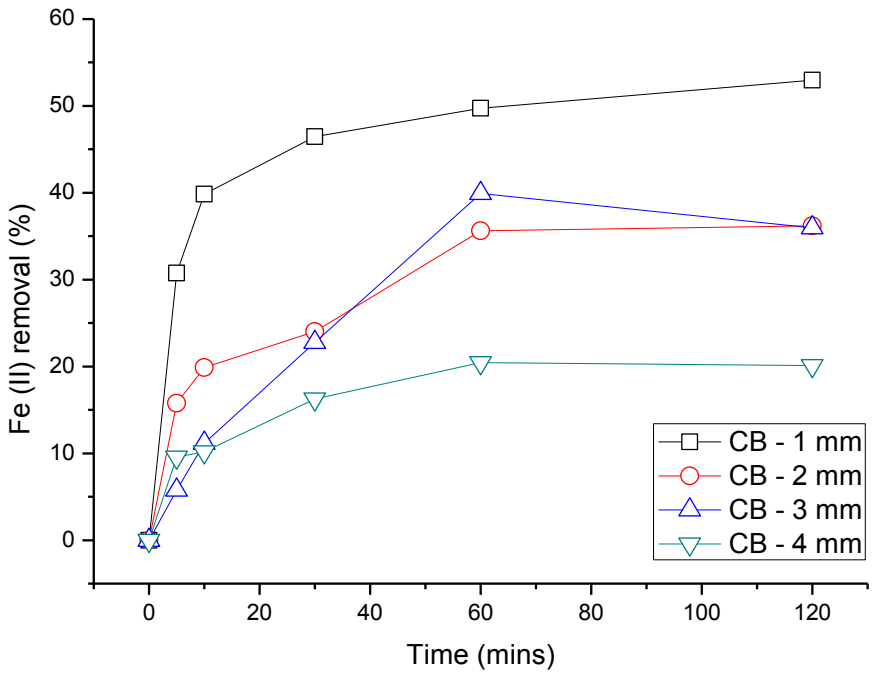


Figure 3.8: Removal Fe (II) ion concentration with time when 1; 2; 3 and 4 mm CB are used.

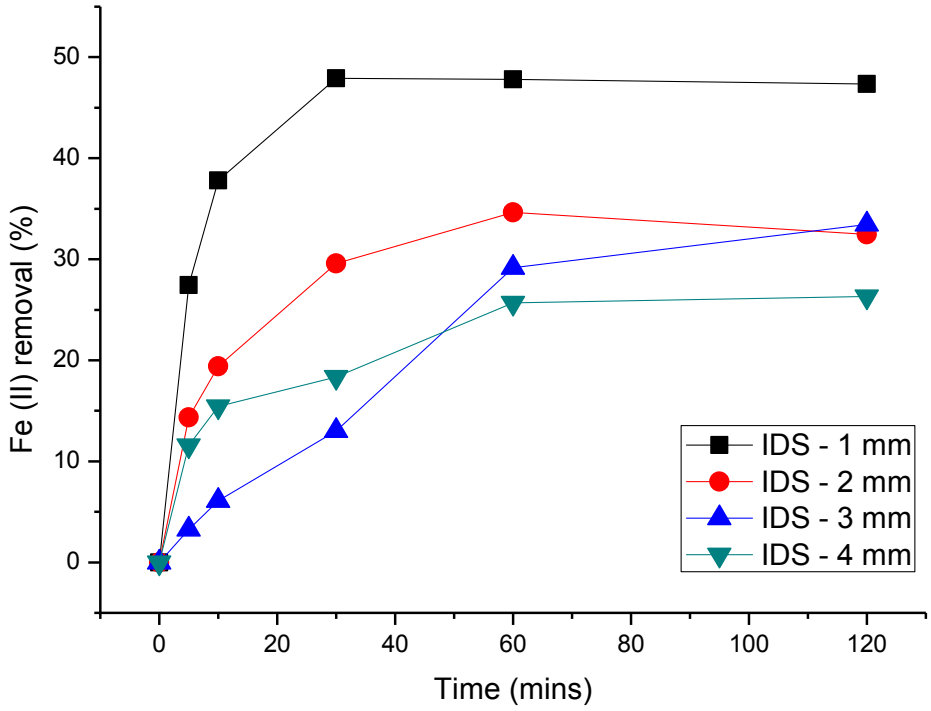


Figure 3.9: Removal of Fe (II) ion concentration with time when 1; 2; 3 and 4 mm IDS are used.

Maximum absorption was reached at 52 % for 1mm after 120 minutes, followed by 4mm at 48 %; 3mm at 40 % and 2mm at 35 % after, 120 minutes, 60 minutes and 120 minutes, respectively. CB obtained maximum absorption of 48 % for 1mm after 30 minutes, followed by 35 % for 2 mm in 60 minutes. Percentage removal for CB for diameter 3 mm was recorded at 34 % after 120 minutes and 27 % for 4mm after 120 minutes. The smallest bead size (1mm) showed to have the most effective Fe (II) uptake.

(c) Effect of biomass concentration on Fe (II) removal from solution

The amount of Fe (II) removed by IDS at bead size 1 mm and initial metal concentration of 120 mg/L was shown to be affected by the variation in biomass concentration (Figure 3.10).

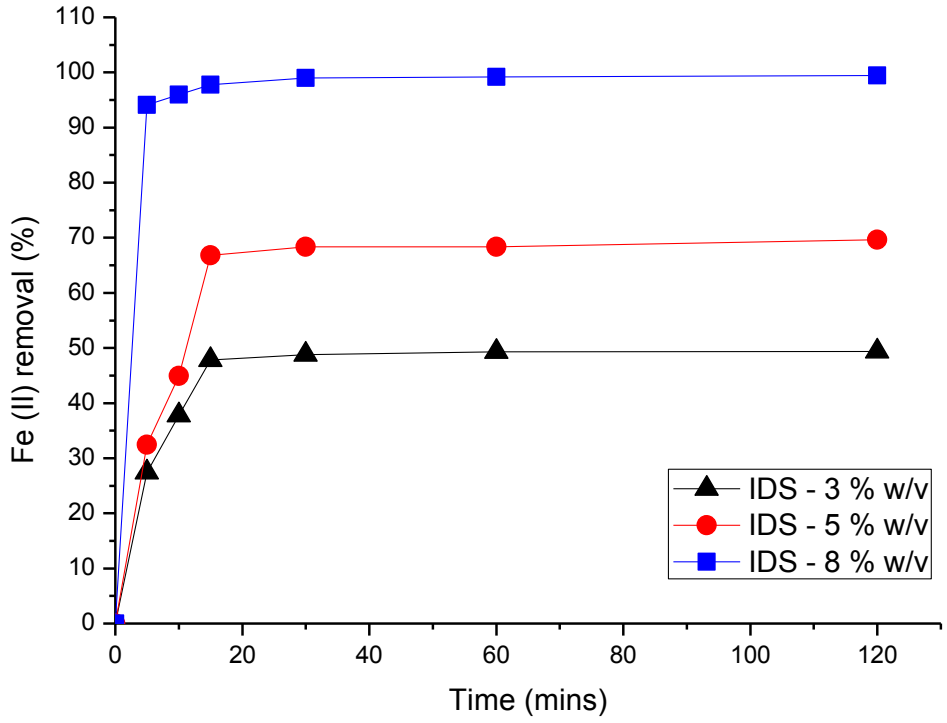


Figure 3.10: Removal of Fe (II) ion concentration in the presence of beads with various biomass concentrations.

In this study, increasing the biomass concentration of microalgae from 3 % w/v, 5 % w/v to 8% w/v showed an increase in metal uptake from 48 %, 69 % and 98, % respectively. This may be attributed to the fact that an increase in biomass concentration leads to a higher number of metal-binding sites available for Fe (II) to bind on. The increase of microalgae concentration in the Ca-alginate matrix has increased its metal binding efficacy. As seen in Figure 3.5, colonies formed by the microcells in the matrix expand and end up leaking from the matrix. These

experiments were conducted with Na-alginate concentration of 3 % wt, which was found to be not form a solid enough matrix (Figure 3.6).

(d) Effect of Na-alginate concentration on Fe (II) removal from solution

The effect of Na-alginate concentration in CB for Fe (II) uptake was investigated and results are represented in Figure 3.11. After 5 minutes 3 % of Fe (II) was removed by CB containing 3 % Na-alginate. CB of 6, 9 and 12 % Na-alginate gave removal % of 22, 23 and 25 in the first 5 minutes of adsorption, respectively. At these Na-alginate concentrations, the rapid removal rate came to a halt after 60 minutes where equilibrium was reached. The equilibrium metal removal was reached at 33, 36, 39 and 45 % for CB of 3, 6, 9 and 12 % Na-alginate, respectively. It is therefore observed that an increase in Na-alginate concentration lead to the increase in metal uptake ability of the beads. When Na-alginate is increased, it is assumed that the number of biopolymer molecules per unit solution volume, which are the binding sites for Ca (II) ions also increase (Blandino et al., 1999). The cross-linking between the biopolymer molecule and Ca (II) ions becomes dense, leading to a more permeable bead structure.

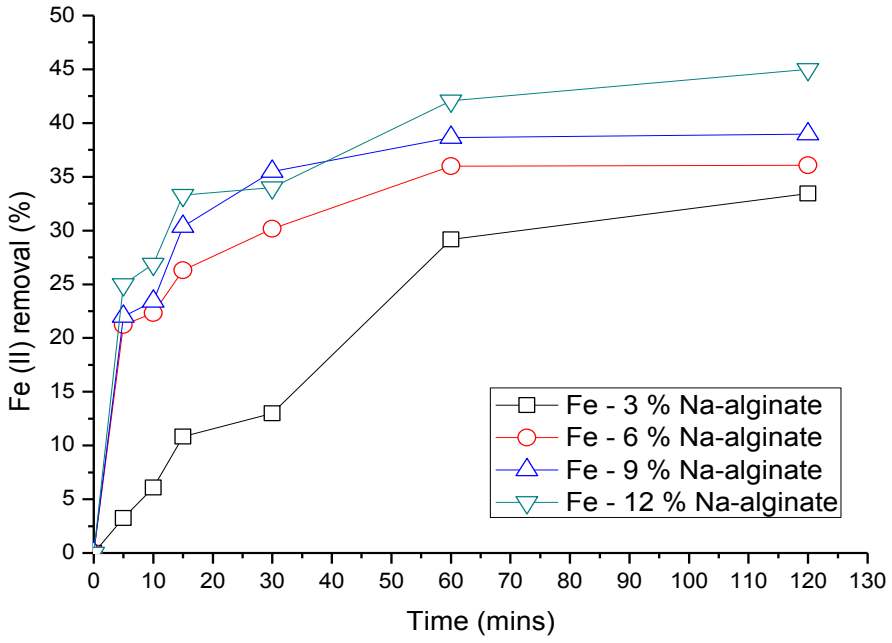


Figure 3.11: Removal of Fe (II) ion concentration in the presence of beads with various Na-alginate concentrations.

(e) Effect of $CaCl_2$ concentration on Fe (II) removal from solution

The effect of $CaCl_2$ concentration in CB for Fe (II) uptake was studied and the results are represented in Figure 3.12. When 2 % wt $CaCl_2$ was used the equilibrium Fe (II) ion removal % was found to be 33 %. This was higher than CB of $CaCl_2$ concentrations at 9 and 12 % wt, but lower than that of CB at 6 % wt of $CaCl_2$. The Fe (II) removal % obtained was 33, 67, 30 and 27 for 2, 6, 9 and 12 % wt of $CaCl_2$ in CB. The increase of $CaCl_2$ concentration when forming Ca-alginate matrix, thickens of the gel film and the gelation time required increases (Blandino et al., 1999). The increased thickness of the gel film might have prohibited the Fe (II) ions from diffusing into the beads, leading to a low metal removal, when $CaCl_2$ concentration was increased.

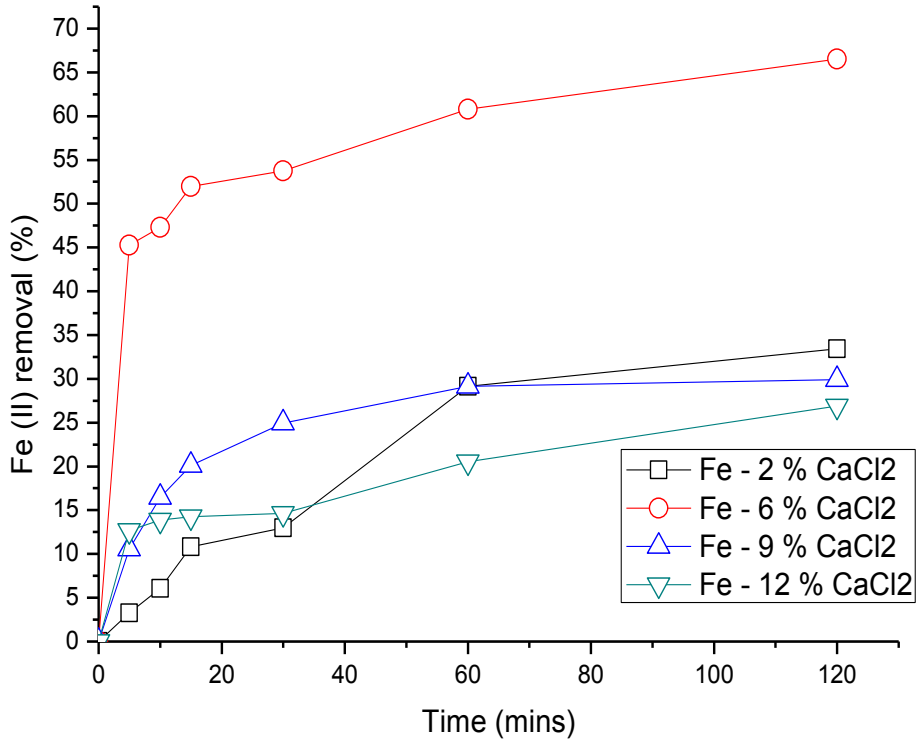


Figure 3.12: The removal of Fe (II) ion concentration in the presence of beads with various $CaCl_2$ concentrations.

3.4 Bead parameters for further adsorption study

The aim of this chapter was to investigate and determine optimal gel formation properties that will be used to create a stable Ca-alginate matrix, suitable for immobilizing DS to be used for heavy metal removal in aqueous solutions. Based on the above observations, the following bead parameters were selected for further work such as: equilibrium batch and packed bed column studies:

Bead size:	3mm
Biomass loading:	8% w/v
Na:	9 % wt
Ca:	6 % wt

In this study it was found that bead diameter 1 mm gave a relatively high metal uptake percentage and should be used for further work. However due to limitations in the laboratory the bead diameter that was chosen was 3 mm. This was due to the viscosity of Na-alginate and DS blend that caused the extrusion of spherical droplets from the syringe and needle almost impossible. The bead diameter of 3 mm was therefore chosen for practical reasons. All other parameters, like: $CaCl_2$ and biomass concentration were chosen based on them giving a better performing Ca-alginate matrix when used. The parameters chosen therefore for this study were combined and investigated. Figure 3.13 shows plots obtained when the parameters listed above where used to make CB and IDS for Fe (II) ion removal in aqueous solution for 5 days (120 hours).

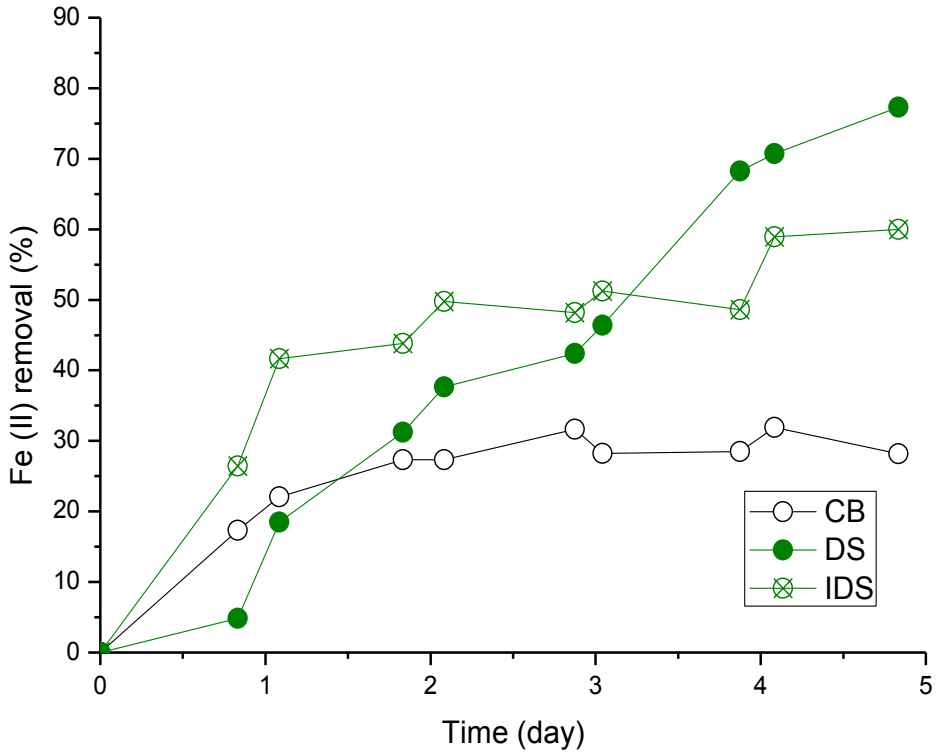


Figure 3.13: Removal of Fe (II) ion concentration in the presence of CB and IDS using parameters observed to be best for metal Fe (II) adsorption and compared to the DS performance.

It was observed that Fe (II) removal was high when IDS was used compared to CB and DS, with removal % of: 5, 17 and 26 reached after 0.83 day, respectively. The removal of Fe (II) ions from solution remained around 32 % after 5 days, when CB was used. A steady increase in Fe (II) ion removal was observed when IDS was used, reaching 60 % removal after 5 days. An exponential increase in metal removal of Fe (II) was observed when DS was used, reaching 77 % removal. Therefore, after 5 days the sequence based on biomass used for Fe (II) removal is:

DS >> IDS >> CB.

3.5 CONCLUSION

Immobilized *Desmodesmus sp.* was effectively used for the removal of Fe (II) ions from aqueous solution.

Inoculated beads showed a porous surface when viewed under an ESEM, confirming active growth within the alginate beads.

Carboxylic acid and hydroxyl, sulphonic acid, alkynes and alcohol groups were functional groups determined by the FTIR to be actively involved in Fe (II) removal from aqueous solution.

The point of zero charge was found at pH 8.6; while the optimum beads size was determined to be 1 mm with biomass loading of 8% (w/v) using Ca-alginate of 9 % Na-alginate and 6 % $CaCl_2$.

Based on the above observations, the following bead parameters were selected for equilibrium batch studies and packed column studies: Bead size: 3mm; Biomass loading: 8% w/v; Na: Ca (%): 6:9.

CHAPTER 4

Fe (II) SORPTION MECHANISM AND KINETIC MODELLING STUDY ON IMMOBILIZED *Desmodesmus sp.*

4.1 Introduction

4.1.1 Adsorption isotherms and kinetic models for immobilized microalgae

The potential use of immobilized microalgae, *Desmodesmus sp.,* and it's efficacy in removing toxic heavy metals from aqueous solutions was studied in the present work. The experimental results were fitted to the Langmuir and Freundlich isotherm models to study the equilibrium loading capacity of the biomass in the presence of heavy metals in aqueous solution. These models are simple, well-established and are easily interpretable, which are some of the important reasons for their frequent and extensive usage (Vijayaraghavan & Yun, 2008). Kinetic studies were conducted and defined if they were either pseudo-first order or pseudo-second order fitting. Water stream heavy-metal contamination from industrial operations such as mining is normally remediated using: limestone neutralization; gypsum crystallization and oxidation by aeration. These methods have been proven to be effective in removal of metal ions, however have also been proven to be difficult and costly processes (Aderhold et al., 1996).

4.1.2 Objectives

The aim of this chapter is to study the maximum loading capacity of IDS when optimized gelling parameters (section 3.4) were used. Also the adsorption kinetics and diffusivity will be studied.

4.2 Experimental methods and materials

4.2.1 Chemicals

Hydrated metal salts of analytical grade: $FeSO_4.7H_2O$; Cr $(NO_3)_3.9H_2O$; $MnSO_4H_2O$ and an anhydrous $NiCl_2$ (all from Merck, South Africa) were used for adsorption experiments. Nitric acid (HNO_3) (65 %), hydrochloric acid (HCl) (37 %) and sulphuric acid (H_2SO_4) (90 – 99 %) were used for pH adjustment. Stock solutions of metal ions (120 mg/L) were prepared with deionized water, obtained from Direct-Q®3, ultrapure water system. Na-alginate and $CaCl_2$ were used for cell immobilization (both obtained from Sigma-Aldrich, South Africa).

4.2.2 Preparation of immobilized algae cells

Preparation of Ca-alginate clear beads (no microalgae present) and IDS (immobilized *Desmodesmus sp.*) are highlighted in section 2.2.2.

4.2.3 Batch adsorption study

Batch sorption experiments were performed by adding 50 mL of metal aqueous solution, with initial concentration of 120 mg/L at pH 2.5; with 5 g of IDS and CB. The experiments were performed on an orbital shaker (MRC Scientific Instruments, UK) at constant agitation of 180 rpm in 250 mL Erlenmeyer flasks. Samples were collected at intervals of 5; 10; 15; 30; 60 and 120 minutes. The solution was filtered on a Whatman cellulose nitrate membrane filters (0.45 µm), diameter of 47 mm, and beads were separated from the supernatant. Heavy metal present in filtrates were quantified using Inductively Coupled Plasma-optical emission spectroscopy (ICP-OES; Perkin Elmer Optima-3300 RL, USA). The amount of Fe (II) ions adsorbed per unit amount of total biomass, represented as Qe, with

unit (mg metal / g alga) ≡ (mg/g) was calculated using the following mass balance equation (equation 4.1):

$$Q_e = \frac{(C_0 - C_e)V}{m} \qquad (4.1)$$

Where,

C_0 = initial concentration (mg/L)

C_e= equilibrium concentration (mg/L)

V = volume of aqueous solution (L)

m = the mass (g) of the adsorbent

Both Qe and qe are concentrations of metal in the solid phase, however these needed to be distinguished as Qe is for isotherm equilibrium study and qe is for kinetics study.

4.2.4 Sorption isotherm and kinetic modelling

In this study equilibrium isotherm models were used to explain experimental behaviour of IDS adsorption of metal ions adsorption. Langmuir and Freundlich sorption isotherms were used to study experimental adsorption data. These sorption isotherms express the relation between the amount of adsorbed metal ions per unit mass of biosorbents and the metal. For Langmuir sorption isotherm the following assumptions are valid (Pathak & Choppin, 2009):

i. Surface that has a specific number of sites where the solute molecules can be adsorbed.

ii. Adsorption involving attachment for only one layer of molecules to the surface, i.e. monolayer adsorption.

The Langmuir sorption isotherm is expressed linearly in equation 4.2, with *b* being the Langmuir constant:

$$\frac{Ce}{qe} = \frac{Ce}{q_{\max}} + \frac{1}{bq_{\max}} \tag{4.2}$$

Freundlich sorption isotherm is assumed to describe both multilayer sorption and sorption on heterogeneous surfaces (Lewinsky, 2007). The empirical Freundlich equation is based on the amount of a substance adsorbed Q_e in relation to the concentration C_e and is represented by the equation 4.3:

$$\log Qe = \log K_f + \frac{1}{n}\log Ce \tag{4.3}$$

Where Qe is the adsorption on the adsorbent at equilibrium, the slope and intercept of the linear Freundlich equation are equal to 1/n and log K_f, respectively. The Freundlich isotherm is linear if 1/n = 1 and 1/n < 1 makes the isotherm nonlinear (Lewinsky, 2007). K_f is the Freundlich isotherm constant and is expressed in unit ($mg^{1-(1/n)}$).

The study of adsorption kinetics in metal removal is paramount as it provides valuable insights into the reaction pathways and into the mechanism of adsorption reactions. In this study, the kinetics of Fe (II) ion uptake rate onto immobilized algal biomass was studied using pseudo-first and pseudo-second order adsorption kinetic models. The solute uptake rate controls the residence time of sorbate

uptake at the solid-liquid interface (Ho, 2004). Pseudo-first order equation 4.4 was first expressed by Lagergren in 1898 as:

$$\frac{d_{q_t}}{d_t} = k_1(q_e - q_t) \tag{4.4}$$

Integrating this for the boundary conditions t = 0 to t = t and q_t = 0 to $q_t = q_t$, equation 4.4 may be rearranged for linearized data plotting as shown by equation 4.5:

$$\log(q_e - q_t) = \log(q_e) - \frac{k_1}{2.303}t \tag{4.5}$$

Where, k_1 is the rate constant of first order sorption (1 / min). A plot of $\log(q_e - q_t)$ against t, gives a straight line. The pseudo-second order equation is not based on concentration of solution like the pseudo-first order, but on adsorption equilibrium capacity (Ho & McKay, 1998a) and is expressed as (equation 4.6):

$$\frac{dq_t}{d_t} = k_2(q_e - q_t)^2 \tag{4.6}$$

and equation 4.6 can be rearranged to give equation 4.7:

$$\frac{t}{q_t} = \frac{1}{k_2 q_e^2} + \frac{1}{q_e} t \qquad (4.7)$$

Where k_2 is the rate constant of second order sorption (g/mg.min). A plot of $\frac{t}{q_t}$ vs. t, gives a straight line. The rate constant can be calculated from the intercept and the adsorption at equilibrium can be obtained from the slope.

4.2.5 Determination of the Effective Diffusivity

When substances are brought together they intermix and diffusion occurs. Diffusion takes place rapidly in case of gases onto a solid and to a lesser extent to liquid. The shrinking core model (SCM), applied by Levenspiel (1972) to fluid particle chemical reactions, and more specifically to ionic exchange of heavy metals by Rao & Gupta (1982), assumes that the diffusion through a reacted shell is the limiting step and that an unreacted core is shrinking as time proceeds (Ara6jo & Teixeira, 1997). The SCM is schematically depicted in Figure 4.1. If *C* is the metal concentration in the bulk solution at any time *t*, the flux of the metal in the spherical clarified sludge particle can be obtained by integrating the diffusion equation at pseudo-steady state taking diffusivity as a constant, concentration independent parameter of the system.

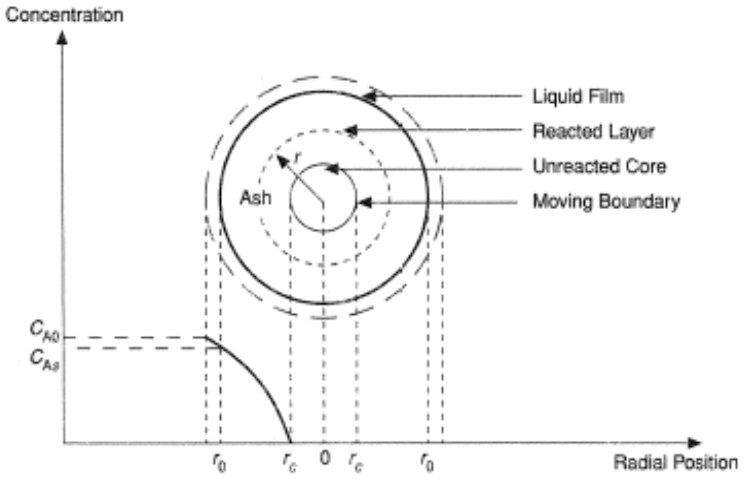


Figure 4.1: Schematic representation of shrinking core model of a spherical particle (Naiya et al., 2009).

The IDS and CB adsorbents are assumed to have a spherical shape with diameter same as that of volume-surface mean diameter of the distribution obtained by screen analysis. Pseudo-steady state diffusion of the adsorbed heavy metal, Fe (II), through a spherical shell in the particle of beads (Figure 4.1) is assumed (Naiya et al., 2009). The rate of uptake of the metal at any instant is equated to the rate of removal of the same from the solution. Liquid side resistance to mass transfer is neglected as the solution is vigorously shaken. The diffusivity of Fe (II) ions through IDS and CB is analysed and in the case of a process controlled by the diffusion of metal ions through the liquid film (*film diffusion control)* the extent of the biosorption process as a function of time will be given by expression, equation 4.2:

$$X = \frac{3D}{\delta R C^0} \int_0^t C dt \qquad (4.8)$$

Where,

X = Ratio between the amount of solute at solid phase at time t and at equilibrium (dimensionless)

R = radius of a spherical bead (cm)

D =Effective diffusion coefficient of the solute in the solid phase ($m^2.s^{-1}$)

C_0 = concentration of Ca ions at the outer surface of the gelled layer (mol/L)

C = concentration of Ca ions in the gelled layer (mol/L)

Da = Diffusion coefficient ($m^2.s^{-1}$)

If the film is diffusion controlled, a plot of X vs $\int_0^t C\ dt$ will yield a straight line relationship. If the process is controlled by the diffusion through reacted shell (*particle diffusion control*), the model is therefore represented by equation 4.3 (Beolchini et al., 2003):

$$F(X) = 1 - 3(1-X)^{\frac{2}{3}} + 2(1-X) = \frac{6Da}{R^2 C^0}\int_0^t C dt \qquad (4.9)$$

Where,

C = concentration of Ca ions in the gelled layer (mol/L)

C^o = concentration of Ca ions at the outer surface of the gelled layer (mol/L)

Da = Diffusion coefficient ($m^2.s^{-1}$)

X = Ratio between the amount of solute at solid phase at time t and At equilibrium (dimensionless)

Consequently, in the case of particle diffusion control a plot of function $F\ (X)$ vs $\int_0^t C\ dt$ will give a straight line.

4.3 Results and Discussion

4.3.1 Metal sorption system

The amount of Fe (II) adsorbed per unit amount of biosorbents using various initial concentrations is represented in Figure 4.2. Initial concentrations of 5; 60; 120; 240; 480 and 1000 mg/L were studied and gave the following Qe values (mg/g): 0.04; 0.22; 0.52; 1.4; 2.13 and 2.16, respectively. An increase in Fe (II) ion concentration showed a direct effect on the amount of metal adsorbed onto the adsorbent. Saturation was observed when concentrations of 480 mg/L and 1000 mg/L were used. The Qe values went from 2.13 to 2.16 mg/g with only a variation of 0.03 mg/g when concentrations were increased by about 2 folds. This is clearly illustrated in Figure 4.2.

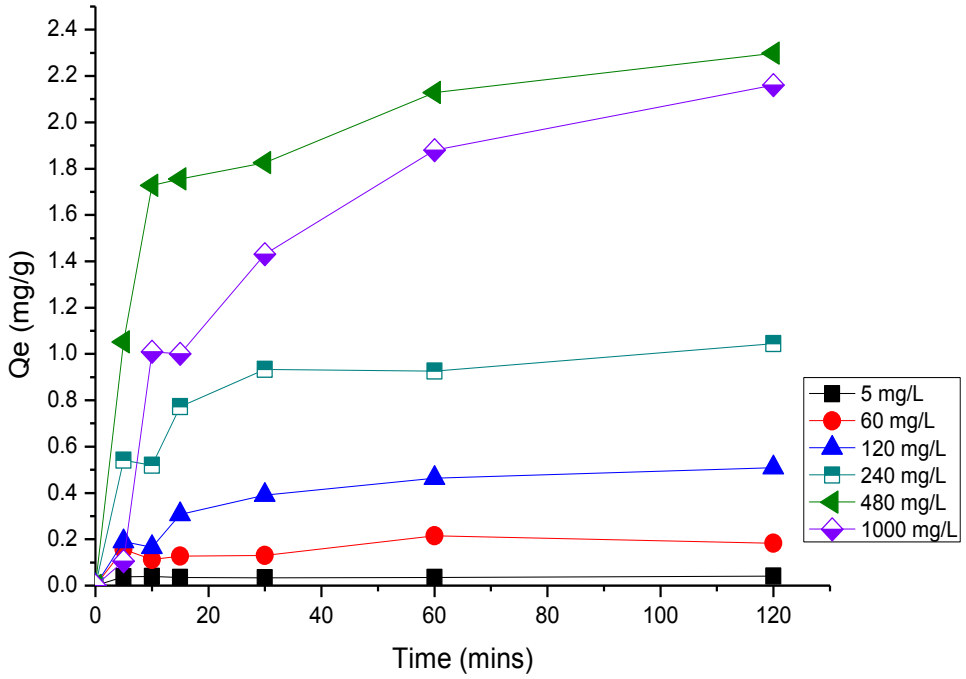


Figure 4.2: Fe (II) ion concentration in solution was increased from 5 – 1000 mg/L, these plots show the loading capacity of IDS at various concentrations used.

Fig. 4.3 shows the maximum amount of Fe (II) adsorbed per unit amount of absorbent in 120 minutes when concentrations of 5; 60; 120; 240; 480 and 1000 mg/L were used. A maximum loading capacity of 2.3 and 2.2 (mg/g) was obtained when concentrations of 480 and 1000 mg/L were used, respectively. No significant change in the amount Qe when these initial concentrations were used ; may imply that all binding sites in the IDS adsorbent are saturated by the Fe (II) ions in solution.

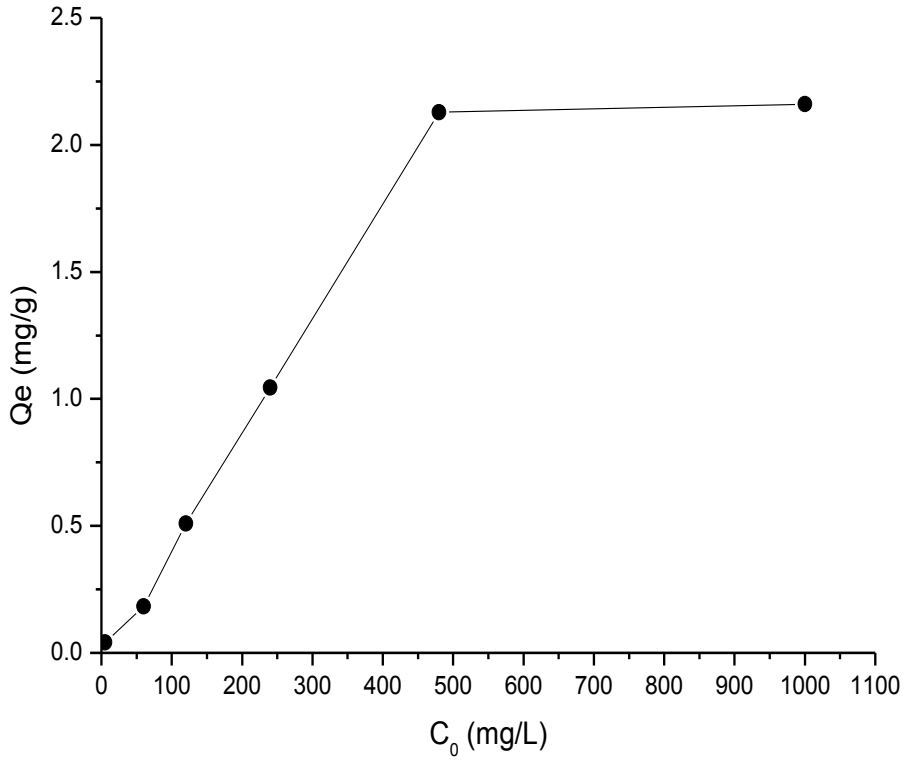


Figure 4.3: Maximum amount of Fe (II) adsorbed per unit amount of absorbent at various initial concentrations

A surface active site model was developed from Figure 4.3 by Prof. Diane Hildebrandt (equation 4.10 – 4.18). This model was used in quantifying the

amount of possible binding sites in IDS. The model is based on the assumption that the loading of metal ions onto the sorbent is a reversible process.

$$k_f C_{Fe}^{\infty} N_e^{\infty} = k_r N_0^{\infty} \tag{4.10}$$

$$N_T = N_e^{\infty} + N_0^{\infty} \tag{4.11}$$

$$N_0^{\infty} = V(C_{Fe}^0 - C_{Fe}^{\infty}) \tag{4.12}$$

$$k_f C_{Fe}^{\infty} (N_T - N_0^{\infty}) = k_r N_0^{\infty} \tag{4.13}$$

$$\frac{k_f}{k_r} C_{Fe}^{\infty} N_T = N_0^{\infty} + \frac{k_f}{k_r} C_{Fe}^{\infty} N_0^{\infty} \tag{4.14}$$

$$\frac{k_f}{k_r} C_{Fe}^{\infty} N_T = N_o^{\infty} \left(1 + \frac{k_f}{k_r} C_{Fe}^{\infty} \right) \tag{4.15}$$

$$\frac{k_f}{k_r} C_{Fe}^{\infty} N_T = V(C_{Fe}^0 - C_{Fe}^{\infty}) \left(1 + \frac{k_f}{k_r} C_{Fe}^{\infty} \right) \tag{4.16}$$

$$\left(\frac{k_f}{k_r} \right) N_T \frac{C_{Fe}^{\infty}}{V\left(C_{Fe}^0 - C_{Fe}^{\infty}\right)} = 1 + \frac{k_f}{k_r} C_{Fe}^{\infty} \tag{4.17}$$

$$\boxed{\frac{C_{Fe}^{\infty}}{V\left(C_{Fe}^0 - C_{Fe}^{\infty}\right)} = \left(\frac{k_r}{k_f} \right) \frac{1}{N_T} + \frac{1}{N_T} C_{Fe}^{\infty}} \tag{4.18}$$

Where,

CFe^{∞} = equilibrium concentrations of Fe (II) solution (mg/L)

CFe^0 = initial concentrations of Fe (II) solution (mg/L)

k_r = rate constant for the reverse reaction

k_f = rate constant for the forward reaction

N_0^{∞} = initial number of binding sites

N_e^{∞} = number of binding sites at equilibrium

N_T = total number of binding sites

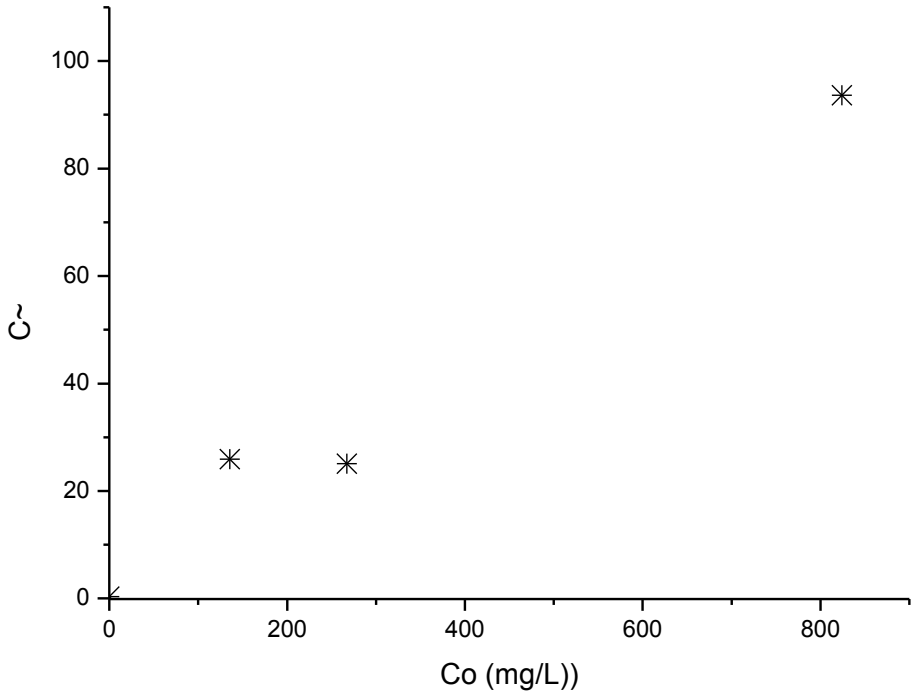


Figure 4.4: Evolution of metal adsorption at various initial concentrations. C_0 = C^{∞} and C~ =

$$\frac{C_{Fe}^{\infty}}{V\left(C_{Fe}^{0}-C_{Fe}^{\infty}\right)}$$

A linear graph was obtained (Figure 4.4) when plotting $\frac{C_{Fe}^{\infty}}{V\left(C_{Fe}^{0}-C_{Fe}^{\infty}\right)}$ vs. C_{Fe}^{∞} equation 4.16. The slope, $\frac{k_r}{k_f}$ was found to be 147.21 and the total number of binding sites N_T was found to be 0.061.

4.3.2 Metal binding mechanism

The FTIR spectra of IDS before and after adsorption of Fe (II) ions were shown in section 3.3.1 (Figure 3.1). In order to understand the Fe (II) binding mechanism the FTIR spectra must be used. It was observed that functional groups that could be responsible for Fe (II) ion sorption are: -OH stretch; symmetrical alkaynes; C=O stretch; symmetric bending of CH_3; -CO stretching of ester groups. Shifts were noticed for bands 3346 and 1604 cm^{-1} after Fe (II) adsorption, suggesting that carboxylic group and hydroxyl group mainly participated in Fe (II) ions interaction on immobilized algal beads. The changes in IDS FTIR spectra before and after Fe (II) adsorption are summarized in Table 4.1.

Table 4.1: The FTIR spectral characteristics of immobilized algal beads before and after adsorption of Fe (II) ions

IR peak	**Frequency (cm^{-1})**			**Assignment**
	Before adsorption	**After Adsorption**	**Differences**	
1	3346	3370	+24	-OH stretch
2	2133	2147	+14	Symmetrical alkynes
3	1604	1640	+36	C=O stretching
4	1421	1421	0	Symmetric bending of CH_3
5	1034	1036	+2	-CO stretching of ester groups
6	-	2363	-	

At pH 2.5, the carboxylic group may have formed into carboxylate ions due to deprotonation. Anions on the surface of the microalgae (DS) could be responsible for electrostatic interaction with positively charged Fe $(OH)_2$ species (Aryal & Liakopoulou-Kryriakides, 2013). Hydroxide ion (-OH) has three lone pair on the oxygen atom making it negatively charged. As a ligand, it can act as a Lewis base by donating a lone pair from O – atom to Fe (II) -atom forming a covalent bond. Thus possible mechanism of Fe (II) binding with carboxylic and hydroxyl groups on biomass surface is given by reactions (4.1 – 4.4):

$$R\text{-}COOH \longleftrightarrow R\text{-}COO^- + H^+ \quad (4.1)$$

$$2R\text{-}COO^- + Fe^{2+} + (OH)^- \longleftrightarrow (R\text{-}COO\text{-})_2\text{-}Fe(OH) \quad (4.2)$$

$$R\text{-}OH^- + H^+ \longleftrightarrow R\text{-}OH_2^- \quad (4.3)$$

$$R\text{-}OH_2^- + Fe(OH)_2 \longleftrightarrow [R\text{-}(OH)^-\text{: } Fe\ (OH_2)]_2 + H^+ \quad (4.4)$$

Fe (II) atom can coordinate four ligands and exhibit an octahedral coordination because; it consists of free d-orbitals presence in its electronic structure ([Ar] 4S03d6). Therefore, the possible structure of the compound obtained by the interaction between Fe $(OH)_2$ ion and biomass surface functional groups may be represented by following scheme (Figure 4.5), this is similar to the study conducted by Aryal & Liakopoulou-Kryriakides (2013) who used *Pseudomonas sp.* biomass to remove Fe (III) ions from aqueous solutions:

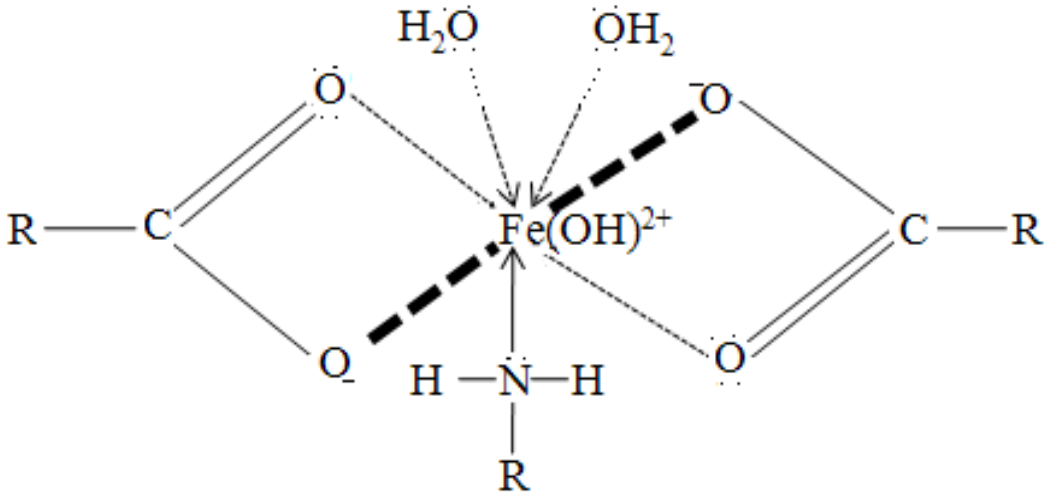


Figure 4.5: Scheme of octahedral coordination formed by Fe (II) adsorption on the function groups found in IDS (Aryal & Liakopoulou-Kryriakides, 2013)

The appearance of a band at 2363 cm^{-1} after Fe (II) interaction (Figure 3.1) confirms the formation of a coordination complex. The band could be a representation of either iron enneacarbonly, $Fe_2 (CO)_9$ or iron tetracarbonyl $Fe_3 (CO)_{12}$. Sheline (1951) however found that the carbonyl stretching frequency of $Fe_2 (CO)_9$ was at 1828 cm^{-1} while $Fe_3 (CO)_{12}$ was found between 2020 - 2043 cm^{-1}.

4.3.3 Comparative study of the removal of Cr (III), Fe (II), Ni (II) and Mn (II) by IDS

Figure 4.6 shows the metal adsorbed per unit amount of immobilized algae in the presence of Cr (III); Fe (II); Ni (II) and Mn (II).

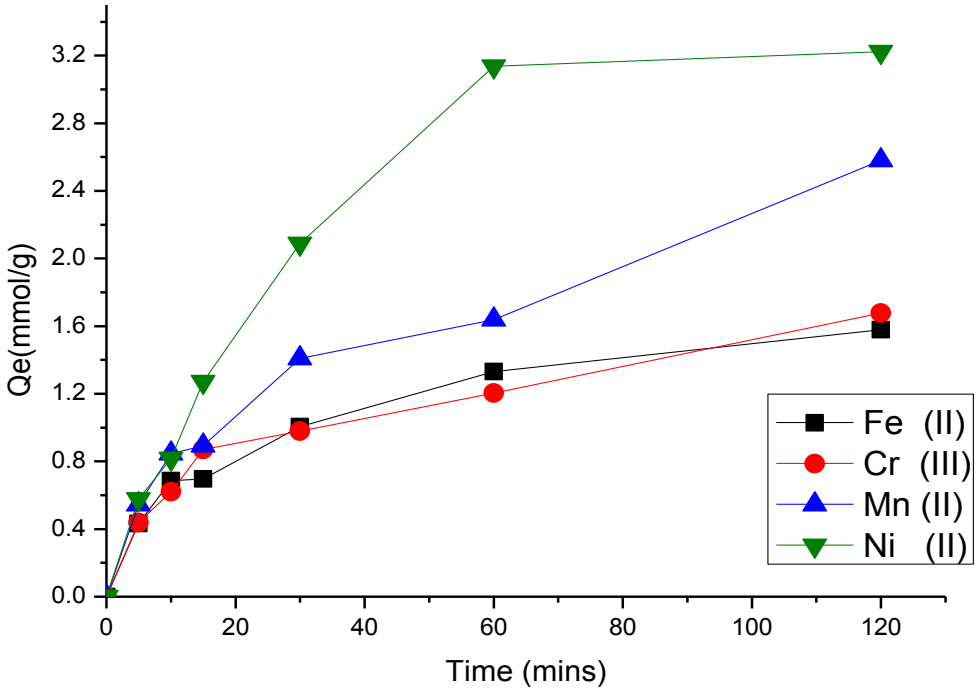


Figure 4.6: Evolution of metal adsorption at various initial concentrations

The uptake of Cr (III); Fe (II); Ni (II) and Mn (II) ions by IDS was remarkably fast in the first 15 minutes. Saturation was reached after 60 mins for Fe (II), Ni (II) and Cr (III), except for Mn (II). The adsorption capacity of Ni (II) was relatively high (3.22 mmol/g) compared to other the other heavy metals. Fe (II), Cr (III) and Mn (II) had maximum adsorption capacities of 1.58, 1.68 and 2.58 (mmol/g), respectively. The trend in binding of metal ions is as follows:

Ni (II) > Mn (II) > Cr (III) > Fe (II).

The increase in loading capacity as a function to time when Fe (II), Ni (II), Mn (II) and Cr (III) are adsorbed by IDS is an indication that microalgae cells are tolerant of toxic heavy metals in solution. The ability of microalgae cells to survive harsh conditions determined from the findings of these experiments is crucial. This can enhance their competitiveness with other commercialized adsorbents. The binding trend of metal ions onto IDS is synonymous to the ionic radii of the heavy metal compounds, represented below:



Ionic radii (picometer):	69	76	80	92

In section 3.3.1, CB of 3 % wt Na-alginate was found to be macroporous. With the Ca-alginate matrix having entrapped microalgae cells and its gelling parameters modified (see section 3.4), the pore diameter could have change from macroporous to either mesoporous or microporous. Ideally, the diameter of pores in IDS should not be smaller than the diameter of the molecules being adsorbed as that would hinder mass transfer or diffusion of the molecules. In this study, it was observed that the smallest metal ion molecule (Ni (II)) was adsorbed the most and the biggest metal ion molecule (Fe (II)) was adsorbed the least.

4.3.4 Biosorption isotherm

Table 4.2 shows Langmuir isotherm and Freundlich isotherm parameters obtained in this study to determine Fe (II) adsorption by CB and IDS. It was observed that the linear regression analysis of Langmuir and Freundlich that IDS had a better fit

compared to CB. In the Langmuir model Fe (II) (Q_{max}) uptake for IDS was found to be 1.05 mg/g and *b* was 0.004.

Table 4.2: Langmuir isotherm and Freundlich isotherm parameters

MATERIAL	Langmuir			Freundlich		
	R^2	Q_{max} (mg/g)	*b* (L/mg)	R^2	*n*	k_F $(L/mg)^{1/n}$
IDS	0.88	1.05	0.004	0.96	0.047	9.22
CB	0.62	0.26	0.025	0.68	0.36	12.25

For a good biosorbent, a high Qmax and steep initial isotherm slope b are desirable (Lichtfouse et al., 2013). Considering this, it was clear that the IDS had high maximum loading capacity (1.05 mg/g) comparable to a system where CB was used (0.26 mg/g). The isotherm slope (b) was steeper for CB than IDS. IDS Freundlich parameters shown in Table 4.2; represent k_f which is an approximate indicator of adsorption capacity and *n* a function of the strength of adsorption in the adsorption process (Lichtfouse et al., 2013). Table 4.2 shows a k_f value of 9.22 for IDS. This value is lower than that of CB. The *n* values obtained were 0.047 and 0.220 for IDS and CB, respectively. A smaller value of k_f and a larger value of *n* seen in the sorption process using CB were also obtained by (Chowdhury et al., 2013). Ideally, higher values of both k_f and n^{-1} indicate that greater metal uptake has occurred. In this study, the parameters from the isotherm plots did not make it clear which of the two are favourable in describing the Fe (II) adsorption process when immobilized algal beads are used. High correlation coefficients was found for the Freundlich models indicating that

it can be used to best describe the adsorption of Fe (II) on the immobilized algal biomass of this study.

An essential feature of the Langmuir isotherm, separation factor (R_L) can be used to determine favourability or unfavourability of the model in describing the adsorption process (Dada et al., 2012). This dimensionless constant is expressed in equation 4.19.

$$R_L = \frac{1}{1 + bC_0} \tag{4.19}$$

R_L values indicate either the adsorption nature to be unfavourable ($R_L > 1$) or favourable ($0 < R_L < 1$) and irreversible $R_L = 0$. Figure 4.7 was obtained when equation 4.19 was plotted, using experimental data. The values of R_L for sorption of Fe (II) on clear beads and immobilized algal beads are shown in Figure 4.7. Figure 4.7 indicated that the adsorption of Fe (II) is favourable on all three biomass. Higher initial concentrations of the metal made the process more favourable, because R_L value was moving closer to zero as opposed to lower initial concentration. A similar trend was observed in the work conducted by Al-Rub et al., (2004).

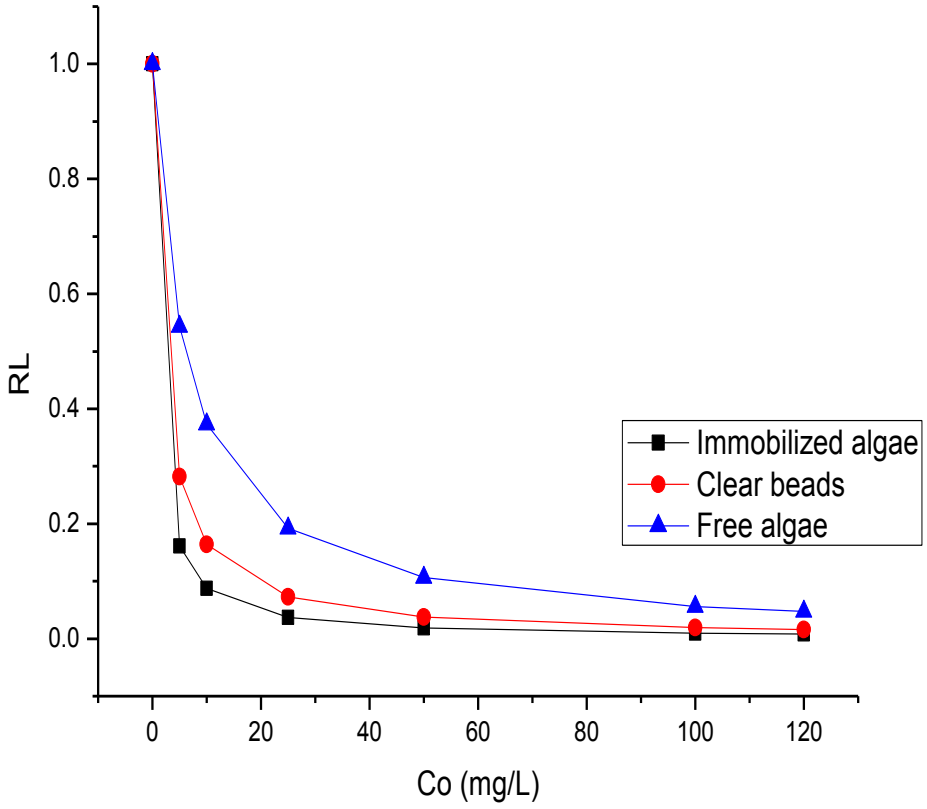


Figure 4.7: Separation factor of Fe (II) ions adsorbed on different biomass

4.3.5 Adsorption kinetics modelling

The adsorption kinetics of Fe (II) ions at various initial concentrations of 5; 60; 120; 240; 480 and 1000 mg/L were analysed using the pseudo-first-order and pseudo-second-order kinetic models. The model parameters are listed in table 4.3 and plots are shown in Figures 4.8 and 4.9, respectively.

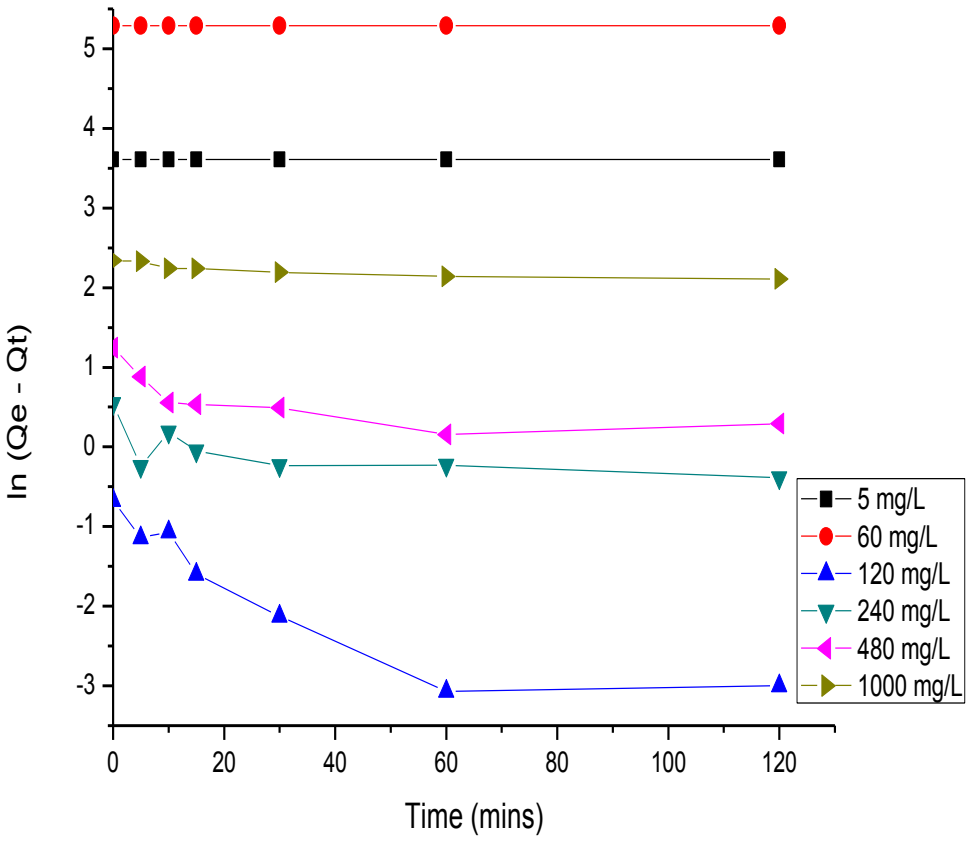


Figure 4.8: Adsorption of Fe (II) by immobilized algal beads on pseudo-first-order kinetic model

The correlation coefficient study showed the R^2 value of Fe (II) adsorption kinetics for pseudo-second order kinetic equation was close to 1. Making it a better fit to the experimental data compared to pseudo-first order where R2 values were 0.18; 0.38; 0.76; 0.41; 0.48 and 0.76 for 5; 60; 120; 240; 480 and 1000 mg/L. Pseudo-second order kinetic model relies on the assumption that chemisorption is the rate-liming mechanism, involving valence forces through sharing or exchange of electrons between sorbent and sorbate (Ho & McKay, 1999).

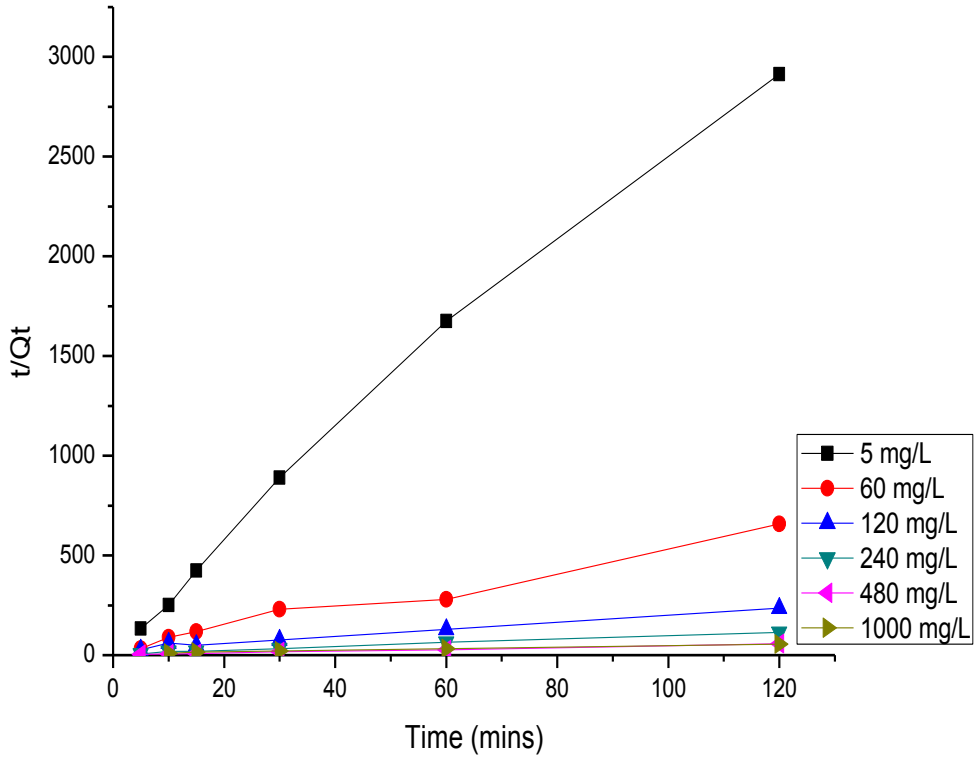


Figure 4.9: Sorption of Fe (II) by immobilized algal beads on pseudo-second-order kinetic model

Therefore for in this study; the sorption of Fe (II) is confirmed as chemisorption. In chemistry, chemisorption is a sub-class of adsorption, where covalent or ionic bonds are formed by interaction with the adsorbent and the substrates surface (Lowell et al., 2004). The comparison of experimental chemisorption capacities and the theoretical values estimated from the above two equations are presented in Table 4.3. The theoretical Q_e values calculated from the pseudo-second order kinetic model gave similar values to that of the experimental Q_e values and the correlation coefficient was significantly high.

Table 4.3: The pseudo-second order kinetic constants for biosorption of Fe (II) on immobilized algal beads

Fe (II) concentration	Experimental capacities	Pseudo first-order kinetic			Pseudo second-order kinetic		
mg/L	Qe (mg/g)	k_1 (1/min)	Q_{eq} (mg/g)	R^2	k_2 (g/mg.min)	Qe (mg/g)	R^2
5	0.04	3.61	1	0.18	0.00043	285.71	0.99
60	0.18	5.29	1	0.38	0.099	43.86	0.98
120	0.51	1.15	0.98	0.76	0.23	49.26	0.98
240	1.05	0.10	1	0.41	0.02	232.55	0.99
480	2.13	0.80	0.99	0.48	0.0034	769.20	0.99
1000	2.16	2.29	0.99	0.76	0.73	67.00	0.47

Both experimental and estimated chemisorption capacities have shown to increase rapidly at the beginning of the experiments where initial concentration of the Fe (II) ions in solution increased. Saturation of IDS adsorbent binding sites was achieved at 480 mg/L concentrations.

4.3.6 Determination of the Effective Diffusivity

The shrinking core model has been used for the fitting of experimental data, considering external film diffusion and intraparticle diffusion control. The kinetic control of the sorption reaction has not been considered because preliminary trials performed with free biomass showed the reaction to be very fast. A good fit has been found in the case of controlling intraparticle diffusion in all experimental trials. Figures 4 and 5 show results obtained considering external film diffusion control (Figure 4) and intraparticle diffusion control (Figure 5) in trials 1, 5, and 12 (see Table 2), as examples. Other courses, not shown here, were similar. These results were expected, since experimental runs have been carried out in good mixing conditions in order to accelerate the external film diffusion.

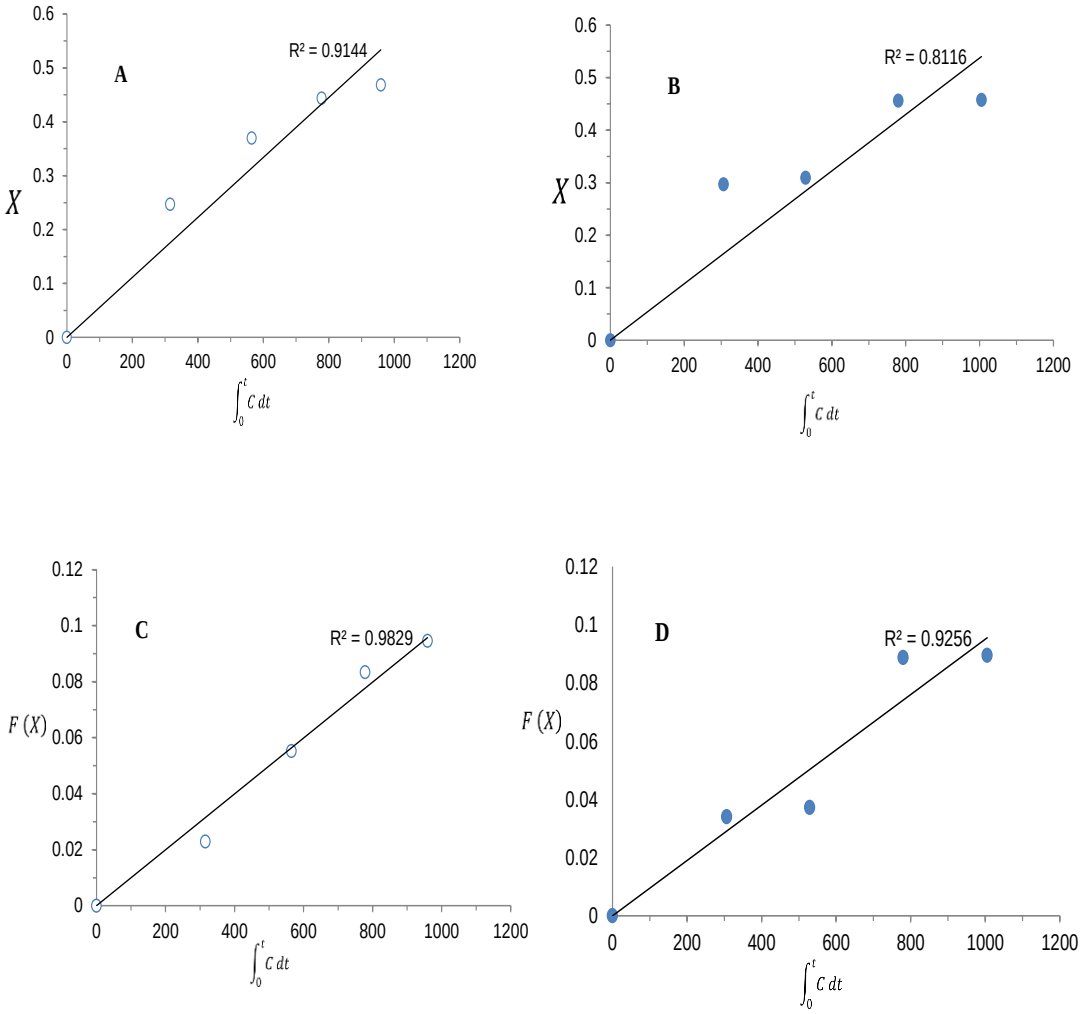


Figure 4.10: SCM plots: (A) CB & (B) IDS when using film diffusion control equation. (C) CB & (D) IDS particle diffusion control equation.

In the case of immobilized biomass mass-transfer resistances inside the particle may take place. Hence, a kinetic model has to be taken into consideration, in order to estimate mass-transfer characteristic parameters. The shrinking core model (Rao & Gupta, 1982) has been used in this work. In the case of a process controlled by the diffusion of metal ions through the liquid film (film diffusion control) the extent of the biosorption process as a function of time will be given by the

following expression: Consequently, if the film diffusion is controlling, a plot of ø vs ∫0 t C dt yields a straight line relationship. If the process is controlled by the diffusion through the reacted shell (particle diffusion control), the model is represented by the following expression: Consequently, in the case of particle diffusion control a plot of function F (ø) vs ∫0 t C dt will give a straight line relationship and the apparent diffusivity in the CB and IDS could be obtained from the slope of such a plot. It was observed that a good fit was only obtained when CB was studies using particle diffusion control equation.

4.4 Conclusion

An increase in Fe (II) ion concentration showed a direct effect on the amount of metal adsorbed onto the adsorbent. Saturation observed when concentrations 480 mg/L and 1000 mg/L were used. The Qe values went from 2.13 to 2.16 mg/g with only a variation of 0.03 mg/g when concentrations were increased by about 2 folds.

The trend in binding of metal ions is as follows: Ni (II) > Mn (II) >Cr (III) > Fe (II). The increase in loading capacity as a function to time when Fe (II), Ni (II), Mn (II) and Cr (III) are adsorbed by IDS is an indication that microalgae cells are tolerant of toxic heavy metals in solution. The ability of microalgae cells to survive harsh conditions determined from the findings of these experiments is crucial. This can enhance their competitiveness with other commercialized adsorbents.

High correlation coefficients was found for the Freundlich models indicating that it can be used to best describe the adsorption of Fe (II) on the immobilized algal biomass of this study.

The correlation coefficient study showed the R^2 value of Fe (II) adsorption kinetics for pseudo-second order kinetic equation was close to 1. Making it a better fit to the experimental data compared to pseudo-first order. Therefore for in this study; the sorption of Fe (II) is confirmed as chemisorption.

A good fit has been found in the case of controlling intraparticle diffusion in all experimental trials

C H A P T E R 5

EXPERIMENTAL AND MATHEMATICAL MODELLING OF BREAKTHROUGH CURVES OF Fe (II) SORPTION ON IMMOBILIZED BIOMASS IN A PACKED BED COLUMN

5.1 Introduction

5.1.1 Packed bed column

Packed bed column sorption processes are ubiquitous in chemical process industries and their applications are typically used in: water purification; air purification; gas dehydration; solvent or hydrocarbon vapour recovery. The process uses a solid mass separating agent, which is packed inside a column so as to allow the separation of one or more component liquid or gas as it flows through the packed bed. The liquid is distributed at the top of the column and flows downward, wetting the packing material. Packed bed sorption experiments are most favourable in wastewater treatment process. In this study entrapped *Desmodesmus sp.* will be packed in a column and Fe (II) ion solution will be pasted through the column.

5.1.2 Objectives

The objectives of these experiments are to examine the performance of immobilized Desmodesmus sp. (IDS) entrapped in a Ca-alginate beads when used in a continuous flow system. The beads will be packed in a column where Fe (II) solution will pass through the beads from the top of the column. Liquid collected will be analyzed for metal uptake. A breakthrough curve will be plotted so as to characterize metal uptake under these conditions. The effect of parameters such as column bed height and influent flow rate on packed bed performance will be studied. The adsorption mechanisms of Fe (II) onto IDS were analyzed using

Thomas and Adam Bohart models. These models were used so as to describe the column's dynamic behaviour.

5.2 Materials and Method

5.2.1 Preparation of CB and IDS beads

Preparation of CB and IDS is described in section 2.2.2

5.2.2 Preparation of heavy metal solution

The preparation of Fe (II) solution is described in section 4.2.1

5.2.3 Packed bed continuous system set-up

Packed bed column experiments were carried out to evaluate column performance for Fe (II) removal using IDS and CB. The experiments were performed at room temperature, with initial concentration of 120 mg/L and a flow rates determined using the using a known hydraulic retention time (equation 5.1):

$$HRT = \frac{V_b}{Q} \tag{5.1}$$

where,

Q = volumetric flow rate (mL/min)

V_b = volume of fixed bed (mL)

The feed stream (influent) containing initial concentration of (Fe (II)) 120 mg/L, was pumped into the column packed containing IDS. A peristaltic pump (Watson, Marlon 520 Du, England), was used to pump the feed via the inlet downward through the column at flow rates as calculated using equation (5.1). A control was also set up using CB. Figure 5.1 shows the schematic diagram for the packed bed column system used in this study.

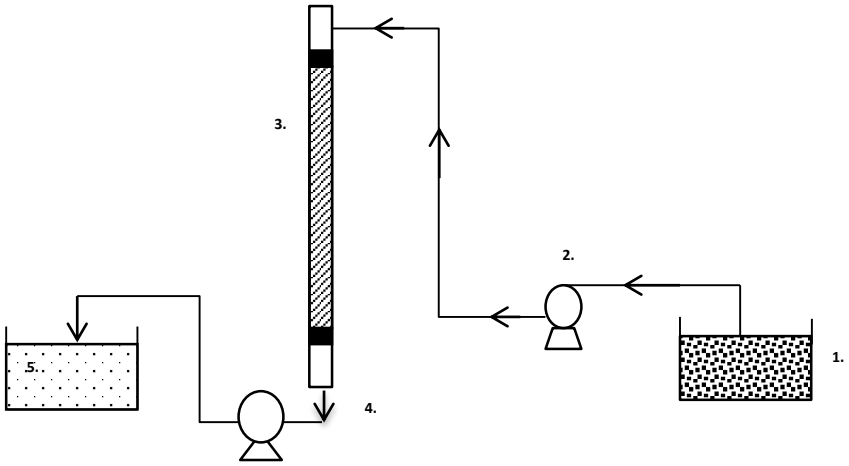


Figure 5.1: Schematic diagram of the experimental column, (1). Feed storage (2); Peristaltic pump (3); Adsorption column and adsorption bed; (4). Outlet liquid; (5) Sample collection

Experiments were conducted in a glass column 5.85 cm internal diameter and 350 mm height, with a total volume of 300 ml. The column was filled with IDS or CB (control experiment) at different bed heights of: 16; 29 and 82 cm. The pH of the solution was maintained at 2.5. Samples were collected from the outlet and quantified using Inductively Coupled Plasma-optical emission spectroscopy (ICP-OES; Perkin Elmer Optima-3300 RL, USA).

5.2.4 Break through curves analysis

A packed bed column is defined to consist of a normalized concentration (C_o / C_f) of the outlet stream vs. time or volume throughout curves, where the shape of the breakthrough curve and breakthrough time can be studied to determine the operation of the adsorption column (Negrea et al., 2011). The adsorption process through the column is unsteady as the concentration of the adsorbate changes as the feed moves through the bed. Figure 5.2, shows a typical plot of the ratio of outlet solute concentration to inlet solute concentration in the fluid as a function of time. The S-shaped curve is called the breakthrough curve. Where:

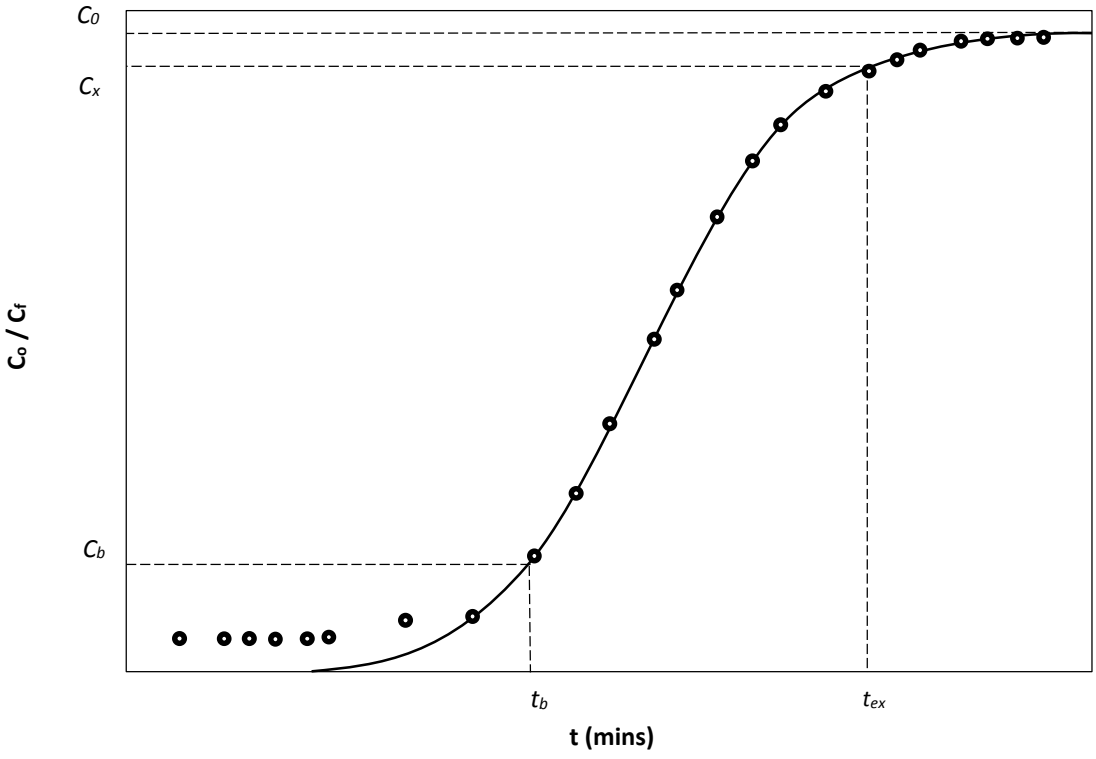


Figure 5.2: A typical S-shaped breakthrough curve

Where,

C_0= initial concentration at inlet

C_{ex}= exhaustion concentration

C_b= breakthrough concentration

t_b= breakthrough time

t_{ex}= exhaustion time

The numerical integration of the area above the breakthrough curve, Figure 5.2, is proportional to the equilibrium capacity (q_{total}) of Fe (II) adsorbed onto the beads.

5.2.5 The adsorption mechanisms of Fe (II)

Three models were used to analyse the adsorption mechanism of Fe (II). These models were:

(a) Thomas model

The Thomas model is an essential model used to determine one of the important parameters needed for successful column design: the maximum bed adsorption capacity of the column. The model is applied based on the following assumptions: (i) The driving force of adsorption obeys pseudo second-order reversible reaction kinetics and (ii) Langmuir kinetics for adsorption-desorption and no axial dispersion (Kotrba et al., 2011) (Ghasemi et al., 2011).

The Thomas model is defined as (Thomas, 1944):

$$\ln\left[\frac{C_f}{C_{out}}-1\right]=\frac{k_{TH}Q_{TH}m}{Q}-k_{TH}C_f t \qquad (5.2)$$

where,

C_f = initial concentration of solute in solution (mg/L)

C_{out} = concentration of solute at the effluent solution at time t (mg/L)

k_{TH} = kinetic constant in the Thomas model (L/g/min)

m = the mass of adsorbent in the column (g)

Q = volumetric flow rate (mL/min)

Q_{TH} = adsorption capacity of the fixed-bed column

t = time (min)

The k_{Th} and Q_{Th} variables can be determined from the intercept and slope of a non-linear plot of $\ln\left[\frac{C_f}{C_{out}} - 1\right]$ against *t*, further prediction and design is then available.

(b) Yoon-Nelson model

This model is based on the assumption that the decrease in the probability of each adsorbate to be adsorbed is proportional to the probability of its adsorption and breakthrough on the adsorbent (Xu et al., 2013). Yoon-Nelson equation regarding to single component system is expressed as:

$$\ln\left[\frac{C_{out}}{C_f - C_{out}}\right] = k_{YN}t - \tau k_{YN} \qquad (5.3)$$

where,

C_f = initial concentration of solute in solution (mg/L)

C_{out} = concentration of solute at the effluent solution at time t (mg/L)

k_{YN} = kinetic constant in the Yoon-Nelson model (1/min)

t = time (min)

A linear plot of $\ln\left[\frac{C_{out}}{C_f - C_{out}}\right]$ against sampling time t will determine the values of k_{YN} and τ from the intercept and slope of the plot.

(c) Adams-Bohart model

This model assumes that the adsorption rate is proportional to both the residual capacity of the adsorbent and the concentration of the sorbent, mainly determined by surface adsorption on the adsorbent surface sites and is used to describe the initial part of the breakthrough curve. The Adams-Bohart model is expressed as (Bohart & Adams, 1920):

$$\ln\frac{C_{out}}{C_f} = k_{AB}C_f t - k_{AB}N_0\left(\frac{Z}{U}\right) \qquad (5.4)$$

A linear plot of $\ln\frac{C_{out}}{C_f}$ against t will determine the value of k_{AB} and N_0 from the intercept and slope of the plot.

where,

C_f = initial concentration of solute in solution (mg/L)

C_{out} = concentration of solute at the effluent solution at time t (mg/L)

k_{AB} = kinetic constant in the Adams-Bohart model (L/g/min)

N_0 = predicted adsorption capacity by the Adams-Bohart model (g/L)

t = time (min)

U = superficial flow velocity of feed to bed (cm/min)

Z = bed depth (cm)

5.3 Results and Discussion

5.3.1 Breakthrough curves

Breakthrough curves show the adsorption dynamics of metal removal from solution in a packed bed column. One of the important parameters for adsorption in a packed bed column is its bed height. To determine the effects of bed heights, three different bed heights: 16; 29 and 82 cm were investigated containing IDS of 5; 70 and 125 ml, respectively. Controls were included for each experiment using CB using the same bed heights. The relative amount of space left between the packed materials was calculated as a fraction of void space volume and bulk volume. This and was found to be 0.29; 0.36 and 0.26 for 16; 29 and 82 cm bed height, respectively. Experimental results using CB as packing material at different bed heights in adsorbing Fe (II) are shown in Figures 5.3 – 5.5.

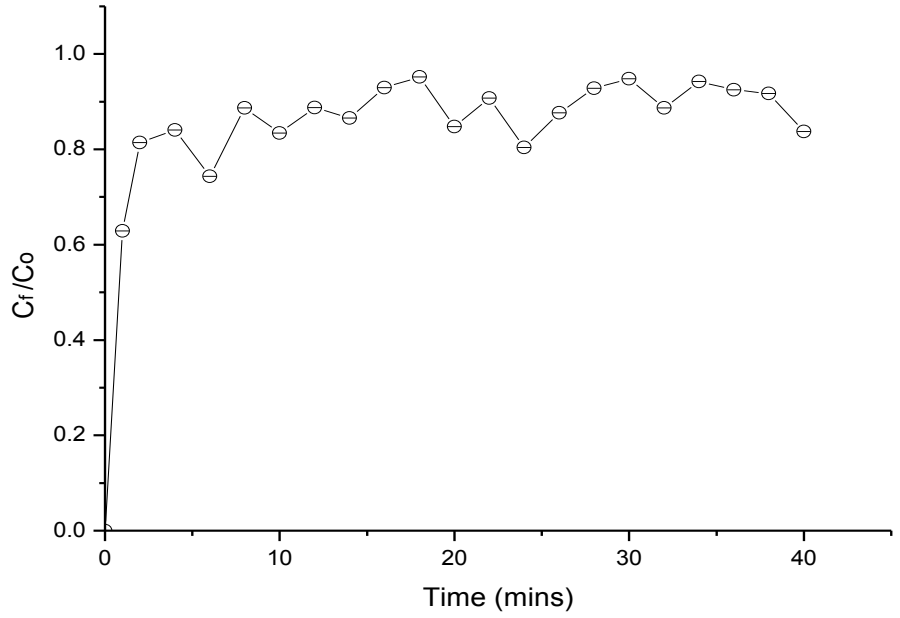


Figure 5.3: Breakthrough curves for Fe (II) adsorption by CB biomass at, Z = 16 cm; C_o = 120 mg/L and Q = 22 mL/min.

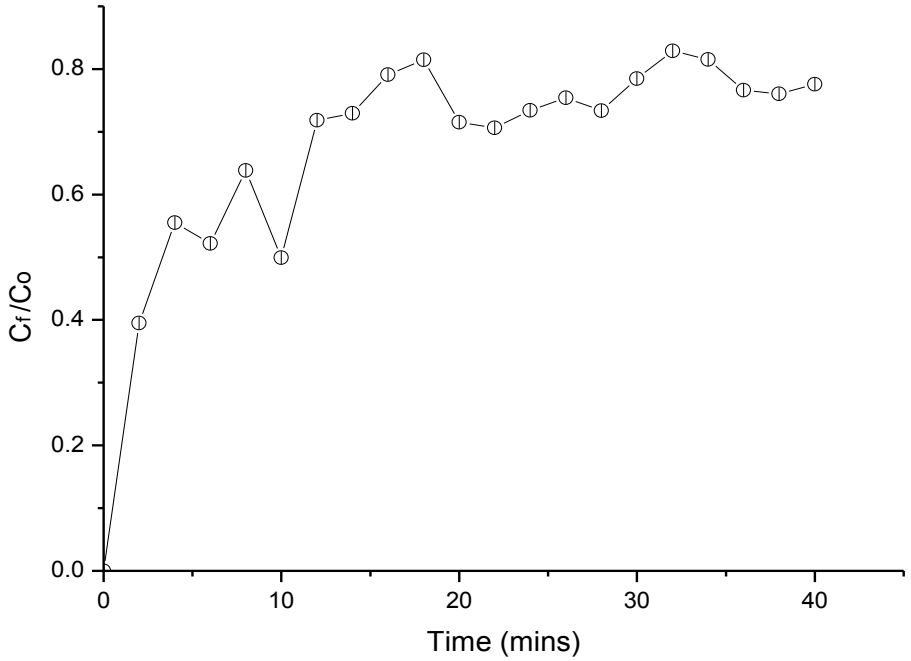


Figure 5.4: Breakthrough curves for Fe (II) adsorption by CB biomass at, Z = 29 cm; C_o = 120 mg/L and Q = 22 mL/min.

The effect of bed height 16 and 29 cm on the breakthrough curve at a constant flow rate of 22mL/min was investigated and it was observed that the shape and gradient of the breakthrough curves exhibited different variation in bed heights. The graphs did not follow the typical s-shape, but rather a steep curve which platued at 0.9 and 0.8 for 16 and 29 cm respectively. The steepness of the breakthrough curve determines the extent to which the capacity of an adsorbent bed can be utilized. Thus, the shape of the curve is very important in determining the length of the adsorption bed. To determine the total column capacity, equation 5.5 was used (Lin et al., 2013).

$$Q_{total} = Q_f C_f \int_0^t \left(1 - \frac{C_{out}}{C_f}\right) dt \qquad (5.5)$$

where,

C_f = initial concentration of solute in solution (mg/L)

C_{out} = concentration of solute at the effluent solution at time t (mg/L)

Q_f = inlet feed flow rate (mL/min)

Q_{total} = total adsorbed quantity of Fe (II) in the column (mg)

This equation uses the numerical integration of the area above the breakthrough curve. The total column capacities (Q_{total}) for 16 and 29 cm bed heights were determined to be 1. 82 mg / g and 25.48 mg / g, respectively. The total amount of Fe (II) adsorbed in the column (Q_{Fe}) was found to be 0.156 mg / g and 0.49 mg / g for 16 and 29 cm bed height, respectively. Bed capacity showed to have increased with an increase in bed height; this was a 3 fold increase from 16 cm to 29 cm. This may have been attributed to the direct impact due to an increase in adsorption surface area resulting from bed height increase (Zeinali et al., 2010). The increase in bed height subsequently increases the mass transfer zone of a packed bed column (Chowdhury et al., 2013). The mass transfer zone in a column moves from the entrance of the bed and proceed towards the exit. An increase in bed height would therefore create longer distance for mass transfer zone to reach the exit subsequently resulting in an extended breakthrough time. Higher contact time between Fe (II) ions and the loaded biomass is achieved when bed height is increased. There are more number of binding sites and ionic groups of biomass available for biosorption of metal ions (Kumar et al., 2012). The breakthrough time was found to increase with increasing bed height, where an increased was seen from 1 to 3.2 minutes.

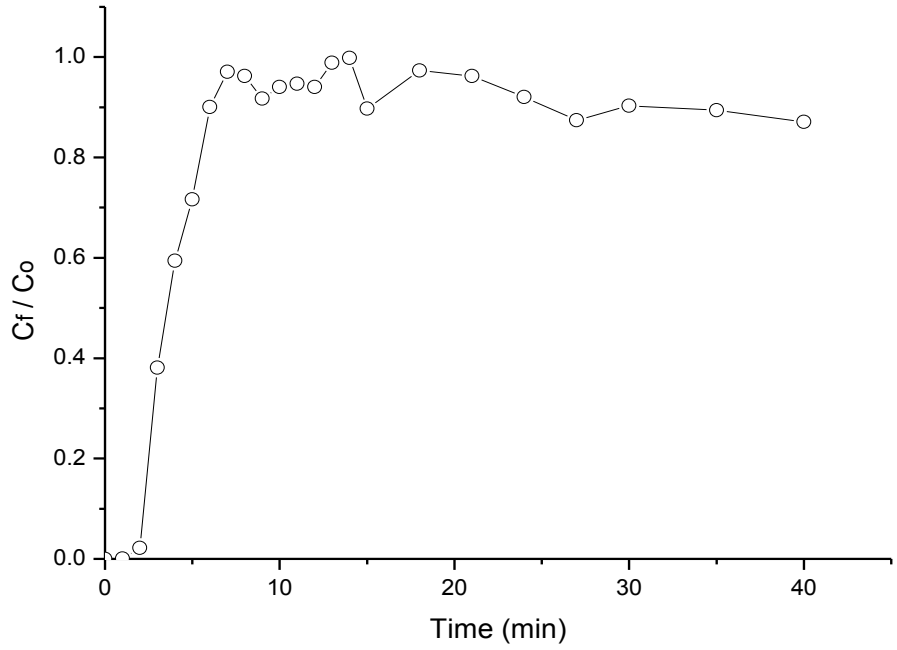


Figure 5.5: Breakthrough curves for Fe (II) adsorption by CB biomass at, Z = 29 cm; C_o = 120 mg/L and Q = 4 mL/min.

The effect of flow rate on Fe (II) adsorption by CB was investigated by varying flow rate from 22 to 4 mL/min, keeping initial concentration (120 mg/L) and bed height (29 cm) constant. It was observed that the breakthrough time increase from 3.2 to 4 minutes with a decrease in flow rate 2 to 4 mL/min (Figure 5.4 -5.5), respectively. An increase in flow rate and a constant bed depth has also been reported to decrease the breakthrough time (Ramesh et al., 2011). As the flow rate increases, breakthrough time is obtained earlier and this can be ascribed to inadequate time for solute inside the column and diffusion limitations of solute into pores of sorbent. Figure 5.5 shows the shape of the breakthrough curve to be saturated (C_t / C_0 = 0.9) within 5 minutes for flow rate of 4 mL/min and saturation was obtained in 16 minutes for flow rate of 22 mL/min. It was found that the sorption capacity increased from 0.09 to 0.49 mg / g when flow rate was

increased (Table 5.1). A comparative study of IDS biomass in absorbing Fe (II) from aqueous solutions using different bed heights are shown in Figures 5.6 and 5.7.

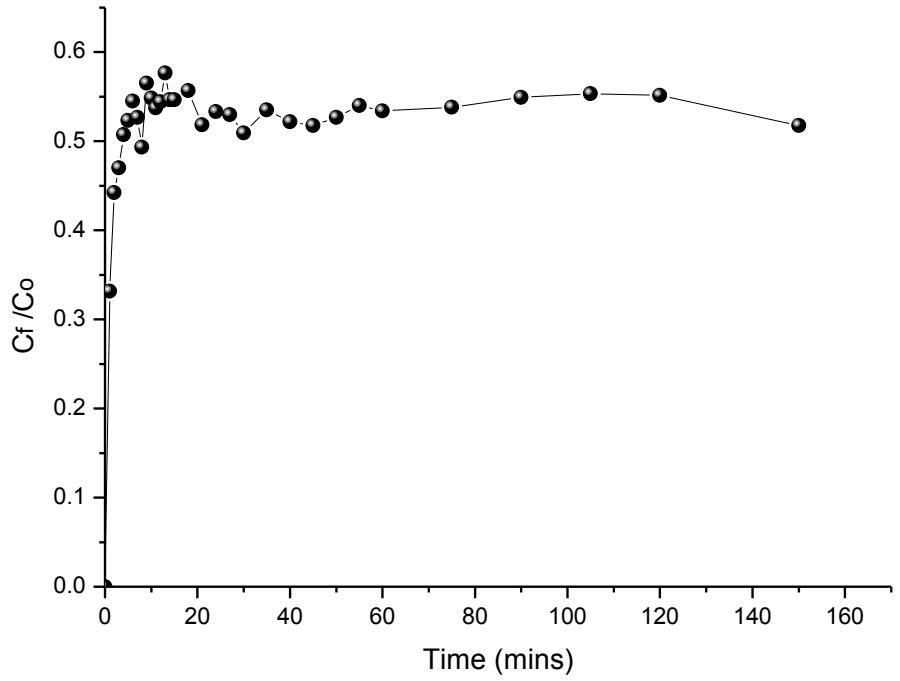


Figure 5.6 Breakthrough curves for Fe (II) adsorption by IDS biomass at, Z = 29 cm; C_o = 120 mg/L and Q = 4 mL/min.

The sorption breakthrough curves were obtained by varying bed heights of 29 and 82 cm at constant flow rate of 4 mL/min and Fe (II) concentration of 120 mg/L. The sorption capacity increased from 0.22 to 0.274 mg / g (Table 5.1) and breakthrough time increased from 4 to 16 minutes, when bed height was increased from 29 to 82 cm, respectively. Breakthrough (C_t/C_0 = 0.9) was not reached after 160 minutes of adsorption. The shape suggests that there may be mass transfer limitation and the rate of consumption of Fe (II) may be slow. In adsorption, atoms, ions or molecules of a solute diffuse to the surface of adsorbent, where they either attach to the adsorbent surface due to the chemical bond or are physically held with weak intermolecular forces. The electrostatic

charge and functional group interactions define the affinity of IDS for Fe (II) adsorption. The Fe (II) ions uptake on IDS mainly depends on: (i) the Fe (II) ions concentration, and (ii) the adsorption and reduction phenomena that simultaneously take place on the IDS surface.

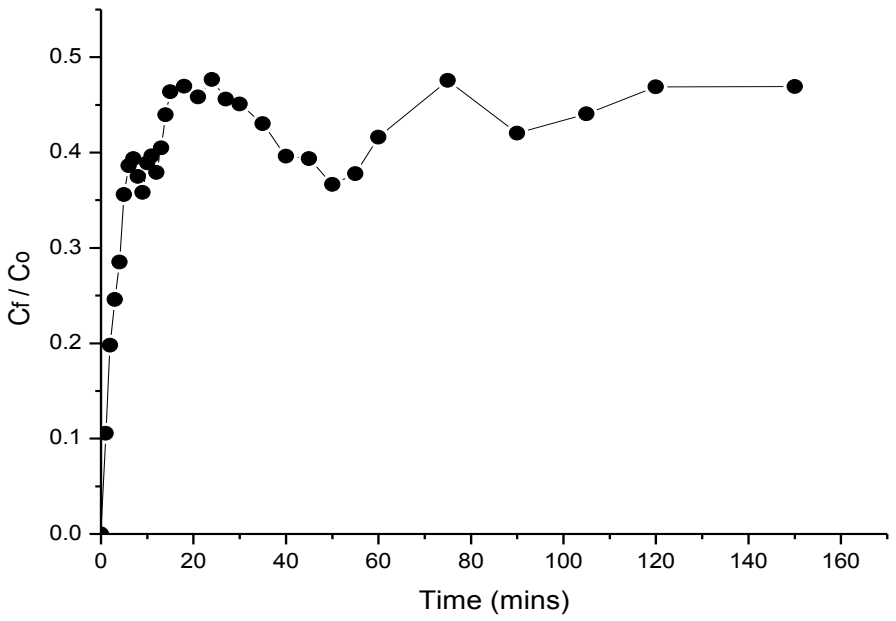


Figure 5.7: Breakthrough curves for Fe (II) adsorption by IDS biomass at, L = 82 cm; Co = 120 mg/L and Qo = 4 mL/min.

Table 5.1: Summary of different process parameters obtained from packed bed adsorption Fe (II). * t_e breakthrough time was not obtained.

Q (mL/min)	C_o (mg/L)	Z (cm)	t_b (min)	t_e (min)	Q_{max} (mg/g)	Q_{Fe} (mg/g)
22	120	16	1	15	2.5	0.16
22	120	29	3	16	25.5	0.49
4	120	29	4	8	25.5	0.095
4	120	29	4	-*	25.5	0.22
4	120	82	16	-*	45.5	0.27

Other important parameters obtained from the breakthrough curves, which are essential for packed bed column design include: volume of treated effluent (V_{eff}); mass transfer zone (Z_m); total amount of metal ion delivered to the column (W_{total}) and total metal removal (%). These parameters are calculated as follows:

The volume of treated effluent, V_{eff} (mL), can be calculated based on the following equation (equation 5.6):

$$V_{eff} = Qt_{total} \quad (5.6)$$

where,

Q = volumetric flow rate (mL/min)

t = time (min)

The length of the mass transfer zone is calculated from the breakthrough curve (equation 5.7):

$$Z_m = Z\left(1 - \frac{t_b}{t_e}\right) \tag{5.7}$$

where,

t_e = time at exhaustion (min)

t_b = time at breakthrough (min)

Z = bed depth (cm)

Z_m = length of the mass transfer zone (cm)

The total amount of metal ion delivered to the column W_{total} (mg) can be calculated from equation 5.8:

$$W_{total} = \frac{C_o Q t_{total}}{1000} \tag{5.8}$$

where,

C_0 = liquid phase concentration (mg/L)

Q = volumetric flow rate (mL/min)

t_{total} = total flow time (min).

and the total metal removal (%) can be calculated from the ratio of metal mass adsorbed (q_{total}) to the total amount of metal ions delivered to the column W_{total} (equation 5.9):

$$A\% = \frac{Q_{total}}{W_{total}} \times 100 \qquad (5.9)$$

The packed column adsorption data were evaluated and presented in Table 5.2.

Table 5.2: Summary of different process parameters obtained from a packed bed column adsorption of Fe (II)

Z (cm)	Z_m (cm)	C_o (mg/L)	V_{eff} (mL)	t_b (min)	t_e (min)	A %
16	14	120	880	1	15	8.54
29	23.56	120	880	3	16	1.92
29	14.5	120	160	4	8	0.37
29	-	120	640	4	-	0.86
82	-	120	640	16	-	0.60

5.3.2 Modelling of breakthrough curves

(a) Thomas model

Thomas model is one of the widely used models for column performance modelling. Its derivation assumes Langmuir kinetics of adsorption-desorption and no axial dispersion (Saadi et al., 2013). The Thomas model's linear regression (R^2) of CB for experimental data from column performance at different bed heights is represented in Figure 5.8 and the values are listed in Table 5.3.

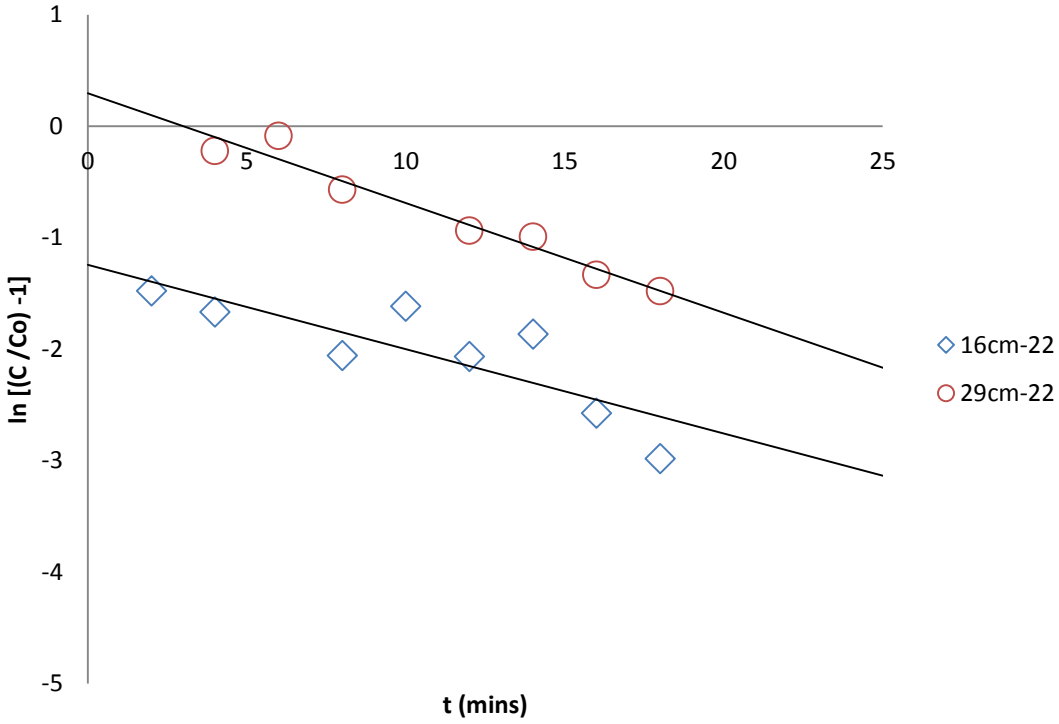


Figure 5.8: Linear plot of Thomas model with experimental data at different bed heights of CB. Z = 16 and 29 cm; C_o = 120 mg/L and Q = 22 mL/min.

The values of R^2 and k_{TH} increased from 0.70 to 0.95 and 6.31 x 10^{-4} to 8.22 x 10^{-4} for bed heights 16 and 29 cm, respectively. Using bed height of 29 cm, agreed with the Thomas model. The calculated Q_{max} from the Thomas model was found

to be greater than the experimental Qe_{max} (exp). Figures 5.9 and 5.10, further showed linear plots of Thomas model when various flow rates and biomass were used.

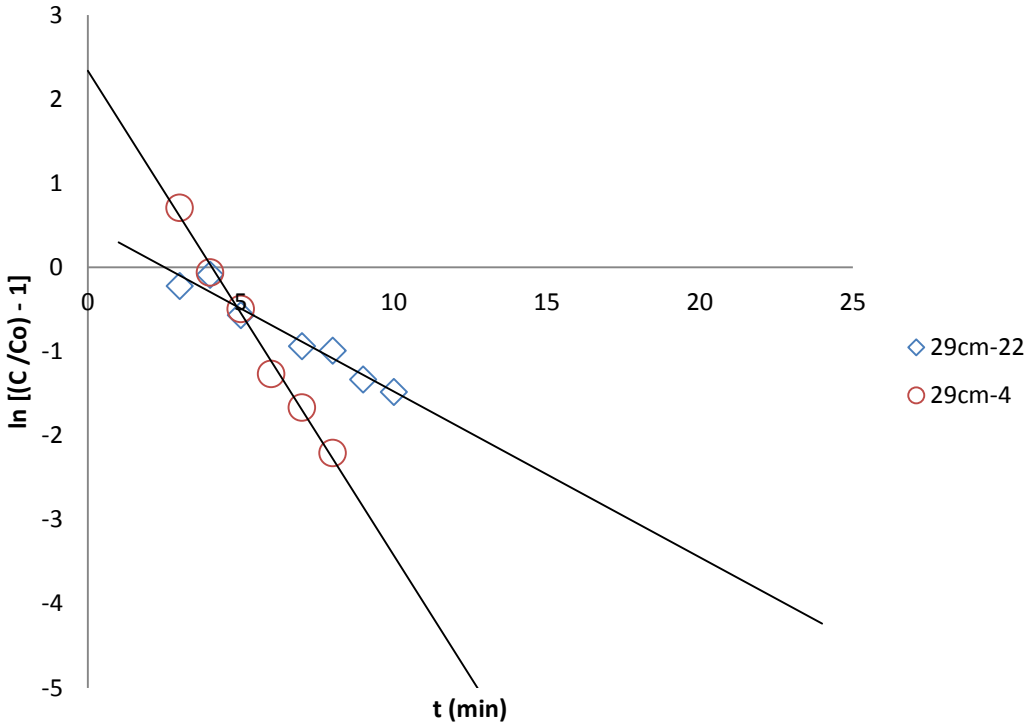


Figure 5.9: Linear plot of Thomas model with experimental data at flow rates of CB. Z = 29 cm; C_o = 120 mg/L and Q = 4 and 22 mL/min.

The bed capacity Q_{max} increased from 28 to 94 mg / g when flow rate was increased from 4 – 22 mL/min and the coefficient (k_{TH}) decreased with increase of flow rate (Table 5.3). This trend was not found when bamboo waste based granular activated carbon (BGAC) was used to remove C.I. Reactive Black (RB5) from aqueous solution, (Ahmad & Hameed, 2010). When flow rate was kept constant and bed height varied, it was found that the bed capacity increased with increase in bed height as well as the coefficient (k_{TH}). Similar trend has been documented by (Chowdhury et al., 2013).

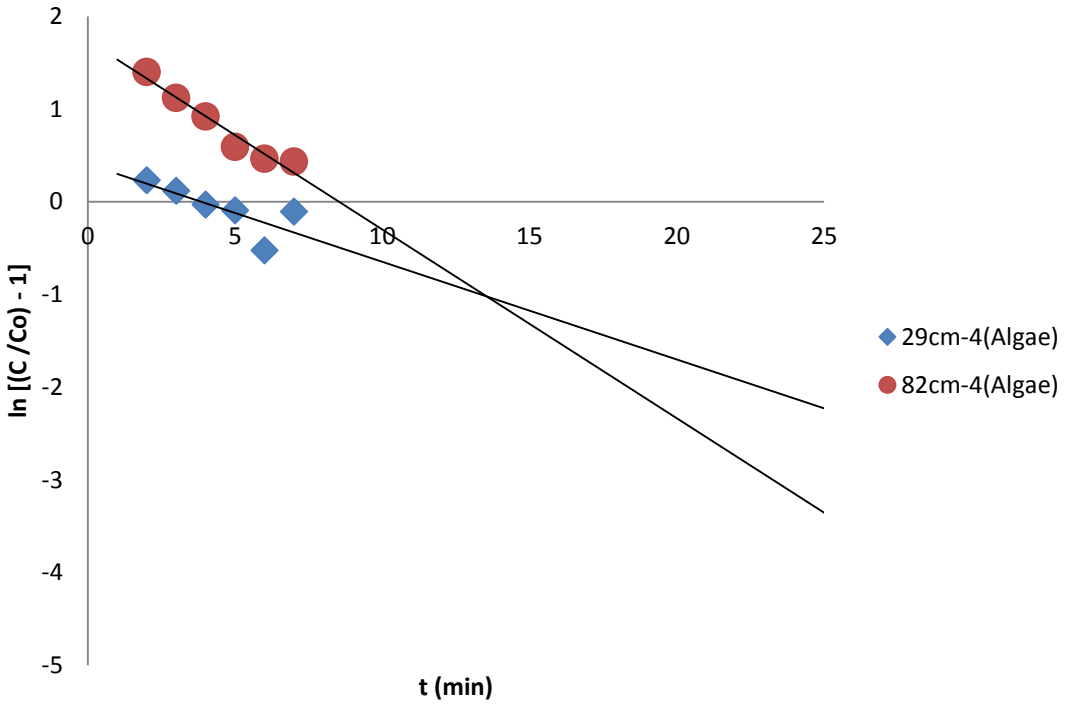


Figure 5.10: Linear plot of Thomas model with experimental data at different heights of IDS. Z = 29 cm and 82 cm; C_o = 120 mg/L and Q = 4 mL/min.

It was observed that a bed height of 16 cm and a flow rate of 22 mL/min and bed height of 82 at a flow rate 4 mL/min did not fit well with the Thomas model. This indicates that the external and internal diffusion are limiting steps of adsorption in CB (Chowdhury et al., 2013). The diffusion -limited adsorption could be attributed to not having enough contact time with the biomass packed bed when a high flow rate of the metal aqueous solution (22 mL/min) is used and not reaching exhaustion point when a longer bed height is used (82 cm), as the mass transfer zone is lengthen.

Table 5.3: Thomas model parameters for the adsorption of Fe (II) onto CB and IDS at different conditions using linear regression analysis

Q (mL/min)	L (cm)	Co (mg/L)	Qe (max) (mg/g)	$k_{TH \times 10^{-3}}$ (ml/min.mg)	R^2	$Qe_{max\ (exp)}$ (mg/g)
22	16	120	86.66	0. 631	0.70	1.8
22	29	120	113.17	0. 822	0.95	25
4	29	120	27.83	4.8	0.99	25
22	29	120	94	1.64	0.95	25
4	29	120	14.81	0.88	0.95	25
4	82	120	32.76	1.70	0.58	45.5

(b) Adams-Bohart model

The Adams-Bohart model was applied to experimental data for the description of breakthrough curves obtained by using various conditions and linear plot are represented by Figures 5.11 - 13. Table 5.4 shows that an increase of height (16 – 29 cm) whilst keeping flow rate (22 mL/min) constant, decreased the saturation concentration (N_0) and increased the mass transfer coefficient (k_{AB}). An increase in flow rate from 4 – 22 mL/min saw an increase in saturation concentration (N_0) and decreased in the mass transfer coefficient (k_{AB}). Finally, the use of IDS at heights 29 – 82 cm decreased the saturation concentration and an increase in the mass transfer coefficient (k_{AB}).

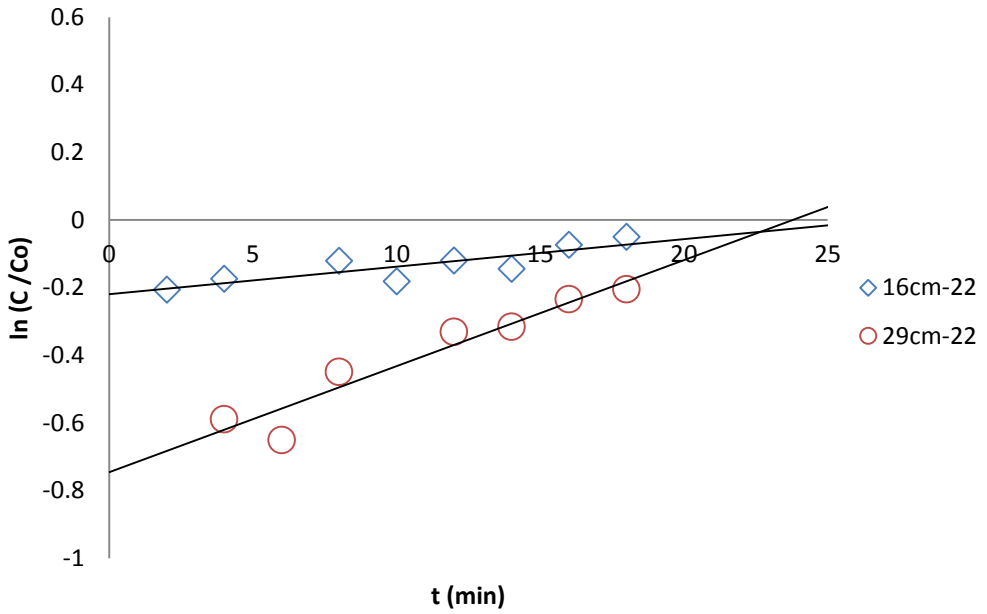


Figure 5.11: Linear plot of Adam-Bohart model with experimental data at different heights of CB. Z = 16 and 29 cm; C_o = 120 mg/L and Q = 22 mL/min.

.

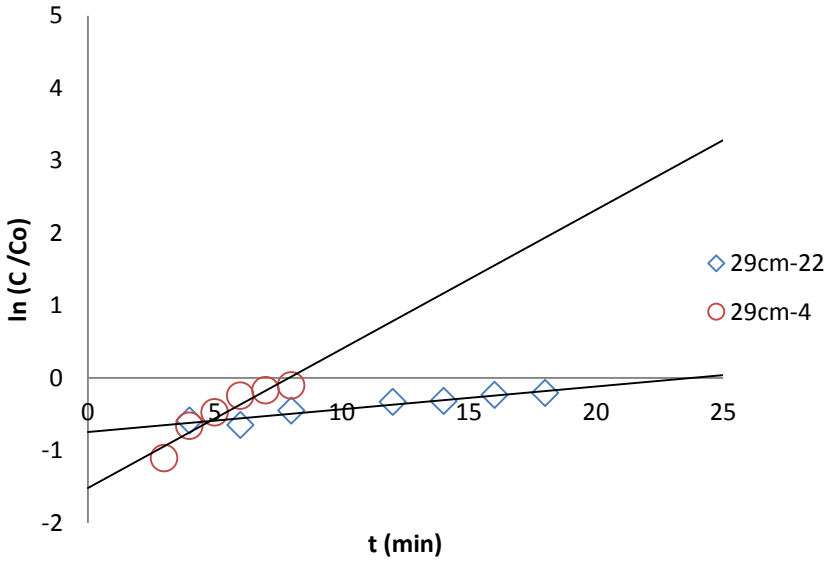


Figure 5.12: Linear plot of Adam-Bohart model with experimental data at different flow rates of CB.
Z = 29 cm; C_o = 120 mg/L and Q = 4 and 22 mL/min.

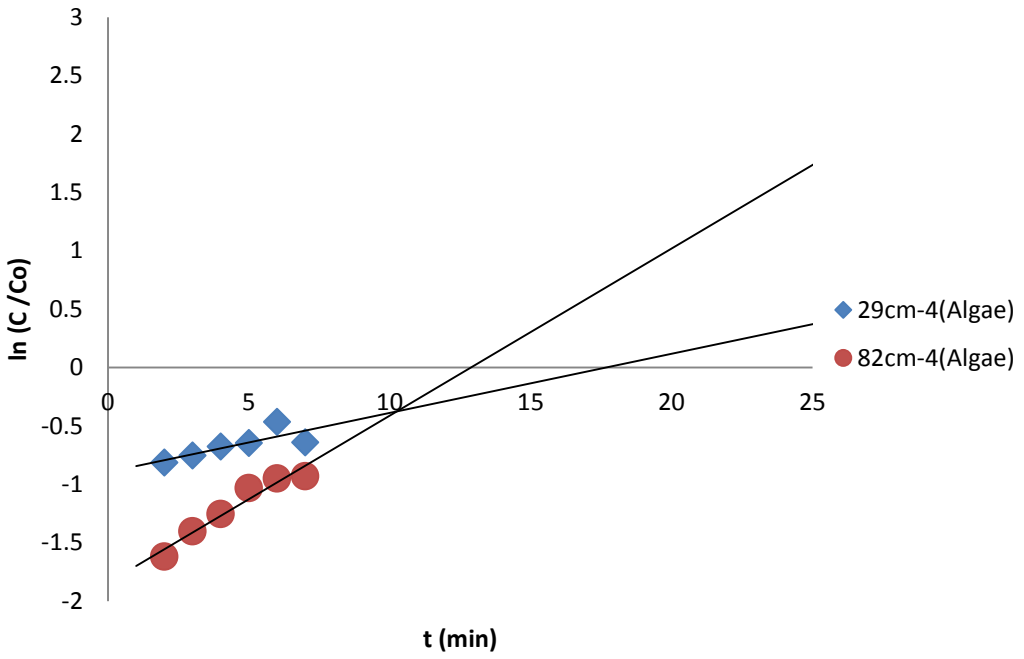


Figure 5.13: Linear plot of Adam-Bohart model with experimental data at different heights of IDS.
Z = 29 and 82 cm; C_o = 120 mg/L and Q = 4 mL/min.

Table 5.4: Adam-Bohart parameters for the adsorption of Fe (II) onto CB and IDS at different conditions using linear regression analysis

Q (mL/min)	L (cm)	C_o (mg/L)	N_0 (mg/L)	k_{AB} x 10^{-3} (ml/min.mg)	R^2
22	16	120	81.03	0.0675	0.73
22	29	120	71.164	0. 262	0.92
4	29	120	7.91	1.60	0.90
22	29	120	61.92	0.0262	0.92
4	29	120	14.12	0.422	0.62
4	82	120	10.30	1.19	0.94

The results showed an increase in bed height caused a decrease in N_0 and an increase in k_{AB}. The increase in k_{AB} experienced when bed height was increased can be attributed to the overall kinetics in the initial part of the adsorption process not being dominated by external mass transfer. This finding is different to that of Kanadasan et al. (2013) who used waste activated sludge (WAS) discharged during the aerobic treatment of palm oil mill effluent (POME) to produce a low cost adsorbent for the removal of methylene blue (MB) from aqueous solution. The linear regression (R^2) values showed a distribution between 0.62 – 0.94 of using bed height 16 cm at flow rate 22 mL/min and bed height 29 cm at flow rate 4 mL/min. This therefore indicates that the data does not fit the model well and that Adam-Bohart model is not suitable to explain the overall adsorption kinetics of the column permanence when these parameters are used.

5.4 Conclusion

Based on the analysis conducted on immobilized *Desmodesmus sp.* (IDS) and clear beads (CB), it was shown that the continuous pack bed system was potentially an efficient method of Fe (II) sequestration from aqueous solution. Experimental data confirmed this; however there were certain limitations observed:

Bed height and flow rate have shown to have a significant influence on IDS and CB adsorption of Fe (II).

Breakthrough time and exhaustion time increased with increase in bed height. Additionally the breakthrough curve became steeper with the increase in flow rate. Breakthrough time and exhaustion time were however not obtained after 160 minutes when IDS was used.

The experimental data showed a better fit when using the Thomas and Adam-Bohart model, as opposed to Yoon-Nelson adsorption model. Hence, these two models can be further used to describe the behavior of the adsorption of Fe (II) in a continuous column using IDS.

When using Thomas model the highest uptake capacity was obtained when 29 cm bed height; at an inlet concentration of 120 mL/g and a flow rate of 22 mL/min According to this study a flow rate of 4 mL/min and a packing height of 82 cm (Co = 120 mg/L) seems to be most effective, which has a potential to increase the metal removal rate significantly.

C H A P T E R 6

GENERAL CONCLUSIONS

6.1 Conclusions

This chapter provides an overview of the conclusions that may be drawn from the current study. Also, areas that require further development and may form the basis of future investigations are highlighted.

The current environmental degradation experienced in the West Witwatersrand basin has received immense attentions from the government. Plans have been put in place to re-establish pumping of underground water filling mined cavities, to avoid uncontrolled decanting. Treatment methods such as the addition of lime (lime-neutralization) for metal removal have been proposed as possible immediate and short term solutions for cleaning water bodies contaminated by previous decants. Although this intervention will greatly improve current situation in the Western Witwatersrand Basin, long term it will prove to be inefficient. The proposed treatment plan will not treat water up to regulated standard. This will create problems such as metal accumulation downstream from the treatment process. An algal based method is proposed be used to either substitute or be incorporated to the current intervention plan. *Desmodesmus sp.* immobilized into Ca-alginate matrix has a huge potential improve the recovery efficiency of heavy metals from contaminated water bodies. This will assist in increasing the success of controlling environmental degradation caused by gold mining in the Witwatersrand basin.

Desmodesmus sp. was entrapped into a Ca-alginate matrix (the blend referred to as IDS) in an effort to immobilize it for heavy metal removal from aqueous solutions. The beads formed by the immobilization process showed considerable swelling upon storage in various aqueous media, especially Beijerinck media. A humidified storage medium proved not to transform the material physically and chemically, hence the storage media of choice for this study. The successful use Ca-alginate as an immobilization matrix relies on understanding its chemical composition, behavior of cross-linkage on a macroscopic and molecular level. Na-alginate containing high guluronic acid blocks is mostly preferred for bioreactor application, because of its high mechanical stability, high porosity and tolerance to salts and chelating agents. The Na-alginate used in this study had high guluronic acid blocks content and the modification of chemical composition improved its stability. Fe (II) removal was found to be 25 % and 29 % for CB and IDS, respectively. Upon optimizing the gel forming properties the Fe (II) removal was improved to 32 % and 60 % recovery for CB and IDS, respectively. This was a clear indication that immobilizing of *Desmodesmus sp.* had a potential for efficient heavy metal removal from aqueous solutions.

Quantification of the ion exchange capacity of IDS was carried out. The maximum adsorption capacity was found to be 0.26 mg / g for CB and 1.05 mg /g for 1.05. The reactivity of IDS towards metal ions in acidic (pH 2.5) aqueous solutions was attributed to the strong affinity of metal ions with carboxylate groups present in the biosorbents. The immobilized *Desmodesmus sp.* species in the current study sequester metal ions following the selectivity series: Ni (II) > Mn (II) > Cr (III) > Fe (II). Fe (II) ions are thought to engage in chelation-type surface reactions in addition to simple ion exchange with protons of weakly acidic surface functional groups. Ni (II), Cr (III) and Mn (II) ions most likely undergo simple ion exchange reactions as well as electrostatic interactions with the negatively charged algal surface as verified by zeta-potential measurements. Stoichiometric release of

protons during metal biosorption has been observed and suggests a bidentate binding mechanism between metal ions in solution and protons on the algal surface.

The Fe (II) metal adsorption process is reversible. Inorganic mineral acids are capable of eluting previously sequestered metal ions. However, degradation of the cellular polysaccharides due to hydrolysis reactions results in reduced potential for multiple reuses. Ni (II), Mn (II) and Cr (III) may be eluted using less aggressive eluents such as acidified ammonium chloride and sodium chloride solutions. Covalently bound Fe (II) ions might be eluted by using strong complexing agents or strong acids capable of breaking the covalent bonds. The rate of metal biosorption is limited by diffusional resistance to transport of metal ions within the matrix. Steric hindrance and specific interactions of metal ions with functional groups within the cellular matrix of algal particles significantly can limit the rate of metal biosorption. For smaller particles, where the effective path length for ion migration is reduced, the biosorption rates are significantly increased.

Fe (II) adsorption under continuous operation conditions was studied employing a packed bed flow-through sorption column. As expected, the optimal lowest sorbent usage rate was found to be in the region of low flow rates (loadings) when the sorbent material was properly contacted and the dynamic bed mass transfer "front" was relatively short. Biosorption breakthrough curves for single metal solutions as well as synthetic metal plating solutions have shown promising potential.

6.2. Future work

The past three years have been spent studying the feasibility of heavy metal sorption by microalgal based biosorbent. It is clear from the work, that the material has tremendous potential for removal of toxic metals from AMD contaminated aqueous solutions. The high Fe (II) sorption capacity of the immobilized *Desmodesmus sp.* coupled with their relatively inexpensive cost suggests that this material could be competitive adsorbents in the water treatment market.

Follow-up work that needs to be evaluated includes:

- The column performance over several sorption / desorption cycles at varying flow rates must be carried out.

- Further detailed investigation needs to be carried out for biosorbents' regenerability. The possible regeneration of the sorbent is essential in prolonging its usability when used for water treatment and help to increase the economic viability of a treatment process based on algae.

- The effective disposal of the biosorbents will need to be investigated: both in recovering the metal adsorbed and the disposal of the remaining biomass.

REFERENCES

Aderhold, D., Williams, C. J. & Edyvean, R.G. J. (1996). The Removal of Heavy Metal Ions by Seaweed and Their Derivatives. Bioresource Technology, 58 (1).

Adsorption design guide. (2001). Engineering and Design, Department of army, U.S. Army Corps of Engineers, DG 1110-1-2.

Ahemad, M. & Kibret, M. (2013). Recent Trends in Microbial Biosorption of Heavy Metals: A Review. Biochemistry & Molecular Biology, 1(1), pp (19 – 26).

Ahmad, A.A. & Hameed, B.H. (2010). Fixed-bed adsorption of reactive azo dye onto granular activated carbon prepared from waste. Journal of Hazardous Materials, 175 (1 -3), pp (298 – 303).

Ahmad, S.A., Shamaan, N.A., Noorliza, M.A., Koon, G.B., Shuko, M.Y.A. & Syed, M.A. (2012). Enhanced phenol degradation by immobilized Acinetobacter sp. strain AQ5NOL 1. World Journal of Microbiology and Biotechnology, 28, p (47 - 352).

Aksu, Z. & Ac¸ikel, Ü. (1999). A single-staged bioseparation process for simultaneous removal of copper (II) and chromium (VI) by using C. vulgaris. Process Biochemistry. 34, pp (589 – 599).

Alberts, B., Johnson, A. & Lewis, J. (2002). Molecular Biology of the Cell. 4th edition. New York. Garland Science.

Alhakawati, M.S. & Banks, C.J. (2004). Removal of copper from aqueous solution by Ascophyllum nodosum immobilised in hydrophilic polyurethane foam. Journal of Environmental Management, 72, pp (195 – 204).

Al-Rub, F.A.A., El-Naas, M.H., Benyahia, F., Ashour, I., 2004. Biosorption of nickel on blank alginate beads, free and immobilized algal cells. Process Biochemistry, 39, pp (1767 – 1773).

Amjad, Z. (1998). Reverse Osmosis Technology: Fundamentals and Water Applications, Association of Water Technologies, Inc. 1998 Annual Convention & Exposition, Washington, DC

An, S.S., Friedl, T., & Hegewald, E. (1999). Phylogenetic relationships of Scenedesmus and Scenedesmus-like coccoid green algae as inferred from ITS-2 rDNA sequence comparisons. Plant Biology, 1, pp (418 – 428).

Applegate, L. E. (1984). Membrane separation processes, Chemical Engineering, 91 (12), pp. 6489.

Araújo, M. M. & Teixeira, J.A. (1997). Trivalent Chromium Sorption on Alginate Beads. International Biodererioration & Biodegradation, 4 (1), pp (63-74).

Aryal, M., & Liakopoulou-Kyriakides M. (2013). Binding Mechanism and Biosorption Characteristics of Fe (III) by Pseudomonas sp. Cells. Journal of Water Sustainability, 3 (3), pp (117–131).

Aubé, B. (2006). The Science of Treating Acid Mine Drainage and Smelter Effluent, EnvirAbé, 361 Aumais, Ste-Anne-de-Bellevue, Québec, Canada, H9X 4A9.

Bailliez, C., Largeau, C., & Casadevall, E. (1985). Growth and hydrogen production of Botryococcus braunii immobilized in calcium alginate gel. Applied Microbiology and Biotechnology, 23, pp (99 – 105).

Bashan, L.E. & Bashan, Y. (2010). Immobilized microalgae for removing pollutants: Review of practical aspects. Bioresource Technology, 101, pp (1611 – 1627).

Baytak, S. & Tu¨rker, A.R. (2005). The use of Agrobacterium tumefaciens immobilized on Amberlite XAD-4 as a new biosorbent for the column preconcentration of iron(III), cobalt (II), manganese (II) and chromium (III). Talanta, 65, pp (938 – 945).

Becker, E.W. (1994). Microalgae, Biotechnology and Microbiology. University Press, Cambridge, Great Britain.

Bellinger, E.G., & Sigee, D.C. (2010). Freshwater Algae: Identification and Use as Bioindicators. John Wiley & Sons, Ltd, Chichester, UK.

Beolchini, F., Pagnanelli, F., Toro, L., Veglio, F. (2003). Biosorption of copper by Sphaerotilus natans immobilised in polysulfone matrix: equilibrium and kinetic analysis. Hydrometallurgy, 70, pp (101 – 112).

Bickerstaff, G.F. (ed.) (1997). Methods in biotechnology: Immobilization of enzymes and cells, 1. Humana Press Inc., Totowa, New Jersey.

Blanco, A., Begoña, S., Llama, M.L., Serra, J.L. (1999) Biosorption of heavy metals to immobilised Phormidium laminosum biomass. Journal of Biotechnology, 69, pp (227 – 240).

Blandino, A., Macías, M., & Cantero, D. (1999). Formation of Calcium Alginate Gel Capsules: Influence of Sodium Alginate and $CaC1_2$ Concentration on Gelation Kinetics. Journal of Bioscience and Bioengineering, 88 (6), pp (686 – 689).

Bohart, G.S. & Adams E.Q. (1920). Some aspects of the behavior of charcoal with respect to chlorine. Journal of the American Chemical Society, 42 (3), pp (523 – 544).

Bouklas, N., & Huang, R. (2012). Swelling kinetics of polymer gels: comparison of linear and nonlinear theories. Soft Matter, 8, pp (8194 – 8203).

Bosman, D.J. (1974). The improved densification of sludge from neutralised acid mine drainage. J.S.A Mining and Metallugy, 74, pp (340-348).

Brena, B., González-Pombo, P. & Batista-Viera, F. (2013). Immobilization of Enzymes and Cells: Methods in Molecular Biology, 3rd edition. Springer Science Business Media, New York.

Brunauer, S., Emmett, P.H., Teller, E. (1938). Adsorption of Gases in Multimolecular Layers. Journal of the American Chemical Society, 60 (2), pp (309 – 319).

Burdin, K.S. & Bird, K.T. (1994). Heavy metal accumulation by carrageenan and agar producing algae. Botanica Marina, 37, pp (467 – 470).

Caisová, L., & Gąbka, M. (2009). Charophytes (Characeae, Charophyta) in the Czech Republic: taxonomy, autecology and distribution. Fottea, 9(1), pp (1 – 43).

Carrilho, E.N.V.M., No´brega, J.A. & Gilbert, T.R. (2003). The use of silica immobilized brown alga (Pilayella littoralis) for metal preconcentration and determination by inductively coupled plasma optical emission spectrometry. Talanta, 60, pp (1131 – 1140).

Chaplin, M.F. & Bucke, C., (1990). The preparation and kinetics of immobilized enzymes. In: Chaplin, M.F. Editor, 1990. Enzyme Technology Cambridge University Press, Cambridge, UK, pp (80 – 90).

Chekroun, K.B. & Baghour, M. (2013). The role of algae in phytoremediation of heavy metals: A review. Journal of Material & Environmental Science, 4 (6), pp (873 – 880).

Chowdhury, Z. Z., Zain, S. M., Rashid A. K., Rafique R. F., & Khalid K. (2013). Breakthrough Curve Analysis for Column Dynamics Sorption of Mn (II) Ions from Wastewater by Using Mangostana garcinia Peel-Based Granular-Activated Carbon. Hindawi Publishing Corporation. Journal of Chemistry, p (8).

Clesceri, L. S., Greenberg A. E. & Trussell R. R. (1989). Standard Methods for the Examination of Water and Wastewater. American Public Health Association, American Water Works Association and Water Pollution Control Federation; New York, pp (92-110).

Coates, J. (2006). Interpretation of Infrared Spectra, A Practical Approach: Infrared Spectroscopy. Encyclopedia of Analytical Chemistry.

Cohen, Y. (2001). Biofiltration--the treatment of fluids by microorganisms immobilized into the filter bedding material: a review. Bioresource Technology, 77, pp (257 - 274).

Coulton, R. Bullen, C., Dolan, J., Hallett, C., Wright, J., & Marsden, C. (2003). Wheal Jane mine water active treatment - design, construction and operation. Land Contamination and Reclamation, 11 (2), pp (245 – 252).

Costello, C. (2003). Acid Mine Drainage: Innovative Treatment Technologies. For: U.S. Environmental Protection Agency, Office of Solid Waste and Emergency Response, Technology Innovation Office, Washington, DC, pp. 1 – 52.

Crist, R.H., Martin, J.R., Carr, D., Watson, J.R., Clarke, H.J. & Crist, D.R. (1994). Interaction of metals and protons with algae. 4. Ion exchange vs. adsorption models and reassessment of scatchard plots; ion-exchange rates and equilibria compared with calcium alginate. Environmental Science and Technology, 28, pp (1859 – 1866).

Dada, A.O., Olalekan, A.P., Olatunya, A.M., DADA, O. (2012). Langmuir, Freundlich, Temkin and Dubinin–Radushkevich Isotherms Studies of Equilibrium Sorption of Zn^{2+} Unto Phosphoric Acid Modified Rice Husk. Journal of Applied Chemistry, 3 (1), pp (38 – 45).

Daemi, H., & Barikani, M. (2012). Synthesis and characterization of calcium alginate nanoparticles, sodium homopolymannuronate salt and its calcium nanoparticles. Scientia Iranica, 19, pp (2023–2028).

Das, N., Vimala, R., & R., Karthika P. (2008). Biosorption of heavy metals: An overview, Indian Journal of Biotechnology, 7, pp. (159 – 169).

Davis, T. A., Volesky, B., & Mucci, A. (2003). A review of the biochemistry of heavy metal biosorption by brown algae. Water Research, 37, pp (4311 – 4330).

Diale, P.P., Muzenda, E., & Zimba, J. (2011a). A Study of South African Natural Zeolites Properties and Applications. Proceedings of the World Congress on

Engineering and Computer Science Vol II. WCECS 2011, October 19-21, San Francisco, USA.

Diale, P. P., Muzenda, E., Matambo, T. S., Glasser, D., Hildebrandt, D., Zimba, J. (2011b). Biosorption of Heavy Metals Contaminating the Wonderfonteinspruit Catchment Area using *Desmodesmus sp.* World Academy of Science, Engineering & Technology, 52, p (821).

Diale, P.P. (2001c). The remediation of heavy metal contaminated water in the Wonderfonteinspruit catchment area using algae and natural zeolite, Masters Dissertation, University of Johannesburg.

Do¨nmez, G.C., Aksu, Z., O¨ ztu¨ rk, A. & Kutsal, T. (1999). A comparative study on heavy metal biosorption characteristics of some algae. Process Biochemistry, 34, pp (885 – 892).

Eldridge, D. (2008). Immobilized algae: Immobilized algae for studying photosynthesis. NCBE, University of Reading. Available from: http://www.eurovolvox.org/Protocols/PDFs/ImmobilisedAlgae1.0_UK_eng.pdf. [Accessed: 5th April 2015].

Ertesva˚g, H. & Valla, S. (1998). Biosynthesis and applications of alginates. Polymer Degradation and Stability, 59, pp (85 – 91).

Fagerlund, G. (1973). Methods of characterization of pore structure. Sweden, Division of Building Technology, The Lund Institute of Technology.

Fourest, E. & Volesky B. (1996). Contribution of sulphonate groups and alginate to heavy metal biosorption by the dry biomass of Sargassum fluitans. Environmental Science and Technology, 30(1), pp (277 – 82).

Fraser, J.E., & Bickerstaff, G.F. (1997). Methods in biotechnology: Immobilization of enzymes and cells, 1. Humana Press Inc., Totowa, New Jersey.

Fu, F.L., & Wang, Q. (2011). Removal of heavy metal ions from wastewaters: a review, Journal of Environmental Management, 92, pp. (407–418).

Ghasemi, M., Keshtkar, A.R., Dabbagh, R., Jaber Safdari, S. (2011). Biosorption of uranium (VI) from aqueous solutions by Ca-pretreated Cystoseira indicaalga: breakthrough curves studies and modeling. Journal of Hazardous Materials, 189(1-2), pp (141-149).

Graham, L.F., Wilcox, L.W. (2000). Algae. New Jersey, Prentice Hall.

Grant, G. T., Morris, E. R., Rees, D. A., Smith, P. J.C., Thom, D. (1973). Biological interactions between polysaccharides and divalent cations: The egg-box model. FEBD Letter, 32, pp (195 – 198).

Greene, B. & Bedell, G.W. (1990). Algal gels or immobilized algae for metal recovery. In: Akatsuka, I. (Ed.), Introduction to Applied Phycology. The Hague, The Netherlands. SPB Academic Publishing BV, The Hague, The Netherlands.

Guisán, J.M. (ed.). (2006). Immobilization of Enzymes and Cells (2nd edition). Humana Press, New York.

Habib, M. A. B. (1998). Culture of selected microalgae in rubber and palm oil effluents and their use in the production of enriched rotifers. Doctoral Thesis, University of Putra, Malaysia.

Hallas, L.E., Adam, W.J. & Heitkamp, M.A. (1992). Glyphosate degradation by immobilized bacteria: field studies with industrial wastewater effluent. Applied and environmental microbiology, 58, pp (1215 - 1219).

Hashim, M.A., Tan, H.N. & Chu, K.H. (2000). Immobilized marine algal biomass for multiple cycles of copper adsorption and desorption. Separation and Purification Technology, 19, pp (39 – 42).

Hegewald, E. & Deason, T. (1989). *Pseudodidymocystis*, a new genus of *Scenedesmaceae* (Chlorophyceae). Archiv fu¨r Hydrobiologie / Suppl, 82, Algological Studies, 55, pp (119 – 127).

Hegewald, E. & Hanagata, N. (2000). Phylogenetic studies on *Scenedesmaceae* (Chlorophyta). Algological Studies, 100, pp (29 – 49).

Henning, K.D. & von Kienle, H. (2012). Carbon, 5. Activated Carbon. In Ullmann's Encyclopedia of Industrial Chemistry; Wiley-VCH Verlag GmbH & Co. K.

Hertzberg, S. & Jensen, A. (1989). Studies of alginate-immobilized marine microalgae. Botanica Marina, 32, pp (267 – 273).

Ho, Y.S., & McKay, G. (1998a). A comparison of chemisorption kinetic models applied to pollutant removal on various sorbents. Process Safety and Environmental Protection, 76 B, pp (332 – 340).

Ho, Y.S., & McKay, G. (1999). Pseudo-second order model for sorption processes. Process Biochemistry, 34, pp (451 -465).

Ho, Y. (2004). Citation review of Lagergren kinetic rate equation on adsorption reactions. Scientometrics, 59 (1), pp (171-177).

Horak, S. (2012). Background information document for the activities associated with the immediate, short term in the western, central and eastern Witwatersrand. Digby Wells Environmental.

Jang, L.K., Nguyen, D.V., Kolostyak, K. & Geesey, G.G., (1995a). Addition of copper-sequestering agents to alginate gel to enhance copper recovery from aqueous media. Water Resource, 29, pp (2525 – 2529).

Jang, L.K., Nguyen, D. & Geesey, G.G., (1995b). Effect of pH on the absorption of Cu (II) by alginate gel. Water Resource, 29 (1), pp (315 – 321).

Jang, L.K., Nguyen, D. & Geesey, G.G. (1995c). Selectivity of alginate gel for Cu vs. Co. Water Resource, 29 (1), pp (307 – 313).

Johnson, D.B. & Hallberg, K.B. (2003). The microbiology of acidic mine waters. Research in Microbiology, 154, pp 466 – 473.

Johnson, D. B. & Hallberg, K.B. (2005). Acid mine drainage remediation options: a review. Science of the Total Environment, 338, pp (3 –14).

Johnson, J.L., Fawley, M.W. & Fawley, K.P. (2007). The diversity of *Scenedesmus* and *Desmodesmus* (Chlorophyceae) in Itasca State Park, Minnesota, USA. Phycologia, 46, pp (214 – 229).

Kativu, E. (2011). Carbon dioxide absorption using fresh water algae and identifying potential uses of algal biomass. Masters dissertation, University of Witwatersrand.

Kanadasan, G., Mashitah, M.D. & Vadivelu V.M. (2013). Fixed bed adsorption of methylene blue by using palm oil mill effluent waste activated sludge. Asia Pacific Young Water Professional Conference.

Kessler, E., Schäfer, M., Hümmer, C., Kloboucek, A., & Huss, V.A.R. (1997). Physiological, biochemical and molecular characters for the taxonomy of the subgenera of *Scenedesmus* (Chlorococcales, Chlorophyta). Botanica Acta, 110, pp (244 – 250).

Khoshmanesh, A., Lawson, F. & Prince, I.G. (1997). Cell surface area as a major parameter in the uptake of cadmium by unicellular green microalgae. The Chemical Engineering Journal and the Biochemical Engineering Journal, 65, pp (13 – 19).

Kim, H. (1990). A kinetic study on calcium alginate bead formation. Korean Journal of Chemical Engineering, 7 (1), pp (1 – 6).

Kostenbader, P.D. & Haines, G.F. (1970). High density sludge treats acid mine water. Coal Age, 90.

Kotrba, P., Mackova, M. & Macek, T. (2011). Microbial Biosorption of Metals. Springer Science & Business Media, London & New York.

Kuhn, E.M.R. (2005). Microbiology of fly ash-acid mine drainage co-disposal processes, Master thesis, University of the Western Cape.

Kumar, R., Bhatia, D., Singh, R., Rani, S. & Bishnoi, N.R. (2012). Sorption of heavy metals from electroplating effluent using immobilized biomass Trichoderma viride in a continuous packed-bed column. International Biodeterioration and Biodegradation, 65 (8), pp (1133 – 1139).

Lagergren, S. (1898). Zur theorie der sogenannten adsorption gelöster stoffe, Kungliga Svenska Vetenskapsakademiens. Handlingar, 24 (4), pp (1 – 39).

Lau, P.S., Tam, N.F.Y. & Wong, Y.S. (1998). Effect of carrageenan immobilization on the physiological activities of Chlorella vulgaris. Bioresource Technology, 63, pp (115 – 121).

Levasseur, M., P.A. Thompson, and P.J. Harrison. 1993. Physiological acclimation of marine phytoplankton to different nitrogen sources. Journal of Phycology, 29, pp (87 – 595).

Levenspiel, 0. (1972). Chemical Reaction Engineering (2nd edition). John Wiley & Sons, New York, pp (21-32), (69 -71), (357 – 408).

Lewinsky, A.A. (2007). Hazardous Materials and Wastewater: Treatment, Removal and Analysis. Nova Science Publishers, Inc., New York, pp (59 -60).

Lichtfouse, E., Schwarzbauer, J. & Robert, D. (2013). Pollutant Diseases, Remediation and Recycling (Environmental Chemistry for a Sustainable World). Springer, Cham, Heidelberg, New York, Dordrecht & London.

Lin, X., Li, R., Wen, Q., Wu, J., Fan, J., Jin, X., Q, W., Liu, D., Chen, X., Chen, Y., Xie, J., B, J., & Ying, H. (2013). Experimental and Modeling Studies on the Sorption Breakthrough Behaviours of Butanol from Aqueous Solution in a Fixed-bed of KA-

I Resin. The Korean Society of Biotechnology and Bioengineering and Springer, 18, pp (223 – 233).

Lowell, S., Shields, J. E., Thomas, M. A. & Thommes, M. (2004). Characterization of Porous Solids and Powders: Surface Area, Pore Size and Density. Kluwer Academic Publishers, Dordrecht.

Lukavsky, J., Komarek, J., Lukavska´, A., Ludvı´k, J. & Pokorny´, J. (1986). Metabolic activity and cell structure of immobilized algal cells (*Chlorella*, *Scenedesmus*). Archiv für Hydrobiologie, SMcupplement, 43, pp (261 – 279).

McDowell, H., Gregory, T.M. & Brown, W.E. (1977). Solubility of Ca_5 $(PO4)_3OH$ in the system Ca $(OH)_2$-H_3P0_4-H_20 at 5, 15, 25, and 37 °C. Journal of research of the National Bureau of Standards-A. Physics and Chemistry, 81A (2&3), pp (273 – 281).

Mallick, N., (2002). Biotechnological potential of immobilized algae for wastewater N, P and metal removal: a review. BioMetals, 15, pp (377 – 390).

Maree, J.P, Mujuru, M., Bologo, V., Daniels, N. & Mpholoane, D. (2013). Neutralisation treatment of AMD at affordable cost. Water SA, 39 (2), pp (245 – 250).

Martins, S.C.S., Martins C.M., Fiúza L.M.C.G., & Santaella S.T. (2013). Immobilization of microbial cells: A promising tool for treatment of toxic pollutants in industrial wastewater. African Journal of Biotechnology, 12(28), pp (4412 – 4418).

McCarthy, T.S. (2011). The impact of acid mine drainage in South Africa. South African Journal of Science, 107 (5 &6), pp (1 – 7).

Meyen, F.J.F. (1829). Beobachtungen u¨ber einige niedere Algenformen. Verhandlungen der Kaiserlichen Leopoldinisch-Carololinischen Akademie der Naturforscher, 14, pp (769 – 778).

Moreno-Garrido, I. (2008). Microalgae immobilization: Current techniques and uses. Bioresource Technology, 99, pp (3949 – 3964).

Monteiro, C.M., Marques, A. P. G. C, Castro, P.M.L. & Malcata, F.X. (2009). Characterization of Desmodesmus pleiomorphus isolated from a heavy metal-contaminated site: biosorption of zinc. Biodegradation, 20, pp (629 – 641).

Monterio, C.M., Castro, P.M.L. & Xavier, M.F. (2010). Cadmium removal by two strains of *Desmodesmus pleiomorphus* cells. Water Air Soil Pollution, 208 (1-4), pp (17 – 27).

Monteiro, C., Castro, P.M., Malcata, F.X. (2012). Metal uptake by microalgae: underlying mechanisms and practical applications. Biotechnology progress, 28(2), pp (299 – 311).

Murdoch, D.J., Fox, J.R.W. & Bensely, J.G. (1995). Treatment of Acid Mine Drainage by the High Density Sludge Process. In: Proceedings for Sudbury 95 – Mining and the Environment, Sudbury, Ontario, May 28 – June 01, 2, pp (431 – 439).

Naiya, T. K., Bhattacharya, A. K., & Das, S. K. (2009). Adsorption of Cd (II) and Pb (II) from aqueous solutions on activated alumina. Journal of Colloid and Interface Science, 333 (1), pp (14 – 26).

Negrea, A., Lupa, L., Ciopec M., & Negrea P. (2011). Experimental and Modelling Studies on As (III) Removal from Aqueous Medium on Fixed Bed Column. Chemical Bulletin of "Politehnica" University of Timisoara, Series of Chemistry and Environmental Engineering, 56(70) (2), pp (89 – 93).

Neilands, J.B. (1981). Iron absorption and transport in microorganisms. Annual Reviews Nutrition, 1, pp (27 – 46).

Nestle, N. & Kimmich, R. (1996). NMR microscopy of heavy metal absorption in calcium alginate beads. Applied Biochemistry and Biotechnology, 56, pp (9 – 17).

Pane, L., Feletti, M., Bertino, C. & Carli, A. (1998). Viability of the marine microalga *Tetraselmis suecica* grown free and immobilized in alginate beads. Aquaculture International, 6, pp (411 – 420).

Pathak, P. & Choppin, G. (2009). Effects of pH, ionic strength, temperature and complexing anions on the sorption behaviour of cobalt on hydrous silica. Soil and Sediment Contamination: An International Journal, 5 (18), pp (590 – 602).

Pathak, S. (2015). Acid catalyzed transesterification. Journal of Chemical and Pharmaceutical Research, 7(3), pp (1780 – 1786).

Pohan, A. (2010) Treatment of polluted water (river) by using activated carbon from coir pith. Bachelor's thesis, University of Malaysia.

Prescott, L.M., Harley, J.P. & Klein, D.A. (1999). Microbiology Forth Edition. The McGraw-Hill Companies, Incorporation, New York, pp. 181.

Ramesh, S.T., Gandhimathi, R., Nitheesh, P.V., Nagendra, B., Bharathi, K.S. (2011). Breakthrough data analysis of adsorption of Cd (II) on Coir pith column. Electronic Journal of Environmental, Agricultural and Food Chemistry, 10 (8), pp (2638 – 2658).

Rao, M.G. & Gupta, A.K. (1982). Ion exchange processes accompanied by ionic reactions. The Chemical Engineering Journal, 24, pp (181 – 190).

Réka, H. (2014). Bioremediation of heavy metals by using the microalga *Desmodesmus subspicatus*. Bachelor's thesis. Ostfalia University of Applied Sciences.

Riemer, K.L. & Durrheim, J. R. (2011). Mining Seismicity in the Witwatersrand Basin: Monitoring, Mechanisms and Mitigation Strategies in Perspective. Journal of Rock Mechanics and Geotechnical Engineering, 3 (3), pp (250 – 259).

Robinson, J.W. (1970). Undergraduate Instrumental Analysis, Marcel Dekker, Inc., New York.

Robinson, P.K., Mak, A.L. & Trevan, M.D. (1986). Immobilized algae: a review. Process Biochemistry, pp (122 – 126).

Saadi, Z., Saadi, R., & Fazaeli, R. (2013) Fixed-bed adsorption dynamics of Pb (II) adsorption from aqueous solution using nanostructured γ-alumina. Journal of Nanostructure in Chemistry, 3 (48).

Sartori, C. (1997). The characterisation of alginate systems for biomedical applications. Doctoral Thesis, BruneI University.

Schiewer, S. & Volesky, B. (2000). Biosorption by marine algae. In: Valdes JJ, (ed.). Remediation. Dordrecht, The Netherlands: Kluwer Academic Publishers.

Schoeman, J.J. (1985). The status of electrodialysis technology for brackish and industrial water treatment, Water SA, 11 (2).

Schultz, J., Muller, T., Achtziger, M., Seibel, P.N., Dandekar, T. & Wolf, M. (2006). The internatranscriber spacer 2 database-a web server for (not only) low level phylogenetic analyses. Nucleic Acids Research, 34, pp (704 – 707).

Sheline, R.K., (1951). The Spectra and Structure of Iron Carbonyls. II. Iron Tetracarbonyl. Journal of the American Chemical Society, 73 (4), pp (1615 –1618).

Shubert, E., Wilk-Woźniak, E. & Ligęza, S. (2014). An autecological investigation of Desmodesmus: implications for ecology and taxonomy. Plant Ecology and Evolution, 147 (2), pp (202 – 212).

SmidsrØd, O., & Skjåk-Bræk, G. (1990). Alginate as immobilization matrix for cells. Trends in Biotechnology, 8, pp (71 – 78).

Smith, J.G. (2013). Organic Chemistry, 4th edition. McGraw-Hill Education, New York, USA.

Spinti, M., Zhuang, H. & Trujillo, E.M. (1995). Evaluation of immobilized biomass beads for removing heavy metals from wastewaters. Water Environment Research, 67, pp (943 – 952).

Stark, P.C. & Rayson, G.D. (2000). Comparisons of metal–ion binding to immobilized biogenic materials in a flowing system. Advances in Environmental Research, 4, pp (113 – 122).

TCTA: Witwatersrand Gold Fields: Acid Mine Drainage (Phase 1). BKS Report no.: J01599/05.

Thomas, H.C. (1944). Heterogeneous ion exchange in a flowing system. Journal of the American Chemical Society, 66, pp (1664-1666).

Thu, B., Bruheim, P., Espevik, T., Smidsrod, O., Soon-Shiong, P. & Skjak-braek, G. (1996). Alginate polycation microcapsules. II. Some fuctional properties. Biomaterials, 17, pp (1069 – 79).

Toyub, M.A., Miah, M.I., Habib, M.A.B, & Rahman, M. M. (2008). Growth performance and nutritional value of *Scenedesmus obliquus* cultured in different concentrations of sweetmeat factory waste media. Bangladesh Journal of Animal and Science, 37 (1), pp (86 – 93).

Tosa, T., Sato, T., Mori, T., Yamamoto, K., Takata, I., Nishida, Y. & Chibata, I. (1979). Immobilization of enzymes and microbial cells using carrageenan as matrix. Biotechnology Bioengineering, 21, pp (1697 – 1709).

Trainor, H.R., Cain, J. & Shubert, L.E. (1976). Morphology and nutrition of the colonial green alga, Scenedesmus: 80 years later. Botanical Review, 42, pp (5 – 25).

Trainor, F.R. & Egan, P.F. (1990). Phenotypic plasticity in Scenedesmus (Chlorophyta) with special reference to S. armatus unicells. Phycologia, 29, pp (461 – 469).

Trainor, F.R. (1998). Biological aspects of Scenedesmus (Chlorophyceae): phenotypic plasticity. Nova Hedwigia Beihefte, 117, pp (1- 367).

Travieso, L., Pello´ n, A., Benı´tez, F., Sa´nchez, E., Borja, R., O'Farrill, N.O. & Weiland, P. (2002). BIOALGA reactor: preliminary studies for heavy metals removal. Biochemical Engineering Journal, 12, pp (87 – 91).

Trunschke, A. (2013). Surface area and pore size determination. Modern Methods in Heterogeneous Catalysis Research.

Valdman, E., Erijman, L., Pessoa, F.L.P. & Leite, S.G.F. (2001). Continuous biosorption of Cu and Zn by immobilized waste biomass *Sargassum sp.* Process Biochemistry, 36, pp (869 – 873).

Valero, F., Barcelo, A, & Arbós, A. (2010). Electrodialysis Technology, Theory and Applications. Desalination, Trends and Technologies.

Van Hannen, E.J., Fink, P. & Lürling, M. (2002). A revised secondary structure model for the internal transcribed spacer 2 of the green algae *Scenedesmus* and *Desmodesmus* and its implication for the phylogeny of these algae. European Journal of Phycology, 37, pp (203 – 208).

Velings, N.M. & Mestdagh, M.M. (1995). Physico-chemical properties of alginate gel beads. Polymer gels & networks, 3, pp (311 – 330).

Vijayaraghavan, K., Yun, Y., (2008). Bacterial Biosorbents and Biosorption. Biotechnology Advances, 26, pp (266 – 291).

Vı´lchez, M.J., Vigara, J., Garbayo, I. & Vı´lchez, C. (1997). Electron microscopic studies on immobilized growing *Chlamydomonas reinhardtii* cells. Enzyme and Microbial Technology, 21, pp (25 – 47).

Westmeier, F. & Rehm, H.J. (1987). Degradation of 4-chlorophenol in municipal wastewater by adsorptive immobilized *Alcaligenes sp* A 7-2. Applied Microbiology and Biotechnology, 26, pp (78 – 83).

Widmann, G. (2001). Interpreting TGA curves. Information for users of METTER TOLEDO thermal analysis systems. [Online] Available from: http://www.masontechnology.ie/x/Usercom_13.pdf. [Accessed: 5th April 2015].

Willey, N. (2007). Phytoremediation: Methods and Reviews. Humana Press Inc., Totowa, New Jersey.

Winnicki, T., Szetela, R. & Wisniewski, J. (1982). Immobilized microorganisms in wastewater treatment. Studies in Environmental Science, 19, pp (341-352).

Wozniak, E.W. & Shubert, E. (2008). Systematics of *Desmodesmus* and *Scenedesmus*: a conundrum? In: Proceedings of the 56th meeting of British Phycological Society, January, Bristol, United Kingdom.

Xin, L., Hong-ying, H. & Yu-ping, Z. (2011). Growth and lipid accumulation properties of a freshwater microalga *Scenedesmus sp.* under different cultivation temperature. Bioresource Technology, 102, pp (3098–3102).

Xu, Z., Cai, J. & Pan B. (2013). Mathematically modeling fixed-bed adsorption in aqueous systems. Journal of Zhejiangh University SCIENCE – A, 14 (3), pp (155 – 176).

Zacheus, O.M. Livanainen, E.K. Nissinen, T.K. Lehtola, M.J. & Martikainen, P.J. (2000). Bacterial biofilm formation on polyvinyl chloride, polyethylene and stainless steel exposed to ozonated water. Water Research, 1, pp (63 - 70).

Zeinali, F., Ghoreyshi, A.A. & Najafpour, G.D. (2010). Adsorption of Dichloromethane from Aqueous Phase Using Granular Activated Carbon: Isotherm and Breakthrough Curve Measurements. Middle – East Journal of Scientific Research, 5 (4), pp (191 – 198).

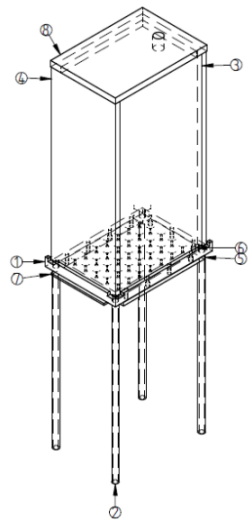
APPENDICES

Appendix A – Beijerinck medium

Modified Beijerinck medium composition

Reagents	**Per 1000mL**
Stock I	100 (mL)
Stock II	40 (mL)
Stock III	60 (mL)
Micronutrients	1 (mL)
Stock I	
NH_4NO_3	1.5 g
KH_2PO_4	0.2 g
$MgSO_4.7H_2O$	0.2 g
CaCl2.2H2O	0.1 g
Stock II	
K_2HPO_4	9.07 g
Stock III	
K_2HPO_4	11.61 g
Micronutrients	
H_3BO_3	10 g
$MnCl_2.4H_2O$	5 g
EDTA	50 g
$CuSO_4.5H_2O$	1.5 g
$ZnSO_4.H_2O$	22 g
$CoCl_2.6H_2O$	1.5 g
$FeSO_4.7H_2O$	5 g
$(NH4).6Mo.7O_{24}.4H_2O$	1g

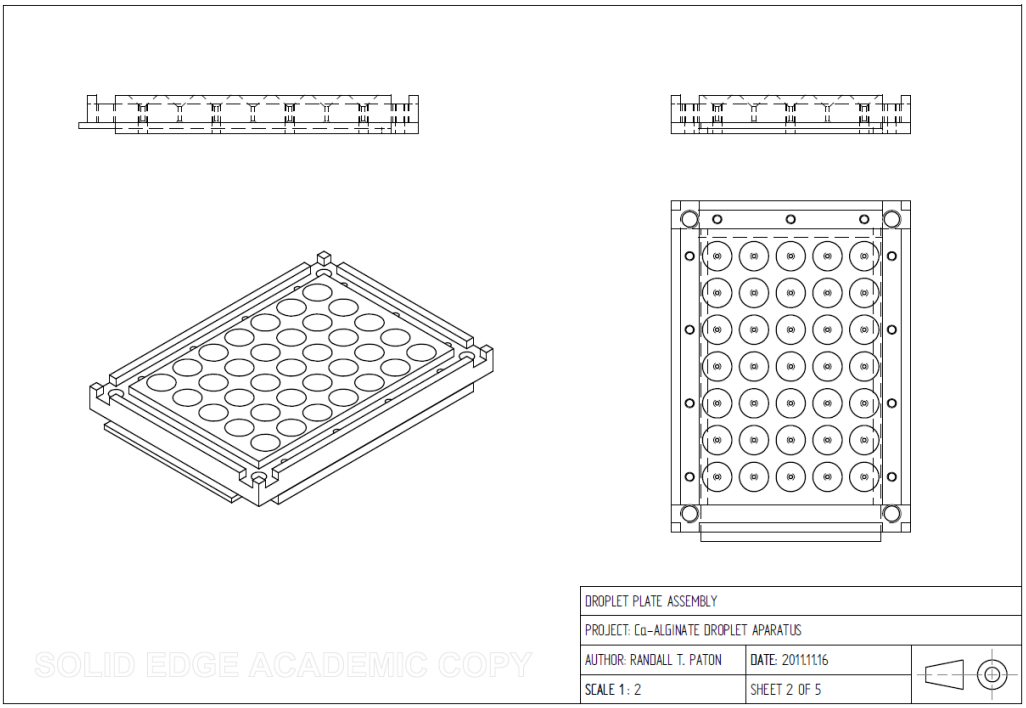
Appendix B – Immobilization, gelling forming system design for large scale production.

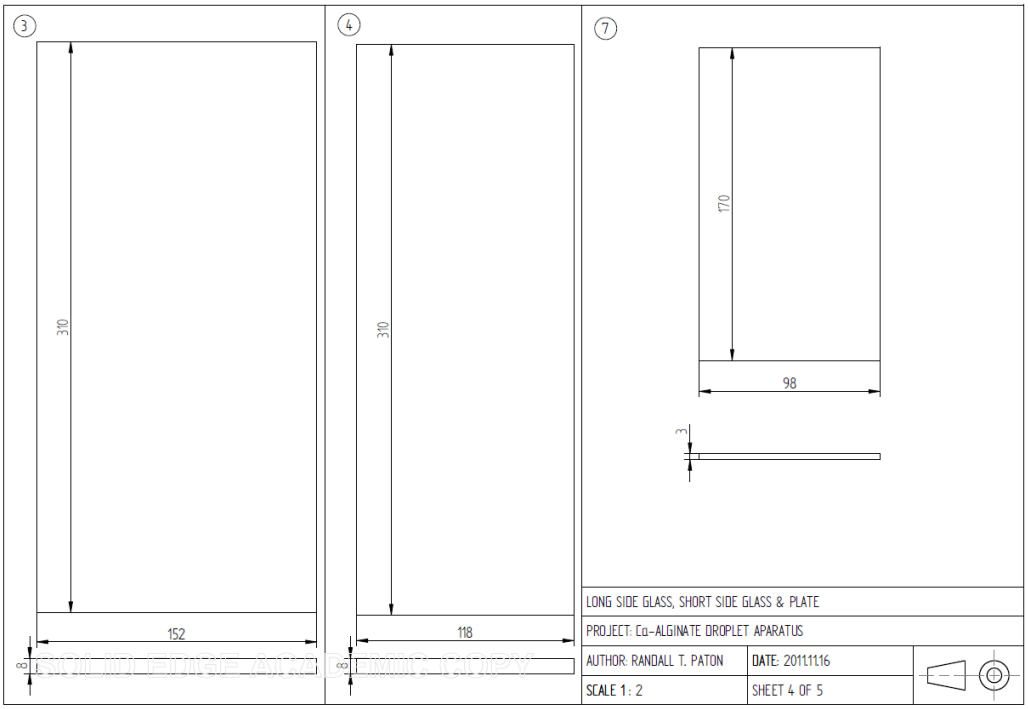


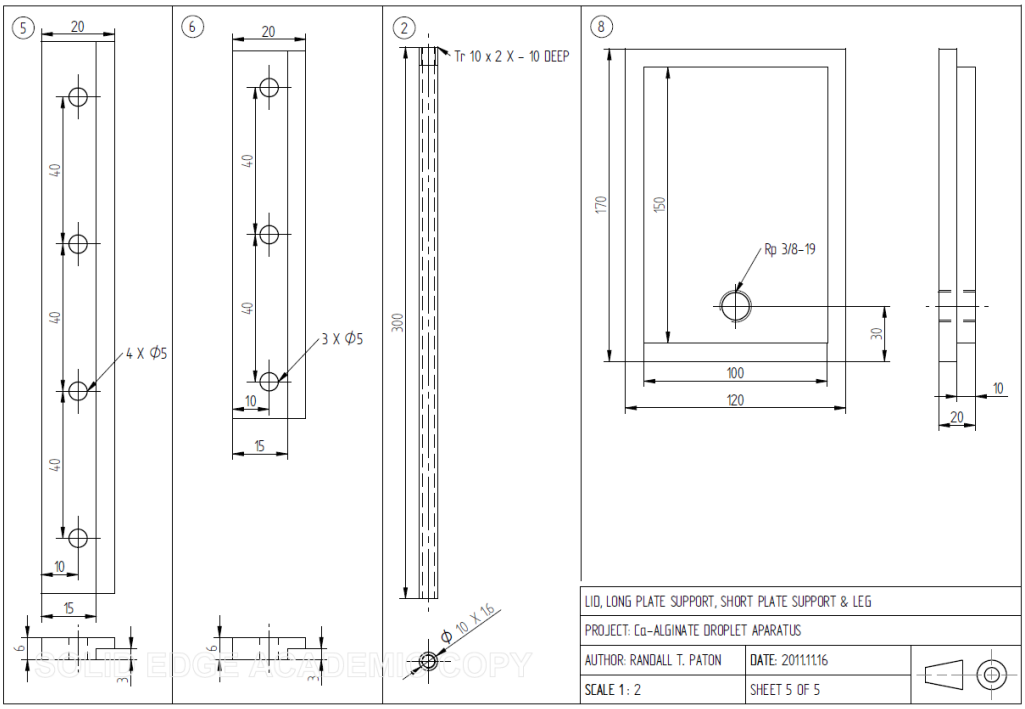
Item Number	Title	Material	Quantity
1	Droplet Plate	Aluminum, 1060	1
2	Support Leg	Aluminum, 1060	4
3	Long Side Glass	Glass, general industrial	2
4	Short Side Glass	Glass, general industrial	2
5	Long Side Plate Support	Aluminum, 1060	2
6	Short Side Plate Support	Aluminum, 1060	1
7	Plate	Aluminum, 1060	1
8	Lid	PVC	1

SOLID EDGE ACADEMIC COPY

DROPLET APPARATUS	
PROJECT: Ca-ALGINATE DROPLET APARATUS	
AUTHOR: RANDALL T. PATON	DATE: 2011.11.16
SCALE 1 : 5	SHEET 1 OF 5


DROPLET PLATE ASSEMBLY
PROJECT: Ca-ALGINATE DROPLET APARATUS
AUTHOR: RANDALL T. PATON
DATE: 2011.11.16
SCALE 1 : 2
SHEET 2 OF 5
SOLID EDGE ACADEMIC COPY


3
310
152
8
4
310
118
8
7
170
98
3
LONG SIDE GLASS, SHORT SIDE GLASS & PLATE
PROJECT: Ca-ALGINATE DROPLET APARATUS
AUTHOR: RANDALL T. PATON
DATE: 2011.11.16
SCALE 1 : 2
SHEET 4 OF 5


5
20
40
40
40
4 X Φ5
10
15
6
3
6
20
40
40
3 X Φ5
10
15
6
3
2
Tr 10 x 2 X – 10 DEEP
300
Ø 10 X 16
8
170
150
Rp 3/8-19
30
100
120
10
20
LID, LONG PLATE SUPPORT, SHORT PLATE SUPPORT & LEG
PROJECT: Ca-ALGINATE DROPLET APARATUS
AUTHOR: RANDALL T. PATON
DATE: 20111116
SCALE 1 : 2
SHEET 5 OF 5
SOLID EDGE ACADEMIC COPY